EVALUATING THE ACCURACY OF KNEE KINEMATICS MEASURED IN SIX DEGREES OF FREEDOM USING SURFACE MARKERS

by

Jesse A. Fisk

BS, Bucknell University, 2001

Submitted to the Graduate Faculty of

The School of Engineering in partial fulfillment

of the requirements for the degree of

Master of Science in Bioengineering

University of Pittsburgh

2004

UNIVERSITY OF PITTSBURGH

SCHOOL OF ENGINEERING

This thesis was presented

by

Jesse A. Fisk

It was defended on

March 23, 2004

and approved by

Zong-Ming Li, Ph.D.,
Departments of Orthopaedic Surgery, Bioengineering, and Occupational Therapy

Jean McCrory, Ph.D.,
Departments of Sports Medicine and Nutrition Sciences and Bioengineering

Mark S. Redfern, Ph.D.,
Departments of Bioengineering, Otolaryngology, Industrial Engineering,
and Rehabilitation Science

Thesis Advisor: Savio L-Y. Woo, Ph.D., D.Sc.
Departments of Bioengineering, Mechanical Engineering, Rehabilitation Science & Technology

EVALUATING THE ACCURACY OF KNEE KINEMATICS MEASURED IN SIX DEGREES OF FREEDOM USING SURFACE MARKERS

Jesse A. Fisk, B.S.

University of Pittsburgh, 2004

Injury to the anterior cruciate ligament (ACL) of the knee can result in joint instability even following reconstruction. This instability may be quantified by measuring *in vivo* knee kinematics in six degrees of freedom. Motion capture systems have been used for measuring kinematics but they are limited by system inaccuracies and error resulting from skin movement. Therefore, the overall objective of this thesis was to determine the level of accuracy that a motion capture system using surface markers provides for measuring knee kinematics.

There are three specific aims in this thesis. The first specific aim was to mathematically investigate the effect of random errors in marker locations on the accuracy of knee kinematics calculated using the point cluster technique (PCT), triad and Helen Hayes marker sets. The results indicated that the PCT marker set had the greatest potential for accurately measuring knee kinematics. The second aim was to determine how inaccuracies of the motion capture system contribute to errors of joint kinematics measured with the PCT. Despite its high accuracy, the average errors of joint kinematics attributed to the system were up to 1° and 2 mm. The final specific aim was to investigate the efficacy of an algorithm called the interval deformation

technique (IDT) for reducing errors of knee kinematics resulting from skin movement. The IDT reduced the errors of kinematics by 90% for an activity with skin movement simulating muscle contraction but was unable to reduce the errors resulting from skin movement at heel strike of gait.

The overall errors of knee kinematics resulting from system inaccuracies and skin movement were estimated to be 2° and 4 mm. While this technique may be useful for measuring the changes in knee kinematics that result from ACL injury, this accuracy may not be sufficient to discern the small differences in knee kinematics between ACL intact and reconstructed subjects or for predicting ligament forces. Thus, further research is suggested in order to better quantify skin movement and provide data for improving the accuracy of kinematics measured with surface markers.

DESCRIPTORS

Anterior Cruciate Ligament
Knee Kinematics
Photogrammetry
Point Cluster Technique
Skin Motion Artifact
Skin Movement

TABLE OF CONTENTS

LIST OF TABLES

LIST OF FIGURES

ACKNOWLEDGEMENTS

I would first like to thank my advisor, Dr. Savio L-Y. Woo, for the privilege of being part of the Musculoskeletal Research Center over the past 3 years. I am very fortunate to have found a research center with such immense opportunities. I am confident that the skills I have learned under the guidance of Dr. Woo will be invaluable throughout my career.

Drs. Zong-Ming Li, Jean McCrory, and Mark Redfern have been essential to my thesis research. Even before they joined my committee, they generously volunteered their insight and resources. Their enthusiasm has shown me the value of my work and sustained my interest in this research.

Several others have also been instrumental in this research. Specifically, Melissa Rollins, Andrew Van Scyoc, and Timothy Sell have been valuable co-investigators and friends. Dr. Gene Alexander has also been very patient in teaching me his techniques and provided vital directions. I am very thankful for the encouragement I have received from the entire MSRC and wish everyone the best of luck with their research and beyond.

Last, but by no means least, I would like to thank my family and friends that have been so supportive. Their understanding and patience has been amazing and truly made this achievement possible.

I would also like to acknowledge the Neuromuscular Research Laboratory and Human Movement and Balance Laboratory for generously sharing their facilities and the University of Pittsburgh Department of Bioengineering and the National Institutes of Health for their financial support.

ABBREVIATIONS

ACL: Anterior cruciate ligament

ATT: Anterior tibial translation

ADL: Activities of daily living

DOF: Degrees of freedom

ITR: Internal tibial rotation

MCL: Medial collateral ligament

LCL: Lateral collateral ligament

PCL: Posterior cruciate ligament

JCS: Joint coordinate system

3D: Three dimensional

RSA: Roentgen stereophotogrammetric analysis

TKA: Total knee arthroplasty

2D: Two dimensional

MRI: Magnetic resonance image

DLT: Direct linear transform

HH: Helen Hayes

ASIS: Anterior superior iliac spine

PCT: Point cluster technique

ROM: Range of motion

IDT: Interval deformation technique

1.0 INTRODUCTION

1.1 ANTERIOR CRUCIATE LIGAMENT INJURY

The anterior cruciate ligament (ACL) of the knee is frequently injured with an estimated annual incidence of 1 in 3,000 for the general population[1, 2]. For those aged between 15 and 45 years, the rate of ACL injury is much larger, estimated to be 1 in 1,750 per year[2]. ACL injuries often occur during athletic activities including skiing[3-6], football[7], basketball[8, 9], and soccer[10-12] and about 70% result from non-contact mechanisms of injury such as rapid deceleration and pivoting motions[2]. Additionally, the incidence of ACL injury is up to 4 times larger for female athletes compared to their male counterparts[12-14].

Injuries to the ACL can frequently result in pathologic joint motion[1]. While a small proportion of ACL deficient patients experience minimal function deficits[15, 16], many report debilitating knee pain and instability that can severely limit activity[11, 17, 18]. In a study of recreational athletes that had suffered an ACL injury, almost all were content with their knees for activities of daily living but only half were satisfied with their knee function during sports[19]. A separate study showed that over 60% of ACL deficient athletes experience "giving way" episodes of the knee even with the use of braces[20]. This instability can cause secondary injuries to the knee such as meniscal tears[21-23] and osteoarthritis[24, 25].

Since the ACL does not heal following injury[17, 26, 27], ACL reconstructions are frequently performed for athletes and laborers that frequently experience high knee loads[28]. A prospective study of 92 patients 8 years after suffering an ACL tear showed that ACL reconstructions gave good to excellent results in 50% more patients that underwent ACL reconstructions compared to patients treated non-operatively[29]. ACL reconstructions have become common and more than 50,000 are performed each year in the United States[28].

Orthopaedic surgeons are faced with several options when performing ACL reconstructions[30]. Many different materials have been used to replace the ACL including hamstring tendon[31-41], patellar tendon[32, 33, 38, 40-42], quadriceps tendon[43], iliotibial band[44], tibialis anterior tendon[45, 46], Achilles tendon[47], and synthetic constructs[48-50]. Additional choices that surgeons face include the tunnel placement[39, 51-56]amount of initial graft tension[37, 57-63], tunnel angle[64, 65], and fixation method[34, 66-73]. While much research has been conducted to compare the biomechanical effects and clinical outcomes of various reconstruction methods, optimal techniques remain unclear[74].

The importance of a rehabilitation phase following ACL reconstruction is widely acknowledged. Early rehabilitation protocols supported the utilization of casts and limited motion for over a month following ACL reconstruction to prevent excessive graft forces[75, 76]. Subsequent studies have shown that resulting quadriceps atrophy can cause limited range of motion and therefore advocate accelerated rehabilitation allowing full range of motion and weightbearing immediately following reconstruction[77-80]. Despite these findings, controversy remains between accelerated and conservative rehabilitation protocols[81]. The use of braces for enhancing knee stability is also controversial[82]; some studies have shown that braces are beneficial[82-85] while others report no

differences[86] or decreases in performance[87, 88] with a brace. Additionally, the risks of open kinetic chain exercises for endangering the graft are unclear[89-93]. Rehabilitation methods are continuously evolving and additional research is needed to investigate the effects of different protocols[94].

A recent study surveyed 397 orthopedic surgeons that were members of the American Academy of Orthopaedic Surgeons on their opinions regarding the treatment of ACL injuries[95]. There was clinical disagreement among the surgeons in response to 48% of the questions. The authors concluded that significant variation exists in the clinical opinions of surgeons and more research is required to clarify appropriate methods for treating ACL injury.

1.2 OUTCOMES OF ACL RECONSTRUCTION

Many retrospective studies have assessed patient outcome following ACL reconstruction[96]. While reconstructions have generally been found to be effective for restoring normal knee function[42, 97], several studies have revealed unsuccessful outcomes for a subset of patients. For example, 3 years after reconstruction, 20% of patients reported that their knee condition was abnormal[98] and 30% of patients had abnormal knee function according to criteria established by the International Knee Documentation Committee[99]. At 7 years post-operatively, 20% of patients complained of knee instability and were not able to return to sports activites[100]. A separate study, also at 7 years after reconstruction, reported that 35% of patients had unsatisfactory results[101].

Several reasons have been proposed to explain the inability of some ACL reconstructed patients to regain normal knee function. First is the inability of ACL reconstructions to restore normal knee mechanics. *In vitro* tests have shown that grafts do not reproduce the *in situ* ligament forces and knee kinematics of cadaveric knees with intact ACLs[33, 54]. A study from our laboratory has shown that even reconstructions designed to replicate the anatomical complexity of the ACL are unable to restore normal knee mechanics immediately following reconstruction[102]. While the long term results are unknown, research using an animal model has shown that these deficits in knee kinematics and graft forces may worsen over the first 6 weeks of healing[103].

Neuromuscular deficits may also contribute to poor knee function following ACL reconstruction. For example, abnormal proprioception of ACL reconstructed patients has been found up to 4 years postoperatively and may be indicative of poor knee function[104-106]. Additionally, reduced quadriceps strength of ACL reconstructed patients has been reported up to 4 years postoperatively[107-109] and has been correlated with decreased functional knee stability[110].

1.3 EFFECT OF ACL INJURY ON KNEE STABILITY

The ACL is the main restraint of the knee to anterior tibial translation (ATT)[111]. Therefore, the ATT of a relaxed knee in response to an anterior tibial load increases 2 to 3 fold when the ACL is transected[54]. Both subjective[112, 113] and instrumented[114-116] clinical exams have been developed to measure ATT for diagnosing ACL injury. These techniques can be conveniently performed and ATT is frequently used to investigate how well normal knee laxity is restored by various treatment techniques[32, 33, 38, 40-42, 44, 47, 99, 101, 117-121]. However, several studies have shown that the

ATT of the relaxed knee may not be an accurate measure of functional outcome for both ACL deficient patients[122-124] and those that have undergone ACL repair[100, 125, 126]. For example, in a comparison of 2 groups of ACL deficient athletes, there were no significant differences in the ATT of patients that had returned to sports activity following injury and of those that had not been able to return to sports[122].

One explanation why ATT in response to an anterior tibial load may not be sufficient for predicting knee function regards the complex loads and motions the knee experiences. During activities of daily living (ADL), the knee is subjected to forces and moments in many directions and experiences rotations and translations in all 6 degrees of freedom (DOF). The ACL has been shown to limit internal tibial rotation (ITR) and valgus rotations in addition to restraining ATT[54, 111, 127]. Therefore, it is important to investigate how the knee responds to external loads in multiple DOF to understand the effect of ACL injury and reconstruction on knee stability. For example, a recent study from our research center compared the performances of two types of reconstructions and showed that while there were no differences in ATT in response to an anterior load, differences in kinematics could be elicited by applying a rotatory load[54].

The ATT of the relaxed knee also may not reflect knee function during ADL because of the stability provided by muscles. Many patients develop complex compensatory muscle activation patterns after ACL injury or reconstruction to stabilize the knee and limit graft forces[15, 16, 128-131]. For example, changes in quadriceps, hamstrings, gastrocnemius, and soleus activation patterns may be used to stabilize the motion of the knee[132-134]. These neuromuscular adaptations can allow patients with high passive knee laxity to function at surprisingly high levels[122].

1.4 CLINICAL MOTIVATION FOR STUDYING KNEE MOTION

Assessing knee kinematics in multiple DOF during ADL will be useful for better understanding the changes in functional knee stability associated with ACL injury and how well different treatment methods restore normal knee motion. In addition to these kinematic outcomes, these data can be combined with kinetic measurements to investigate joint torques using inverse dynamics. Our research center also plans to reproduce these *in vivo* kinematics[135, 136] with a finite element model[137] or a cadaveric knee using a robotic/universal force-moment sensor testing system[138-140] to calculate the *in situ* forces of the ACL and its replacement grafts during different activities. These results will be useful for determining the efficacy of different reconstructions for restoring normal *in situ* forces of the ACL and determining the graft forces associated with different rehabilitation exercises.

2.0 OBJECTIVE

The overall objective of this thesis is to investigate the accuracy of a method for non-invasively measuring knee kinematics in multiple degrees of freedom with a motion capture system and surface markers.

3.0 BACKGROUND

3.1 ANATOMY OF THE KNEE

The purpose of this thesis is to investigate a method of quantifying knee motion. Therefore, a brief overview of the anatomy of the knee will be useful. The knee allows relative motion between the thigh and lower leg or shank. Several diarthrodial joints comprise the knee; the patellofemoral joint between the distal femur and sesamoid patella, the tibiofibular joint between the proximal tibia and fibular head, and the tibiofemoral joint between the distal femur and proximal tibia (Figure 1). The latter provides large motions in addition to supporting high loads and will be the focus of this thesis.

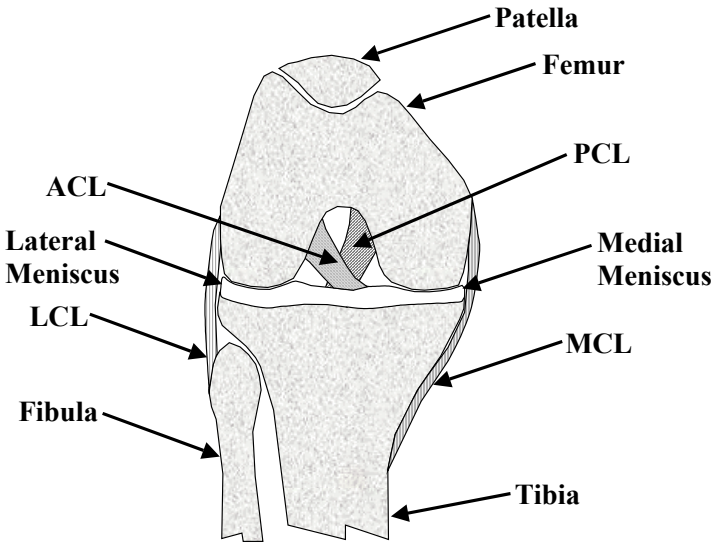

Figure 1: Anterior view of the anatomy for a flexed right knee

The distal end of the femur forms two condyles which rest on the tibial plateau to form the tibiofemoral joint[141]. Both of these articulating surfaces are covered with hyaline cartilage that reduces friction and provides shock absorbance. The tibial plateau is approximately perpendicular to the tibial axis with a slight anterior inclination in the sagittal plane and lateral inclination in the coronal plane[132, 142]. The medial plateau is concave to mate with the femoral condyle while the lateral plateau is slightly convex[143].

The tibiofemoral joint is stabilized by several passive structures[141, 143]. The menisci are semicircular fibrocartilaginous wedges attached primarily to the tibial plateau. The menisci conform to the articulating surfaces of the femur and tibia and increase the contact area of the tibiofemoral joint. Four main knee ligaments connect the tibia and femur. The medial collateral ligament (MCL) is a thickening of the capsule that is composed of superficial and deep fibers[144]. The MCL attaches proximally to the medial femoral epicondyle and inserts distally to the medial meniscus and the tibia. The lateral collateral ligament (LCL) is a round ligament that connects the lateral femoral epicondyle to the head of the fibula. The LCL, popliteus tendon, and popliteofibular ligaments are often referred to as a group as the posterolateral structures[145]. The anterior cruciate ligament (ACL) is attached proximally to the medial aspect of the lateral femoral condyle and distally to the anterior tibia. Anatomically, different bundles of the ACL are difficult to identify[146], while functionally, two can be identified based on tension patterns and are named by the locations of the tibial insertions; the anteromedial and posterolateral bundles[147]. The posterior cruciate ligament (PCL) crosses the ACL intra-articularly with attachments on the lateral aspect of the medial femoral condyle and posterior tibia. The PCL is the larger of the two cruciates with a cross sectional area 18% to 55% greater than that of the ACL[148].

Several muscles of the thigh cross the knee joint[141, 143]. The sartorius is the longest muscle in the body and the most superficial muscle of the anterior thigh. The sartorius originates at the anterior superior iliac spine (ASIS) of the pelvis and inserts on the medial side of the proximal tibia. The quadriceps femoris includes 4 muscles on the anterior thigh. Of these, the rectus femoris originates on the pelvis while the 3 vasti originate on the proximal femur. All 4 quadriceps insert at the tibial tuberosity through the sesamoid patella via the patellar tendon. The 3 hamstring muscles are part of the posterior thigh and originate on the ischial tuberosity of the pelvis. Of these, the semitendinosus and semimembranosus insert on the medial side of the proximal tibia while the biceps femoris inserts laterally at the fibular head. The gracilis originates at the pubic ramus, inserts on the medial tibia near the sartorius and semitendinosus, and is the only hip adductor to cross the knee joint. The tensor fascia lata muscle lies on the lateral thigh and originates on the pelvis. This muscle blends with the gluteus maximus to form the iliotibial tract that inserts into the femur through the intermuscular septum, the lateral femoral condyle by Kaplan's fibers, the patella through the iliopatellar band, and the anterolateral tibia at Gerdy's tubercle[149-151].

Several muscles of the shank also span the knee joint[141, 143]. The gastrocnemius is the most superficial of the triceps surae or calf muscles. Its 2 heads originate from the medial and lateral femoral condyles and insert at the calcaneus through the Achilles tendon. The plantaris is a long, slender muscle with its origin at the lateral femoral condyle and insertion on the medial border of the calcaneus. The popliteus muscle is located posterior to the knee joint. Its short muscle body attaches the medial tibia to the lateral femur and lateral meniscus.

3.2 BIOMECHANICAL CONTRIBUTIONS OF THE KNEE STRUCTURES

The articulating surfaces of the femur and tibia do not provide sufficient geometric constraints to stabilize the knee. Instead, knee motion is controlled by static stabilizers, such as the menisci and ligaments, and active stabilizers, i.e. muscles. These structures interact in a complicated manner to stabilize the knee throughout its range of motion[152-154]. Investigating the biomechanical role of the various knee structures is valuable for understanding the causes and consequences of knee injury.

The role of static stabilizers for providing knee stability has been investigated by sectioning various ligaments of cadaveric specimens and measuring the resulting changes in knee motion in response to applied loads (i.e. "cutting studies")[155, 156]. Other investigators have implanted transducers in cadaveric knees to measure how ligaments are loaded[127, 153, 157, 158] or stretched[159] in response to external loads. A novel non-contact methodology that combines a robotic manipulator and a universal force-moment sensor has been developed at our research center to investigate ligament loading patterns in addition to the changes in joint kinematics that occur with ligament transection[135, 138, 140, 160-162]. These methods have all been used to elucidate the contributions of different structures to knee stability.

The ACL is an important restraint to ATT throughout the range of motion of the knee and also to medial tibial translation near knee extension[111, 147, 155]. The ACL has also been shown to limit ITR and varus-valgus rotations[157-159, 163]. The role of the ACL for providing knee stability is most important near full extension[127]. On the other hand, the PCL limits posterior tibial translation[111, 155, 164] and external tibial rotation, and is most effective near 90 degrees of knee flexion[127, 155, 157,

[163-166]. The MCL is essential for restraining valgus rotation and can also limit ATT and internal-external tibial rotations. The lateral structures of the knee including the LCL are very important for limiting varus and external rotations and may additionally restrain anterior-posterior translations[111, 155]. The menisci have been shown to contribute to the anterior-posterior, varus-valgus, and the internal-external stability of the knee[156, 167].

Muscle activation is used to stabilize the knee joint, in addition to providing motion. The quadriceps are the main knee extensors but also produce an anteriorly directed force and joint compression that causes ATT[132]. The gastrocnemius also provides ATT and is considered an ACL antagonist[168]. On the other hand, the hamstrings[133] and iliotibial band[169] pull the tibia posteriorly and can also regulate internal-external tibial rotation. Despite not crossing the knee joint, the soleus muscle produces a moment about the ankle that also reduces ATT at the knee[134].

3.3 KINEMATICS FOR INVESTIGATING KNEE MOTION

Injury to any of the static or active stabilizers of the knee, such as the ACL, can alter the delicate balance of forces across the joint. While neuromuscular compensation may sometimes reduce the resulting knee instability, pathological movement often occurs. The quantification of this abnormal motion can be useful for understanding the functional deficits that are associated with various musculoskeletal disorders, rating the severity of injury, and assessing the efficacy of different treatment modalities.

3.3.1 Theory

The basics of kinematic analysis have been well described in the literarure[170, 171]. The brief review that follows will focus on the theory utilized in the methods of this thesis. Kinematics describes how a body is positioned in space over time without regard for the forces causing motion. Both the location and orientation of a body must be determined to completely describe how it is positioned. The position of a body may be quantified by describing how a local Cartesian coordinate system or frame fixed to the body is located and oriented with respect to a global coordinate frame[170-172]. For example, the location of body 1 is described as the position of its origin O_1 measured in global coordinate frame-0 (Figure 2). The orientation of body 1 can be described by the unit vectors, I_1, J_1, and K_1 of axes X_1, Y_1, and Z_1 measured in the global coordinate frame.

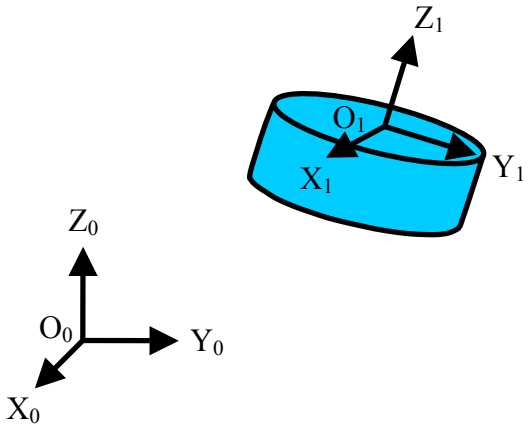

Figure 2: Rigid body with respect to global coordinate frame-0

A transformation matrix is a convenient method of presenting these relationships between coordinate frames. The transformation matrix $[T_{01}]$ describing how frame-1 is positioned with respect to frame-0 can be written as:

$$[T_{01}] = \begin{bmatrix} I_0 \cdot I_1 & I_0 \cdot J_1 & I_0 \cdot K_1 & a_{01} \\ J_0 \cdot I_1 & J_0 \cdot J_1 & J_0 \cdot K_1 & b_{01} \\ K_0 \cdot I_1 & K_0 \cdot J_1 & K_0 \cdot K_1 & c_{01} \\ 0 & 0 & 0 & 1 \end{bmatrix} \tag{1}$$

where a_{01}, b_{01}, and c_{01} are the x, y, and z locations, respectively, of O_1 measured with respect to frame-0.

The location of a point measured in different coordinate frames may be calculated using transformation matrices. If the location of point P with respect to frame-1 is known (Figure 3), its location with respect to the global frame-0 is:

$$\begin{pmatrix} x_0 \\ y_0 \\ z_0 \\ 1 \end{pmatrix} = [T_{01}] \cdot \begin{pmatrix} x_1 \\ y_1 \\ z_1 \\ 1 \end{pmatrix} \tag{2}$$

More commonly, the location of a point can be measured with respect to a global coordinate frame and its location in a local coordinate frame is desired. In this case, the location of the point P with respect to local coordinate frame-1 can be determined as:

$$\begin{pmatrix} x_1 \\ y_1 \\ z_1 \\ 1 \end{pmatrix} = [T_{10}] \cdot \begin{pmatrix} x_0 \\ y_0 \\ z_0 \\ 1 \end{pmatrix} \tag{3}$$

$[T_{10}]$ can be calculated as the inverse of $[T_{01}]$ and Equation 3 becomes:

$$\begin{pmatrix} x_1 \\ y_1 \\ z_1 \\ 1 \end{pmatrix} = [T_{01}]^{-1} \cdot \begin{pmatrix} x_0 \\ y_0 \\ z_0 \\ 1 \end{pmatrix} \tag{4}$$

If two local coordinate frames exist, the location of point P with respect to frame-2 can be calculated using several methods. If the relationship between frame-2 and the global frame-0 is known:

$$\begin{pmatrix} x_2 \\ y_2 \\ z_2 \\ 1 \end{pmatrix} = [T_{20}] \cdot \begin{pmatrix} x_0 \\ y_0 \\ z_0 \\ 1 \end{pmatrix} \tag{5}$$

If instead the relationship between frame-1 and frame-2 is given:

$$\begin{pmatrix} x_2 \\ y_2 \\ z_2 \\ 1 \end{pmatrix} = [T_{21}] \cdot \begin{pmatrix} x_1 \\ y_1 \\ z_1 \\ 1 \end{pmatrix} \tag{6}$$

Equation 3 may then be substituted into Equation 6 to give:

$$\begin{pmatrix} x_2 \\ y_2 \\ z_2 \\ 1 \end{pmatrix} = [T_{21}] \cdot [T_{10}] \cdot \begin{pmatrix} x_0 \\ y_0 \\ z_0 \\ 1 \end{pmatrix} \tag{7}$$

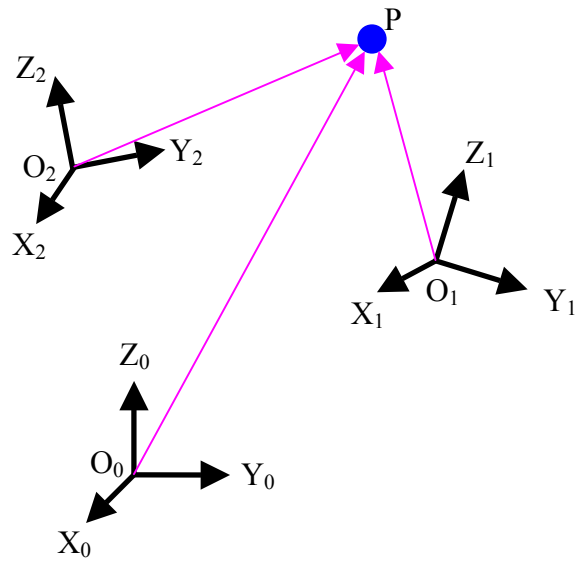

Figure 3: Location of point P with respect to 3 coordinate frames

When 2 body segments are connected through a joint, it is often desirable to obtain the relative kinematics of the two segments. For some applications, an anatomic joint can be modeled as a revolute joint, a universal joint, or a ball and socket joint[173, 174], however, the most general description provides joint kinematics in 6 DOF. For adjoining body segments 1 and 2, the joint kinematics may be fully described by the transformation matrix $[T_{12}]$. However, joint kinematics are more clearly given as the 3 translations and 3 rotations that describe how frame-2 is located and oriented with respect to frame-1. The translations represent the location of O_2 with respect to frame-1. Two conventions exist for describing the orientation of frame-2 with respect to frame-1[171]. Both methods explain how frame-1 can be rotated in 3 steps such that it is aligned with frame-2. Using the method of fixed angles, frame-1 is rotated about the 3 axes of the initial orthogonal frame-1. Alternatively, the Euler method describes 3 rotations that are taken about the

axes of the moving frame-1. The sequence of rotations must be specified for both methods and the solutions of all 24 angle set conventions are available in the literature[171]. Method utilizing Euler angles are common for the description of human joint kinematics[175, 176] and will be used in this thesis.

As an example of calculating joint kinematics using Euler angles, consider the relationship between frames 1 and 2 (Figure 3). Translating frame-1 to O_2, rotating the translated frame-1 an angle α about X_1, rotating the resulting frame-1' an angle β about Y_1', and lastly rotating frame-1'' an angle γ about Z_1'' can be represented as the transformation:

$$[T_{12}] = \begin{bmatrix} 1 & 0 & 0 & a_{12} \\ 0 & 1 & 0 & b_{12} \\ 0 & 0 & 1 & c_{12} \\ 0 & 0 & 0 & 1 \end{bmatrix} \begin{bmatrix} 1 & 0 & 0 & 0 \\ 0 & \cos\alpha & -\sin\alpha & 0 \\ 0 & \sin\alpha & \cos\alpha & 0 \\ 0 & 0 & 0 & 1 \end{bmatrix} \begin{bmatrix} \cos\beta & 0 & \sin\beta & 0 \\ 0 & 1 & 0 & 0 \\ -\sin\beta & 0 & \cos\beta & 0 \\ 0 & 0 & 0 & 1 \end{bmatrix} \begin{bmatrix} \cos\gamma & -\sin\gamma & 0 & 0 \\ \sin\gamma & \cos\gamma & 0 & 0 \\ 0 & 0 & 1 & 0 \\ 0 & 0 & 0 & 1 \end{bmatrix}$$

$$= \begin{bmatrix} \cos\beta\cos\gamma & -\cos\beta\sin\gamma & \sin\beta & a_{12} \\ \cos\alpha\sin\gamma + \sin\alpha\sin\beta\cos\gamma & \cos\alpha\cos\gamma - \sin\alpha\sin\beta\sin\gamma & -\sin\alpha\cos\beta & b_{12} \\ \sin\alpha\sin\gamma - \cos\alpha\sin\beta\cos\gamma & \sin\alpha\cos\gamma + \cos\alpha\sin\beta\sin\gamma & \cos\alpha\cos\beta & c_{12} \\ 0 & 0 & 0 & 1 \end{bmatrix} \quad (8)$$

By equating the numerical values of $[T_{12}]$ with the right side of Equation 8, the 3 orthogonal translations, a_{12}, b_{12}, c_{12}, and the 3 Euler angles, α, β, γ, can be solved[170, 171].

For investigating knee kinematics, anatomical coordinate frames are defined for the femur and tibia to allow clinically meaningful joint kinematics to be determined. Several conventions may be used to define these anatomical axes[174, 177-181]. While uniformity between different investigators is advantageous, the adopted conventions are dependent upon the anatomical landmarks that may be measured and the specific application[182]. For this thesis, the x-axes are oriented to the subject's left, the y-axes distally, and the z-axes posteriorly (Figure 4). These directions were adopted to match the conventions used by our laboratory's high payload robotic testing system[177]. The origins of both the tibial and femoral anatomic coordinate frames are centered between the femoral epicondyles when the subject is relaxed with the knee at full extension (separation of these coordinate frames is exaggerated in Figure 4).

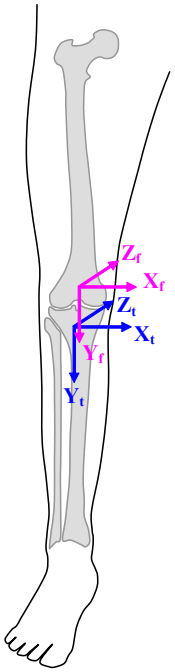

Figure 4: Anatomical coordinate frames for the right knee

The orientation of the tibial frame with respect to the femoral frame can be described using a specific sequence of Euler angles; the femoral frame is sequentially rotated α about the x-axis, β about the z'-axis, and γ about the y''-axis. For a right knee, α corresponds to knee flexion, β to valgus rotation, and γ to external tibial rotation. These rotations can be calculated from the transformation matrix, $[T_{ft}]$, describing the position of the tibial anatomic frame with respect to the femoral anatomic frame:

$$\alpha = \tan^{-1}\left(\frac{(T_{ft})_{3,2}}{(T_{ft})_{2,2}}\right) \tag{9}$$

$$\beta = \tan^{-1}\left(\frac{-(T_{ft})_{1,2}}{\cos(\alpha)\cdot(T_{ft})_{2,2} + \sin(\alpha)\cdot(T_{ft})_{3,2}}\right) \tag{10}$$

$$\gamma = \tan^{-1}\left(\frac{(T_{ft})_{1,3}}{(T_{ft})_{1,1}}\right) \tag{11}$$

Two options for describing knee translations will be considered. The basic method of presenting translations is to give the location of the tibial origin, O_t, with respect to the orthogonal femoral frame. These 3 translations can be obtained directly from the right column of $[T_{ft}]$. For an extended right knee, a_{ft} represents lateral tibial translation, b_{ft} distal tibial translation and c_{ft} posterior tibial translation.

An alternative method of describing knee translations uses the joint coordinate system (JCS)[178]. Rather than knee translations being described along the orthogonal femoral axes, a non-orthogonal coordinate system is used (Figure 5). Medial-lateral translation occurs along X_f, proximal-distal translation along Y_t, and anterior-posterior translation along a floating axis that is mutually perpendicular to the body-fixed axes X_f and Y_t. Using the JCS description of joint

kinematics for the right knee, the femoral coordinate frame is rotated α about the x-axis, translated medially along the x-axis, rotated β about the z' or floating axis, translated posteriorly along the z'-axis, rotated γ about the y''-axis, and finally translated distally along the y''-axis to become coincident with the tibial frame. Equations 9 - 11 remain valid for calculating knee rotations while the JCS translations for the right knee can be calculated from the transformation matrix (Appendix A):

$$d_{medial} = \frac{\cos(\beta)\cdot(T_{ft})_{1,4} + \cos(\alpha)\cdot\sin(\beta)\cdot(T_{ft})_{2,4} + \sin(\alpha)\cdot\sin(\beta)\cdot(T_{ft})_{3,4}}{\cos(\beta)} \tag{12}$$

$$d_{posterior} = -\sin(\alpha)\cdot(T_{ft})_{2,4} + \cos(\alpha)\cdot(T_{ft})_{3,4} \tag{13}$$

$$d_{distal} = \frac{\cos(\alpha)\cdot(T_{ft})_{2,4} + \sin(\alpha)\cdot(T_{ft})_{3,4}}{\cos(\beta)} \tag{14}$$

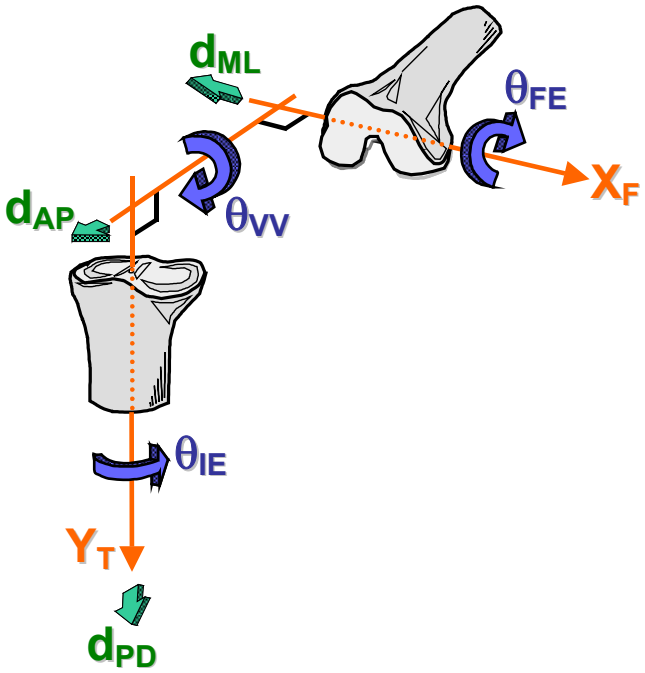

Figure 5: Diagram of joint coordinate system conventions

The JCS was developed to facilitate communication between engineers and clinicians[174]. It has been utilized by several investigators[178, 179, 183] and has been recommended by the International Society of Biomechanics for the standardization of reporting kinematic data[181]. A simple example can demonstrate the advantages of describing kinematics with the JCS rather than reporting translations with respect to the orthogonal femoral frame: with the knee extended, translation along the Z_f axis corresponds to posterior tibial translation, however, with the knee flexed, translation along Z_f is in the distal direction of the tibia. With the JCS, translation along the floating axis will always correspond to posterior tibial translation and have a clear clinical interpretation.

3.3.2 Measurement Methods

Many methods have been used to measure knee kinematics. In this section, several common traditional techniques will be described in addition to methods more recently developed. Instrumented spatial linkages or electrogoniometers have been used for over 30 years to directly measure joint motion[175, 184]. These devices consist of a linkage with transducers attached across an anatomical joint. By measuring the rotation or translations of each mechanical joint electronically, the kinematics of the anatomical joint are calculated[185, 186]. An early device that allowed joint rotations to be measured in 3 DOF was described in 1969 by Johnson and Smidt for the hip[187] and in 1970 by Kettlekamp and coworkers for the knee[188]. In 1972, Kinzel and associates presented a thorough description of the theory and applications of a 6 DOF device[189, 190]. These device have remained popular and recent studies have used both 4 DOF[191-194] and 6 DOF[129, 195, 196] devices to quantify knee motion. While instrumented spatial linkages are relatively inexpensive, the accuracy of these devices suffers from machining tolerances,

difficulty aligning or determining the relationship between the mechanical axes of the device and the anatomical axes, and soft tissue movement between the device and the bone. Suntay and coworkers showed the accuracy of an instrumented spatial linkage to be within 0.5 mm and 0.5°, but did not consider errors resulting from misalignment or slippage of the device[197]. Additionally, these devices can be bulky and awkward, thus encumbering subject motion.

Photogrammetry and videogrammetry have a long history in the study of human motion[198, 199]. Unlike instrumented spatial linkages, these methods have been used to measure joint motion without contacting the subject. By using multiple cameras, the three dimensional (3D) locations of surface markers attached to the skin of subjects may be measured and joint kinematics calculated. In 1967, Sutherland explained a system that used 2 cameras to record gait in 3D using mathematics developed for the aeronautic industry[200]. This method required the markers to be hand-digitized in each movie frame and was very time intensive. During the mid 1970's, investigators such as Furnée, Paul, Jarrett, Andrews, and Winter began to develop automated video systems and, by 1980 commercial systems including VICON and Selspot became available[198]. With rapid improvements in computer technology, these motion capture systems became common for clinical gait analysis. Example applications for this technology that have been recently published include investigating risk factors for ACL injury[201] and the effect of ACL injury[202] on motion patterns. Motion capture systems are generally non-invasive and convenient to use, however, the accuracy of this method suffers from relative motion between the skin and bone. The resulting errors are not fully understood but, in most cases, knee translations cannot be accurately measured using these systems.

Unlike instrumented spatial linkages and motion capture systems, radiographic methods have been used to measure skeletal motion directly. Roentgen stereophotogrammetric analysis (RSA) uses radiographs simultaneously recorded from 2 perspectives to determine the 3D positions of the skeleton[203]. Since it may be difficult to accurately identify anatomical landmarks on radiographs, metal beads have been implanted in the skeleton to provide distinct radiopaque markers. An early description of this technique for recording joint kinematics of cadavers was given by Lysell in 1969[204] and was later developed extensively by Selvik and coworkers[205-207]. By the late 1980's, RSA had been used for investigating the effect of ACL injury on *in vivo* knee motion[208-210] and this method continues to be used to investigate knee kinematics[211-213]. RSA has been shown to have a repeatability better than 0.25 mm and 0.6°[203, 214] and has been used as a gold-standard for the validation of other measurement techniques[215, 216]. Despite its high accuracy, RSA requires the subject to remain in a small measurement volume, be exposed to radiation, and perform the activity slowly so quasistatic radiographs may be taken.

Instrumented spatial linkages, motion capture systems, and RSA have been used for several decades to investigate a variety of joint pathologies. However, each method has associated limitations and improved techniques are in continuous development. The optimal method of recording *in vivo* knee kinematics in 6 DOF would use non-contact measurements, allow the subjects to perform ADL in a normal setting, and have high accuracy. With this objective in mind, some investigators are developing markerless motion capture systems and algorithms to correct for skin movement[217, 218]. However, these methods still require the subject to wear specialized, tight fitting clothing, are technically demanding, and have not yet been validated.

While recently developed dynamic radiographic methods do not allow as flexible a testing environment as motion capture systems, errors from skin movement are overcome. For example, Banks has developed a system utilizing fluoroscopy for recording knee kinematics of total knee arthroplasty (TKA) patients[219-221]. Three dimensional computer-aided design models of the implanted components are fit to the two dimensional (2D) fluoroscopic images recorded during subject motion. Knee kinematics can be obtained with an accuracy of 1° for rotations, 0.2 mm for translations in the plane of the 2D image, and 2-3 mm for translations perpendicular to the image plane[219]. Komistek and coworkers have used a similar model-fitting approach with fluoroscopy to investigate knee kinematics of normal and ACL reconstructed subjects[222]. This system can record images at 30 Hz and provide kinematics in 6 DOF with an accuracy of 0.7° for rotations and 0.6 mm for translations in the plane of the image.

To allow translations to be measured accurately in the direction perpendicular to the image plane, Tashman and Anderst have developed a biplanar fluoroscopic system that uses implanted metal markers, similar to RSA. This system has been shown to record marker locations with an accuracy and precision of 0.1 mm and provide kinematics with an intertrial repeatability of 1.7° and 0.2 mm[223]. This method has recently been used for calculating knee kinematics and tibiofemoral joint space of normal and ACL reconstructed subjects at sampling rates of 250 Hz[224-226]. Knee kinematics have also been calculated with biplanar fluoroscopy by fitting 3D computer models of the femur and tibia to the fluoroscopic images but the errors of knee kinematics determined with this approach are up to 3.9° and 0.8 mm[227]. While the accuracy and sampling rate of biplanar fluoroscopy are impressive, this method is invasive and exposes the subject to radiation. Cine phase-contrast magnetic resonance imaging (MRI) overcomes these

limitations while recording bone positions with an accuracy on the order of a millimeter[228, 229]. However, this method requires the subject to repeatedly perform the same motion within a small measurement volume and may not be well suited for investigating ADL.

3.3.3 Kinematics of the Knee after ACL Injury

When choosing between the various methods of measuring pathologic joint motion, it is necessary to ensure that the equipment will have sufficient accuracy to resolve the anticipated differences in kinematics. Many investigators have quantified the effect of ACL injury on the kinematics of a relaxed knee. Bach and coworkers showed that the ATT of an ACL deficient knee is 3 to 5 mm greater than that of a normal knee during an instrumented clinical exam[115]. The ATT of a cadaveric knee increases up to 13 mm following ACL rupture in response to a 134 N anterior tibial load[54].

The effects of ACL rupture on knee kinematics during ADL are not well understood, however several recent studies have begun to elucidate these patterns. Tashman used a canine model to investigate dynamic knee stability during gait prior to and following ACL transection[223, 230]. Differences of ATT up to 10 mm were found even 2 years after injury. Other investigators have shown that ACL injury affects ITR in addition to ATT. During a step-up activity, Brandsson found differences up to 5° in ITR and 2 mm in ATT as a consequence of ACL rupture[212]. Zhang reported significant changes in ITR of 5° throughout the gait cycle and in ATT of 10 mm during swing phase[129].

While ACL reconstruction can often restore the ATT of the relaxed knee to normal, the effect of ACL reconstruction on *in vivo* knee kinematics is unclear. For example, Brandsson measured knee kinematics in 6 DOF during a step-up activity but found no significant differences for injured knees before and after reconstruction[211]. However, Tashman and Anderst reported mean differences of 4° in ITR and 3° in varus-valgus rotation for ACL reconstructed and normal contralateral knees following heel strike of downhill running[226].

These data demonstrate that a measurement system with accuracies of 2 mm and 3° might be adequate for showing how ACL injury effects knee motion. However, if kinematics with these magnitudes of error were used to estimate the *in situ* force of the ACL, unacceptably large errors would result. For example, 1 mm of error in knee translation could result in an incorrect estimation of the *in situ* force of the ACL of 250 N or over 10% of the ultimate load of the ligament[231]. Therefore, knee translations with accuracies of less than 1 mm will likely be required for reproducing knee kinematics to estimate the force of the ACL.

3.4 MOTION CAPTURE SYSTEMS

Motion capture systems are well suited for measuring knee kinematics during ADL because large measurement volumes are possible and subject motion is not restricted. These systems are also noninvasive, allowing studies to be conducted with large numbers of subjects. Therefore, motion capture systems may be useful for investigating the effect of ACL injury on knee kinematics in 6 DOF during ADL.

3.4.1 System Overview

Motion capture systems utilize multiple video cameras to determine the 3D locations of markers based on 2D camera views. The associated photogrammetric calculations were described by Abdel-Aziz and Karara in 1971 and called the direct linear transform (DLT)[232] although it is interesting to note that Das published a similar method in 1949[233]. Several alternatives and modifications to the basic DLT have been proposed[234-239] but for the purpose of this thesis, only a basic summary of the method is necessary.

A light ray can be thought of as following a straight line from marker M, through the image plane of the camera, to the perspective center of the lens P (Figure 6).

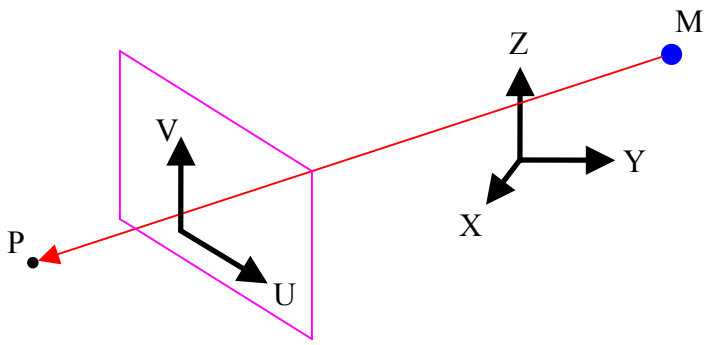

Figure 6: Marker locations in 3D object space and the 2D image plane

Using the DLT, the relationship between the location of the marker in 3D object space (X, Y, Z) and its projection on the recorded image (u,v) can be written in the form[232]:

$$u + \frac{L_1 X + L_2 Y + L_3 Z + L_4}{L_9 X + L_{10} Y + L_{11} Z + 1} = 0 \quad (15)$$

$$v + \frac{L_5 X + L_6 Y + L_7 Z + L_8}{L_9 X + L_{10} Y + L_{11} Z + 1} = 0 \quad (16)$$

where L_1 to L_{11} are parameters that characterize the camera set-up including location, orientation, and magnification. These parameters are determined by a calibration procedure that uses markers with known X, Y, Z locations in the object space. Subsequently, if a marker is simultaneously recorded by 2 cameras, Equations 15 and 16 can be written for both to give 4 equations with 3 unknowns (X,Y,Z). While only 2 cameras are mathematically required to determine the 3D location of markers, more cameras are often used to increase the redundancy of the system.

Motion capture systems can be classified as active or passive based upon the type of marker used. Active systems use markers such as light emitting diodes that generate light while passive systems use retroreflective markers that reflect light generated by lamps mounted adjacent to the cameras. Since several calibration parameters for a camera depend upon the recorded wavelength of light, monochromatic light, such as infrared or visible-red, is usually used[234].

Several methods can be used to determine the 2D locations of the markers in the camera images including fitting an ellipse to the markers or calculating the centroid of each marker[240]. While the latter method is computationally faster, fitting an ellipse to the marker images is more accurate when markers may be partially blocked from view, thus not providing a round image. Modern

motion capture systems have been reported to record marker locations with accuracies of 1/20 to 1/50 of a pixel if each marker covers 8-50 pixels for the ellipse method or 3-5 pixels for the centroid method[240].

Many investigators have attempted to quantify the accuracy of motion capture systems. A basic method of measuring joint angles uses one marker at the axis of the joint, a second proximal to the joint, and a third distal to the joint. Two vectors are defined, V_1 between the first and second marker and V_2 between the first and third marker, and the angle between the vectors is calculated. Therefore, several investigators have recorded known angles formed by 3 markers to assess the accuracy of motion capture systems[241-245]. These studies assessed the reliability of intermarker angles measured with a variety of 2 camera motion capture systems under both static and dynamic conditions. Both the accuracy and repeatability of angular measurements were generally under 0.5°.

Several investigators have also quantified the accuracy of motion capture systems by measuring the distance between 2 markers[242, 244, 246, 247]. Vander Linden and coworkers measured intermarker distances with a passive motion capture system and found mean errors of 0.9 to 4.5 mm and standard deviations of 1.4 to 3.0 mm[242]. Using another system, Haggard and Wing reported mean errors of 1.7 to 2.3 mm and standard deviation of 2.1 to 3.4 mm[246].

It is difficult to directly compare the accuracies of these 2 camera systems since the authors utilized somewhat different methods. However, several general conclusions can be made from these studies. First, the accuracy of intermarker angles and distances decreases as the plane

containing the markers is rotated away from the plane of the cameras[241, 243, 244]. Additionally, the error of motion capture systems can increase with the velocity of the subject[245] and wide angle lenses may introduce a systematic error that varies through the measurement field[244].

The Clinical Gait Analysis Forum of Japan recently held the 2002 Comparison Meeting of Motion Analysis Systems to assess the reliability of several commercial motion capture systems[248]. The cameras were set-up within a 7m x 7m area to record a subject during gait and there were no restrictions on the number of cameras. To investigate the reliability of intermarker angles, 3 markers were attached to an L-shaped frame to form a 90° angle while 2 markers were attached to a 900 mm rigid bar to determine the accuracy and repeatability of intermarker distances. Marker locations were recorded while the subject carried these objects throughout the measurement volume and the mean error and standard deviation of the angle and distance were calculated. There was a large variability between systems, with mean errors ranging from 0.2° and 0.4 mm to over 0.7° and 4.7 mm (Table 1). Since there were such large differences between system, the authors suggested that the reliability of all motion capture systems be determined using a similar protocol prior to clinical use.

Table 1: Error of intermarker angles and distances for motion capture systems[248]

System	Angle (°)		Distance (mm)	
	Mean	SD	Mean	SD
Eagle Digital	0.5	0.2	2.8	0.4
Frame-DIASII	0.7	0.5	3.6	3.8
Peak Motus	0.6	0.4	4.7	1.0
ProReflex	0.3	0.2	2.3	0.8
VICON	0.2	0.2	0.4	0.2

3.4.2 Marker Sets for Measuring Knee Motion

Knee kinematics can be calculated with motion capture systems using many different arrangements of markers or marker sets. While some investigators have developed custom marker sets for specialized applications, standardization is advantageous. The Helen Hayes and triad marker sets have been used for measuring knee motion by several investigators while the point cluster technique is a recently developed marker set that has seen much less widespread use. Each of these 3 marker sets will be explained in this section.

The Helen Hayes (HH) marker set was developed by Kadaba and coworkers in the late 1980s[249-251]. This method is sometimes referred to as a wand-based marker set because, in addition to markers placed over anatomical landmarks, markers are attached to the thigh and shank using short wands (Figure 7). The HH marker set allows hip, knee, and ankle joint rotations to be calculated in 3D and was described by its developers as "a simple marker system that can be easily implemented for routine clinical gait evaluations"[251].

Vaughan and coworkers developed a similar method to Kadaba's that used an additional marker on the foot[252]. This method has been thoroughly described in the literature and will be referred to as the Helen Hayes marker set for the purposes of this thesis. Markers are attached over the sacrum (SAC) and bilaterally over the anterior superior iliac spine (ASIS), mid-thigh on the femoral wand (FW), over the lateral femoral epicondyle (FE), mid-shank on the tibial wand (TW), over the lateral malleolus (LM), at the heel (HL), and over the head of the 4th metatarsal (MT) (Figure 7, Figure 8).

Figure 7: Lateral (left) and anterior (right) views of subject with Helen Hayes marker set

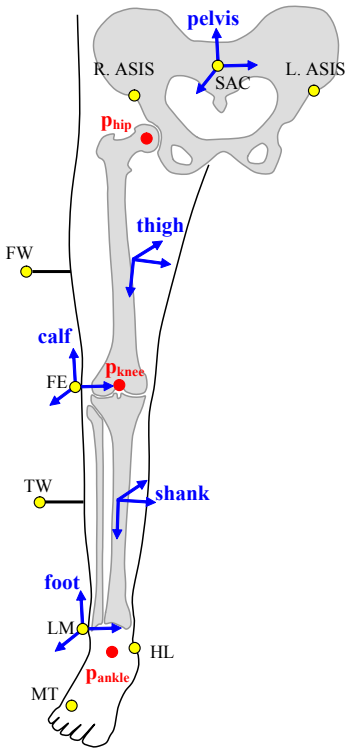

Figure 8: Marker locations and coordinate frames for the Helen Hayes marker set

Anatomical coordinate frames for the pelvis, calf, and foot can be defined using marker locations (Figure 8). Three non-colinear markers are required to construct each of these orthogonal coordinate frames. For example, the x and y-axes of the pelvis frame are located in a plane defined by markers over the sacrum, right ASIS, and left ASIS. The y-axis is parallel to the line between the right and left ASIS:

$$j_{pelvis} = \frac{L.ASIS - R.ASIS}{|\, L.ASIS - R.ASIS \,|} \tag{17}$$

while a second vector in the x-y plane can be defined between the right ASIS and the sacrum:

$$V_1 = R.ASIS - SAC \tag{18}$$

The z-axis, oriented in the proximal direction, is then:

$$k_{pelvis} = \frac{V_1 \times j_{pelvis}}{|\, V_1 \times j_{pelvis} \,|} \tag{19}$$

where "x" denotes the cross product of two vectors. Lastly, the x-axis in the anterior direction is:

$$i_{pelvis} = j_{pelvis} \times k_{pelvis} \tag{20}$$

The anatomic frame for the calf is obtained from marker locations of the lateral malleolus, tibial wand, and femoral epicondyle using similar calculations while the anatomic frame for the foot is defined from markers on the lateral malleolus, heel, and metatarsal head. The origins of the pelvis, calf, and foot frames are the sacrum, epicondyle, and malleolus markers, respectively.

The joint centers p_{hip}, p_{knee}, and p_{ankle} can be calculated using 2 methods. The first approach uses anthropometric measurements from the subject and morphological correlations to estimate the locations of joint centers with respect to anatomical frames. For example, the right hip joint center can then be estimated as[252]:

$$\begin{aligned} p_{hip} &= SAC + 0.598 \cdot (ASIS_{breadth}) \cdot i_{pelvis} \\ &- 0.344 \cdot (ASIS_{breadth}) \cdot j_{pelvis} \\ &+ 0.290 \cdot (ASIS_{breadth}) \cdot k_{pelvis} \end{aligned} \tag{21}$$

where $ASIS_{breadth}$ represents the distance between the right and left ASIS. The alternative method uses a functional approach to determine joint centers with respect to anatomical frames[253, 254].

The locations of the thigh and shank segment centers of mass can then be estimated:

$$p_{thigh} = p_{hip} + 0.39\left(p_{knee} - p_{hip}\right) \tag{22}$$

$$p_{shank} = p_{knee} + 0.42\left(p_{ankle} - p_{knee}\right) \tag{23}$$

These provide the origins of the thigh and shank coordinate frames. The orientations of these frames are determined using the joint centers and wand markers. For example, the axes of the thigh are:

$$j_{thigh} = \frac{p_{knee} - p_{hip}}{\| p_{knee} - p_{hip} \|} \tag{24}$$

$$V_2 = FW - p_{hip} \tag{25}$$

$$k_{thigh} = \frac{j_{thigh} \times V_2}{\| j_{thigh} \times V_2 \|} \tag{26}$$

$$i_{thigh} = j_{thigh} \times k_{thigh} \tag{27}$$

Similar calculations are performed to determine the orientation of the shank coordinate frame. The transformation between the thigh and shank frames may then be calculated and decomposed using Equations 9 - 11 to obtain knee rotations. The location of the knee joint is used to construct the coordinate frames of both the thigh and shank, implicitly assuming the knee is a ball and socket joint. The HH method is therefore unable to provide knee translations.

The most basic method of determining the position of a body segment in 6 DOF requires 3 points. While the HH method does use 3 markers attached to the pelvis, the thigh and shank segments do not have 3 unique markers and therefore joint translations cannot be determined. Several investigators have used an alternative marker set with triads or clusters of 3 markers on each segment to determine joint kinematics[255-260]. In theory, the positions of these markers are arbitrary with the exception that they must not be colinear (Figure 9).

Figure 9: Lateral view of subject with the triad marker set

A coordinate frame can be defined for each marker triad to define the location and orientation of the thigh and shank (Figure 10**).** The origin of these coordinate frames can be defined as the position of 1 of the 3 triad markers. The axes of these frames are determined such that one axis is perpendicular to the plane formed by the 3 markers, another connects 2 markers, and the third is mutually perpendicular to the first 2 (Equations similar to 17 - 20). This allows the transformations $[T_{gth}]$ and $[T_{gsh}]$ of the thigh and shank with respect to the global coordinate frame to be determined.

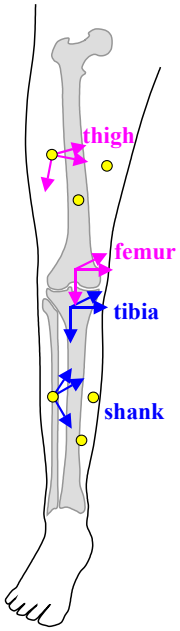

Figure 10: Marker locations and coordinate frames for the triad marker set

While the triad markers allow the positions of the thigh and shank to be determined, joint kinematics must be described in anatomical terms (Figure 4). Anatomical coordinate frames can be obtained by attaching markers over anatomical landmarks. For the purposes of this thesis, markers are placed at the medial and lateral femoral epicondyles (MC, LC) and on the proximal

and distal femur and tibia (FP, FD, TP, TD) with the subject supine and the knee fully extended. The anatomical axes for a right knee may be calculated as:

$$i_{femur} = \frac{MC - LC}{|MC - LC|} \tag{28}$$

$$V_3 = FD - FP \tag{29}$$

$$k_{femur} = \frac{i_{femur} \times V_3}{|i_{femur} \times V_3|} \tag{30}$$

$$j_{femur} = k_{femur} \times i_{femur} \tag{31}$$

$$j_{tibia} = \frac{TD - TP}{|TD - TP|} \tag{32}$$

$$k_{tibia} = i_{femur} \times j_{tibia} \tag{33}$$

$$i_{tibia} = j_{tibia} \times k_{tibia} \tag{34}$$

The origins of both the tibial and femoral coordinate frames are centered between the condyle markers in this reference position. This allows the transformations $[T_{gf}]$ and $[T_{gt}]$ of the femur and tibia with respect to the global coordinate frame to be determined.

The triad marker set is implemented by first determining the relationships between the anatomical coordinate frames and the triad frames. The triad markers and markers over anatomical landmarks are simultaneously recorded and the transformations $[T_{gth}]$, $[T_{gsh}]$, $[T_{gf}]$, and $[T_{gt}]$ are determined. This allows the fixed transformations of the femoral anatomy with respect to the thigh triad $[T_{thf}]$ and the tibial anatomy with respect to the shank triad $[T_{sht}]$ to be calculated. After this registration, the positions of the anatomical frames and the 6 DOF joint kinematics may be determined by measuring the locations of the triad markers.

The point cluster technique (PCT) is a recently described marker set that also allows knee kinematics to be measured in 6 DOF[261, 262]. This method was developed by Andriacchi and coworkers in the late 1990s and has been used by the same authors to investigate the effects of TKA[263] and ACL injury[264] on knee motion. Similarly to the triad marker set, the positions of the thigh and shank segments are measured using separate sets of markers. However, the PCT uses clusters of markers attached to each segment while the triad market set only uses 3 on each segment. For this thesis, 6 markers were used for the shank cluster while 9 markers were attached to the thigh (Figure 11).

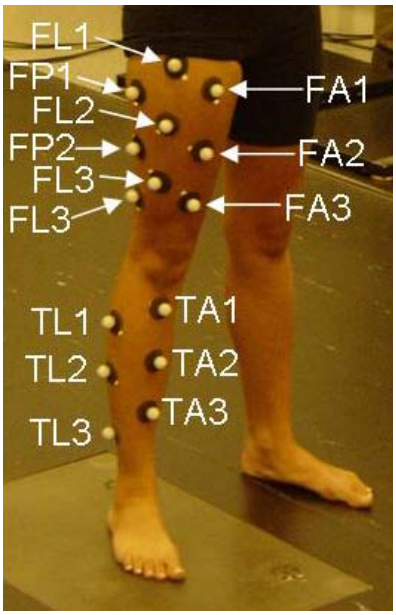

Figure 11: Anterolateral view of subject with point cluster technique marker set

The position of each cluster is defined as the center of mass of the cluster while the orientation is calculated as the principal axes (Figure 12). To determine these values, a weighting factor or "mass" must be assigned to each marker. For the basic PCT, unity masses are used for all markers. In general, the center of mass, C, of an n marker cluster is:

$$C = \frac{\sum_{i=1}^{n} Pg_i \cdot m_i}{\sum_{i=1}^{n} m_i} \tag{35}$$

where Pg_i is the location of marker i in the global coordinate frame and m_i is the mass of marker i. The global marker locations are then shifted to a coordinate frame located at the cluster center of mass to give marker locations Pg'_i

$$Pg'_i = Pg_i - C \tag{36}$$

This allows the inertia tensor, I, of the cluster to be calculated

$$I = \begin{bmatrix} \sum_{i=1}^{n}\left[\left(Pg'_{i,y}\right)^2 + \left(Pg'_{i,z}\right)^2\right]\cdot m_i & \sum_{i=1}^{n} Pg'_{i,y}\cdot Pg'_{i,x}(-m_i) & \sum_{i=1}^{n} Pg'_{i,z}\cdot Pg'_{i,x}(-m_i) \\ \sum_{i=1}^{n} Pg'_{i,x}\cdot Pg'_{i,y}(-m_i) & \sum_{i=1}^{n}\left[\left(Pg'_{i,x}\right)^2 + \left(Pg'_{i,z}\right)^2\right]\cdot m_i & \sum_{i=1}^{n} Pg'_{i,z}\cdot Pg'_{i,y}(-m_i) \\ \sum_{i=1}^{n} Pg'_{i,x}\cdot Pg'_{i,z}(-m_i) & \sum_{i=1}^{n} Pg'_{i,y}\cdot Pg'_{i,z}(-m_i) & \sum_{i=1}^{n}\left[\left(Pg'_{i,x}\right)^2 + \left(Pg'_{i,y}\right)^2\right]\cdot m_i \end{bmatrix} \tag{37}$$

Finally, the principal axes of the cluster are determined by calculating the eigenvectors of the inertia tensor, $\text{eigenvec}(I)_1$, $\text{eigenvec}(I)_2$, and $\text{eigenvec}(I)_3$. Therefore, the position of the cluster coordinate frame with respect to global can be described by the transformation matrix

$$T_{gc} = \begin{bmatrix} eigenvec(I)_{1,x} & eigenvec(I)_{2,x} & eigenvec(I)_{3,x} & C_x \\ eigenvec(I)_{1,y} & eigenvec(I)_{2,y} & eigenvec(I)_{3,y} & C_y \\ eigenvec(I)_{1,z} & eigenvec(I)_{2,z} & eigenvec(I)_{3,z} & C_z \\ 0 & 0 & 0 & 1 \end{bmatrix} \tag{38}$$

The PCT is implemented similarly to the triad marker set. First, markers for each cluster and markers over anatomical landmarks are simultaneously recorded in a reference position. This allow the transformations [T_{thf}] between the thigh cluster and the femoral anatomy and [T_{sht}] between the shank cluster and the tibial anatomy to be determined. Alternatively, these relationships may be determined using MRI with specialized MR opaque/retroreflective markers. During activity, only the locations of the cluster markers are measured, from which the positions of the anatomic frames are calculated using [T_{thf}] and [T_{sht}].

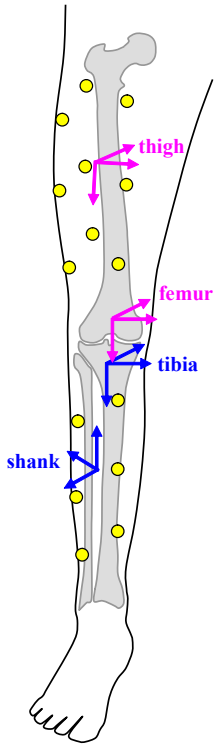

Figure 12: Marker locations and coordinate frames for point cluster technique marker set

3.4.3 Skin Movement

When Sutherland approached the Lockheed Aircraft Corporation in the late 1960's and presented his goal of recording skeletal joint kinematics using surface markers, the response was "you mean you would like to measure the movements of the skeleton from surface markers with skin movement confounding the interpretation. Is not that like trying to measure the movements of a broomstick within a gunny sack?"[198]. In 1978, Chao acknowledged that "accurate reconstruction of skeletal axes based on cinematographic data is extremely difficult because of the relative motion existing between the skin and bone"[258] and as recently as 2003 researchers such as Manal have concluded that "it is not feasible to routinely obtain sufficiently accurate estimates of detailed knee joint translations using superficial tracking target attachment methods"[265]. However, several investigators have attempted to characterize this skin movement to evaluate the resulting errors and ultimately allow correction methods to be developed.

Skin movement, also referred to as skin motion artifact, is the relative motion that occurs between surface markers attached to the skin and the underlying bone. Several factors contribute to skin movement including muscle contraction, vibration of soft tissue, and skin deforming as joints move. Cappozzo and coworkers investigated skin movement of surface markers by attaching markers to external fixation devices, allowing the true skeletal motion to be recorded, and additional markers directly to the leg[266]. Seven patients were included in this study, 2 with an external fixation device on the femur and 5 with a device on the tibia. Normal gait and cycling were investigated in addition to simple tasks of hip or knee joint flexion. The results showed that skin movement is related to the angle of adjacent joints regardless of the task. For example, a marker attached to the head of the fibula moved medially with knee flexion (Figure 13).

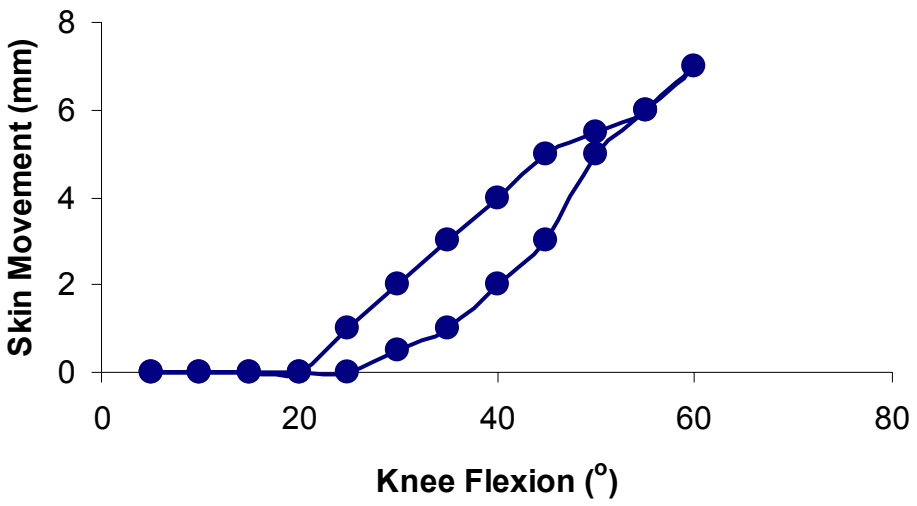

Figure 13: Skin movement in medial direction at fibular head (from Cappozzo, 1996[266])

The magnitude of skin movement varied considerably for different locations and ranged from 10 to 30 mm during gait. When all the activities were considered, skin movement was up to 40 mm for the lateral epicondyle, 30 mm for the greater trochanter, 25 mm for the head of the fibula, and 15 mm for the lateral malleolus. In general, markers attached to the thigh experienced larger skin movement than those on the shank. Markers near the hip had the largest movements while skin movement on the distal thigh was lower. Markers over the gastrocnemius on the posterior shank experienced much larger skin movement than those on the anterior shank. Cappozzo and coworkers concluded that surface markers should be located on the lateral portions of the thigh and shank and away from joints to minimize errors from skin movement.

More recently, Fantozzi, Stagni, and colleagues have assessed skin movement using both a motion capture system with surface markers and fluoroscopy during stair climbing and while rising from a chair[267, 268]. Markers on the shank experienced skin movement up to 30 mm while than those on the thigh moved up to 50 mm with respect to the skeleton. This skin movement resulted in average errors of knee rotations less than 30% for flexion-extension but up to 350% for varus-valgus rotation.

While much research has shown that skin movement is systematically related to joint rotations, others have investigated how inertial effects during rapid motion can cause skin movement. Tashman and Anderst measured marker locations while a subject landed from a one-legged hop and found that markers vibrated with a dominant frequency of 10-20 Hz[269]. Karlsson and Tranberg measured the resonant frequencies of markers attached to wands and found that markers vibrated at 20 to 50 Hz[270]. However, typical low-pass filters used for gait analysis have cut-off frequencies around 10 Hz and may reduce some of this error resulting from vibrations[271].

Several investigators have used motion capture systems to accurately record knee kinematics by attaching the markers directly to the skeleton using intracortical bone pins[183, 271-275]. While this approach avoids errors resulting from skin movement, problems have been reported with pins bending, loosening, and vibrating. Further, pin impingement with muscle can constrain the motion of the subject[276]. Despite the accuracy of this method, it is invasive and not suitable for studies with a large number of human subjects.

3.4.4 Methods to Improve Accuracy

Both skin movement and inaccuracies of motion capture systems can result in substantial errors of joint kinematics determined using surface markers. While these errors may be acceptable for some applications, many investigators have developed algorithms to improve accuracy. These techniques range from relatively simple methods that assume segments remain rigid during motion to complex optimizations that explicitly address systematic skin movement.

Mun noted that different kinematics can be calculated from the same experimental marker data with the triad marker set depending upon how the local coordinate frame is defined from the 3 markers[255]. As a result of skin movement and other experimental errors, using different markers as the origin of the local coordinate frame will result in different kinematics. Therefore, a method was proposed where the Euler angles describing the orientation of the body segment in the global coordinate frame were calculated separately using coordinate frames located at each of the 3 markers. By averaging the Euler angles, random errors could be reduced.

A least-squares method that also assumes that marker clusters are rigid was developed by Selvik for RSA and later modified by Spoor and Veldpaus[277] and others[259, 278, 279]. This technique utilizes clusters of at least 3 markers on each segment. The locations of the markers with respect to a local coordinate frame of the cluster are first determined with the subject in a reference position. Marker locations are then recorded while the subject performs an activity and the transformation matrix defining the position of the local cluster frame with respect to the global frame is calculated at each time step. This calculation is performed by minimizing the differences between the locations of the markers with respect to the local coordinate frame in the

reference position and the locations of the markers with respect to the local coordinate frame during activity. Holden and coworkers used this technique to record the position of the shank during gait but found errors up to 10 mm[280]. Manal and colleagues subsequently investigated several methods for attaching markers to the shank but even with the optimum arrangement, the calculated origin of the tibial anatomical coordinate frame had errors up to 14 mm during gait[265, 281]. While this method can reduce random errors in marker location and has become integrated into several software packages (e.g. Move3D, NIH, Bethesda, MD), errors resulting from systematic skin movement can remain large.

The least-squares method calculates the position of the thigh and shank separately and can result in large, non-physiologic knee translations being calculated. Lu and O'Connor developed a similar method using a least-squares minimization, however, the knee was modeled as a 3 DOF ball and socket joint, thus preventing translations[260]. To validate the method, marker locations were mathematically generated and skin movement of a sinusoidal form was added. Calculating knee kinematics with the basic triad marker set resulted in average knee translations of 32 mm. This value was improved to 7 mm using the least-squares method and to 0 mm, by definition, for the proposed method. Internal-external tibial rotation had the largest errors of the 3 knee rotations with an average error of 14° for the basic triad marker set, 5° after the least-squares minimization, and 3° after the proposed method. These results showed that large improvements in calculated knee rotations can be obtained using both the least-squares method and the proposed method that modeled the knee as a ball and socket joint. However, the assumption that knee translations can be neglected may not be appropriate for the study of ACL injury.

Several investigators have acknowledged that markers experience unequal amounts of skin movement and have attempted to reduce the effect of markers with large movements. Cheze and coworkers proposed using clusters of greater than 3 markers but calculating the position of the segment with the triad that experienced the least amount of skin movement[282]. Andriacchi and colleagues also developed a method for use with the PCT to lessen the effects of markers undergoing large skin movement[262]. Skin movement deforms the shape of the marker cluster and consequently changes the eigenvalues of the cluster inertia tensor. Therefore, the weighting values assigned to each marker were optimized such that changes in the eigenvalues were minimized. To investigate the efficacy of this method, marker locations were generated with simulated skin movement and the maximum error in the location of the anatomical coordinate frame was reduced from 35 mm to 10 mm with mass optimization.

The previous methods model the marker clusters as rigid bodies and assume that the locations of anatomical landmarks with respect to the clusters are constant. However, it has been shown that relative movement occurs between anatomical landmarks of the skeleton and surface markers. Further, Cappozzo has shown that this skin movement is not random but is instead systematically related to the positions of adjacent joints. In 1997, Cappello and coworkers devised a double-calibration method to specifically correct for non-rigidity of surface marker clusters[283]. The locations of anatomical landmarks with respect to the marker clusters were first determined with the subject at 2 positions. During activity, these locations were assumed to change linearly between the 2 positions. To demonstrate this method, the relationships between anatomical landmarks of the femur and a cluster of thigh markers were determined with the leg of a cyclist flexed and extended. The position of the femur during cycling was then determined by

measuring the position of the thigh cluster using rigid body calculations and interpolating the location of anatomical landmarks with respect to the cluster. Markers were also attached to an external fixation device to allow the true position of the femur to be determined. The double calibration method reduced the errors of the calculated femoral orientation and location from 5 to 4° and from 7 to 4.5 mm.

Lucchetti and coworkers proposed a similar method that assessed the skin movement of each subject, allowing marker locations subsequently recorded to be corrected for this error[284]. Rather than assuming that skin movement followed a linear trend between 2 positions, skin movement was quantified throughout the range of motion (ROM). With 4 markers attached to a rigid plate on the pelvis, 5 markers attached to the thigh, and 4 on the shank, the subject performed hip flexion-extension and abduction-adduction tasks with a hyperextended knee. During this activity, the shank markers were assumed to be unaffected by skin movement. The skin movement of the thigh markers could then be estimated as a function of hip rotation. In subsequent trials, a first estimation of hip rotation was determined, and then thigh marker locations were corrected for skin movement. This method was validated using 2 methods. First, 3 subjects repeated the hip ROM exercise with a hyperextended knee. The knee was assumed to be locked in this position such that all knee rotations and translations could be viewed as errors. Correcting for skin movement reduced the root mean square error from 1.1 - 5.0° to 0.4 – 3.0° and from 3 - 13 mm to 1 - 3 mm. The second validation method used a subject fitted with a 1 DOF knee arthroprosthesis. The axis of knee flexion-extension was defined to coincide with the axis of the prosthesis so all measured knee kinematics besides flexion represented error. During gait, errors were reduced to 2.5° and 3 - 4 mm. This method allowed skin movement to be conveniently

assessed and the accuracy of knee kinematics to be significantly improved for activities involving hip rotation, even without accounting for skin movement of the shank markers. However, during many ADL, not only the hip joint but also the knee and ankle joints undergo significant motion. The correlation of skin movement with combined rotations of all 3 major joints of the lower extremity may be necessary to further improve the accuracy of knee kinematics measured during ADL.

Alexander and Andriacchi developed a method called the interval deformation technique (IDT) for use with the PCT marker set that does not require the amount of skin movement to be known, only the pattern of the movement[285]. The IDT uses an optimization method to predict the skin movement of each marker such that the deformation of the cluster over the recorded interval of time may be explained. The recorded marker locations may then be corrected for skin movement to provide a more accurate estimate of the motion of the skeleton.

The IDT defines two local coordinate systems for each cluster, one that is constructed from the recorded marker locations and another that is embedded in the bone (Figure 14). In the reference position, these coordinate frames are coincident but during motion, these frames separate due to skin movement. While the basic PCT uses the recorded marker locations to calculate the positions of the cluster, the IDT estimates the position of the bone embedded frame.

To implement the IDT, the global locations, $Pg_i(t)$, of each marker i are recorded over time, t. This allows the position of the cluster in the global coordinate frame, $[T_{gc}]$, to be calculated using Equations 35 - 38. However, $[T_{gc}]$ does not represent the position of the bone embedded frame, $[T_{gb}]$, due to skin movement. The position of the bone embedded frame can be written as

$$T_{gb} = T_{gc} \cdot T_{bc}^{-1} \tag{39}$$

where $[T_{bc}]$ is the unknown position of the cluster with respect to the bone embedded frame. Therefore, if $[T_{bc}]$ can be determined, the position of the bone embedded frame may be calculated.

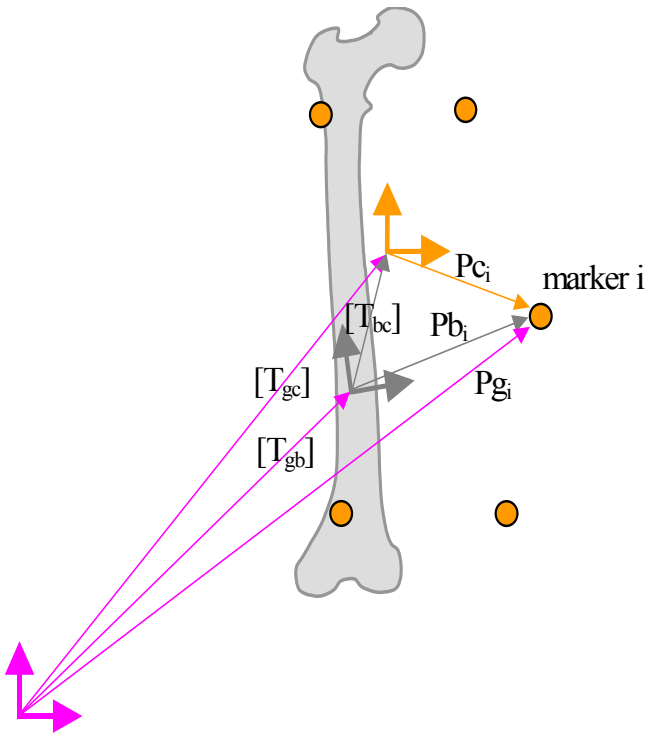

Figure 14: Coordinate frame definitions for the interval deformation technique

The relationship between the bone and cluster is determined by predicting the skin movement of each marker such that the changing shape of the cluster can be explained. Specifically, skin movement is estimated such that the changing location of each marker with respect to the cluster can be accounted for throughout the activity. The location of marker i in direction j with respect to the bone embedded frame is given by $Pb_{ij}(t)$ and is the sum of the marker location with respect to bone measured in the reference position, $Pb_{ij}(ref)$, and the unknown skin movement $\varepsilon_{ij}(t)$ during the activity.

$$Pb_{ij}(t) = Pb_{ij}(ref) + \varepsilon_{ij}(t) \tag{40}$$

The IDT uses an optimization approach to determine $\varepsilon_{ij}(t)$. For any predicted $\varepsilon_{ij}(t)$, the corresponding locations of the markers with respect to bone, $\hat{P}b_{ij}(t)$, can be determined using Equation 40. The position of the cluster with respect to the bone, $[T_{bc}(t)]$, can then be calculated by evaluating Equations 35 – 38 using $\hat{P}b_{ij}(t)$. The predicted locations of each marker with respect to the cluster may be calculated as

$$\begin{pmatrix} \hat{P}c_{ix}(t) \\ \hat{P}c_{iy}(t) \\ \hat{P}c_{iz}(t) \\ 1 \end{pmatrix} = \left[T_{bc}(t)\right]^{-1} \cdot \begin{pmatrix} \hat{P}b_{ix}(t) \\ \hat{P}b_{iy}(t) \\ \hat{P}b_{iz}(t) \\ 1 \end{pmatrix} \tag{41}$$

The optimized $\varepsilon_{ij}(t)$ minimizes an error function defined as the sum of the squared differences between the predicted, $\hat{P}c_{ij}(t)$, and measured, $Pc_{ij}(t)$, marker locations over all time frames t, for all N markers i, and in all 3 orthogonal directions j:

$$Error = \sum_{t=1}^{t_{\max}} \sum_{i=1}^{N} \sum_{j=1}^{3} (\hat{P}c_{ij}(t) - Pc_{ij}(t))^2 \tag{42}$$

The IDT requires that the functional form of skin movement, $\varepsilon_{ij}(t)$, is known. For simple tasks where the subject begins and ends in the same position, skin movement can be approximated as a Gaussian curve:

$$\varepsilon(t) = \delta \cdot e^{\frac{-1}{2}\left(\frac{t-\mu}{\sigma}\right)^2} \tag{43}$$

where δ is amplitude, μ is the mean time, and σ is the standard deviation. For example, if a subject performs knee flexion-extension at a constant angular velocity, the skin movement shown in Figure 13 can be estimated by a Gaussian function with an amplitude of 7 mm, a mean of 0.5 s, and a standard deviation of 0.2 s (Figure 15).

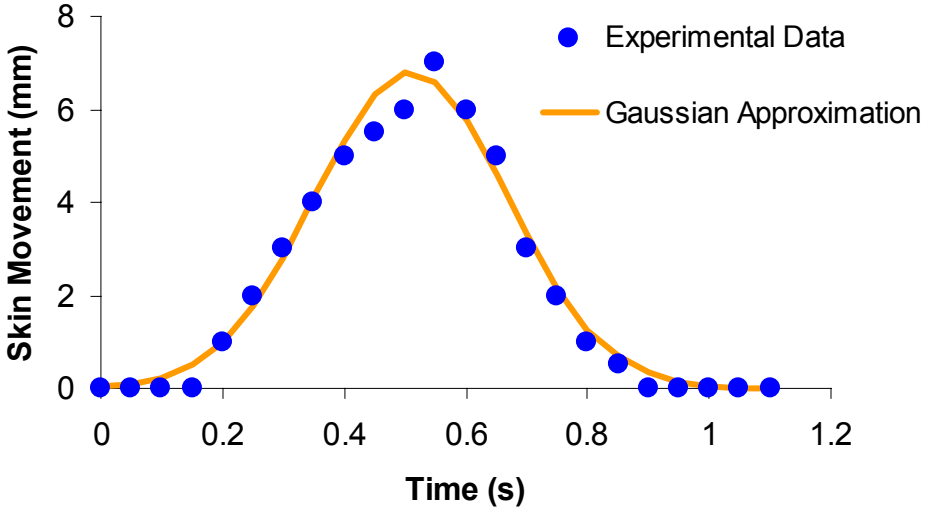

Figure 15: Gaussian approximation of skin movement

The IDT was mathematically validated by generating 50 trials of marker locations for an 8 marker cluster[285]. Seventy-two random values were generated to describe the skin movement of the markers using Gaussian functions. The cluster position was determined using both the least-squares rigid body method and the IDT. The mean errors of the cluster location and orientation were 71% and 81% lower for the IDT, respectively, compared to the rigid body method.

The IDT was also validated using a subject with an external fixation device on the tibia[285]. The position of the tibia was recorded using 4 markers attached directly to the fixation device and a cluster of 6 surface markers attached to the skin during a step-up activity. The maximum errors of the tibial location and orientation were about 7 mm and 7° when the least-squares rigid body method was used but only 3 mm and 4° after correction with the IDT.

Stagni and coworkers have recently investigated the efficacy of the IDT using 2 TKA patients[286]. Knee kinematics were simultaneously collected using fluoroscopy and surface markers during a step-up/down activity. The position of the femoral anatomical frame was calculated using the basic PCT, IDT with a Gaussian model of skin movement, IDT with a cubic polynomial model of skin movement, and the least-squares rigid body method. Mean errors of the femoral position were up to 10° and 2 mm for the basic PCT, 1° and 2 mm for the cubic IDT, and 8° and 5 mm for the least-squares method. The root mean square error of the location of the femur was 3.6 mm for the cubic IDT and 4.5 mm for the Gaussian IDT. While the IDT did provide decreased error compared to the least-squares method, the kinematics calculated with the IDT were highly dependent upon the functional form, $\varepsilon(t)$, used to model skin movement.

4.0 SPECIFIC AIMS

4.1 Aim 1

The first step of this research was to decide which marker set would be most useful for accurately measuring the knee kinematics of subjects with ACL injury. While all marker sets are susceptible to similar errors from the motion capture system and skin movement, propagation of this error affects the accuracy of the measured knee kinematics differently. Therefore, the first specific aim was to compare the effect of random errors in marker locations on the accuracy of knee kinematics measured with the Helen Hayes, triad, and point cluster technique marker sets.

4.2 Aim 2

To understand the accuracy of knee kinematics measured using surface markers, errors resulting from inaccuracies of the motion capture system must be understood. Therefore, the second specific aim was to evaluate the accuracy of a commercial motion capture system for measuring a) angles and distances formed between markers and b) joint kinematics with the point cluster technique marker set.

4.3 Aim 3

Skin movement is the largest source of error for knee kinematics measured using surface markers. However, the interval deformation technique has recently been developed to reduce these errors. Therefore, the third specific aim was to evaluate the efficacy of the interval deformation technique for correcting errors in knee kinematics caused by systematic skin movement.

5.0 AIM 1: MARKER SET COMPARISON

5.1 INTRODUCTION

Several marker sets can be used to record the motion of the knee. Since the objective of this thesis is to investigate the accuracy of knee kinematics, the first specific aim was to compare the errors in knee kinematics that result from inaccuracies in marker locations for the Helen Hayes, triad, and point cluster technique marker sets. These results were used to determine which marker set is least affected by skin movement and errors of the motion capture system. This analysis was performed by mathematically generating marker locations that corresponded to known knee kinematics. Random errors in marker locations were then added and the resulting knee kinematics were calculated. The resulting errors in kinematics were compared between marker sets.

5.2 METHODS

5.2.1 Subject Geometry

To generate marker locations, the relationship between the anatomical frames and the markers were required for each marker set. This geometry was obtained from the right extremity of a typical female subject (24 y, 1.7 m, 61 kg) using a protocol approved by the Institutional Review Board of the University of Pittsburgh.

For the Helen Hayes marker set, 9 retroreflective markers were attached to the subject and a motion capture system (VICON Motion Systems, Inc., Lake Forest, CA) was used to record the locations of the markers. The orientations of the femoral and tibial anatomic coordinate frames in the global system were then calculated using Equations 17 – 27 while the origins were taken as the knee joint center. The locations of the right and left ASIS, sacrum, femoral wand, and lateral epicondyle markers with respect to the femur and the tibial wand, lateral malleolus, heel, and metatarsal markers with respect to the tibia could then be determined.

A similar method was used for the PCT. Nine markers were attached to the subject for the thigh cluster and 6 for the shank cluster (Appendix B). Two additional markers were placed on the medial and lateral femoral epicondyles and the motion capture system was used to record marker locations. The transformation matrices describing the anatomic frames were obtained with Equations 28 – 34 using FA1 and FA3 as the proximal and distal femoral markers and TA1 and TA3 as the proximal and distal tibial markers, respectively. The locations of the thigh markers with respect to the femoral frame and the shank markers with respect to the tibial frame were then determined.

For the triad marker set, markers FA1, FA2, and FL2 were used as the thigh triad and markers TA2, TA3, and TL2 for the shank triad. Markers were also attached to the greater trochanter, medial and lateral epicondyles, and medial and lateral malleoli. Equations 28 – 34 were again used to calculate the anatomical coordinate frames with the greater trochanter as the proximal femoral point, the midpoint of the 2 malleoli markers as the distal tibial point, and the midpoint of the 2 epicondyle markers as the distal femoral and proximal tibial points. This allowed the locations of the 3 thigh triad markers and the 3 shank triad markers with respect to the femur and tibia, respectively, to be calculated.

5.2.2 Generating Marker Locations

Marker locations corresponding to known knee kinematics during a simple activity were mathematically generated (MATLAB, The MathWorks, Natick, MA). These skeletal kinematics were chosen to simulate an ACL reconstructed subject flexing the knee to perform a step-up activity and were estimated from a study using RSA performed by Brandsson and coworkers[211].

During this activity, flexion increased from 1 to 55° while kinematics in the other 5 DOF had a range up to 6° and 15 mm (Table 2). The simulated knee kinematics increased linearly in each DOF over the 55 frames of data (Figure 16).

Table 2: Simulated knee kinematics of a step-up activity

Knee Motion	Start	End
Flexion (°)	1	55
Valgus Rotation (°)	0	-1
Internal Tibial Rotation (°)	-4	2
Medial Tibial Translation (mm)	0	1
Anterior Tibial Translation (mm)	0	-15
Proximal Tibial Translation (mm)	1	7

The location of the femoral anatomic coordinate frame in the global system was first specified. The transformation matrix defining the relationship between the tibia and the femur was then calculated for each data frame using the specified skeletal kinematics. For the HH marker set, translations cannot be calculated so only knee rotations were modeled. However, complete 6 DOF knee motion was used to construct the transformation matrix between the femur and tibia for the triad and PCT marker sets. This allowed the position of the tibial frame in the global coordinate system to be obtained. The marker locations in the global frame could then be generated based on the subject geometry from Section 5.2.1.

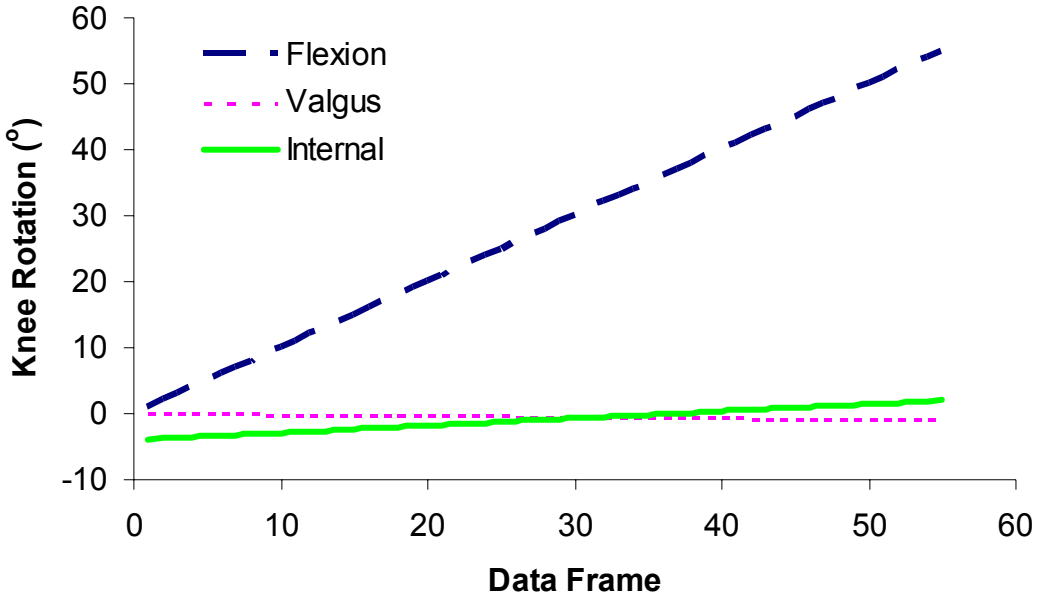

Figure 16: Skeletal knee kinematics changed linearly through the simulated activity

Random errors in marker locations were used to simulate both skin movement and inaccuracies of the motion capture system. Random errors were generated from uniform distributions between -5 and 5 mm, -10 and 10 mm, -15 and 15 mm, and -20 and 20 mm. These were added to the marker locations in each orthogonal direction for each data frame. Knee kinematics were then calculated from these marker locations to represent the kinematics that would be measured by a motion capture system. To validate this method, marker locations were generated with random errors of 0 mm and knee kinematics were calculated to verify that the measured and skeletal kinematics matched.

5.2.3 Data Analysis

Error was calculated in each DOF as the magnitude of the difference between the skeletal and the measured kinematics (Figure 17). A 2 factor analysis of variance was used to compare these errors in each DOF for 1) the different marker sets and 2) the different amounts of errors in marker locations (SuperANOVA, Abacus Concepts, Inc., Berkeley, CA). The mean kinematic errors were then compared for factors found to be significant using multiple contrasts. Statistical significance was set as $p < 0.05$.

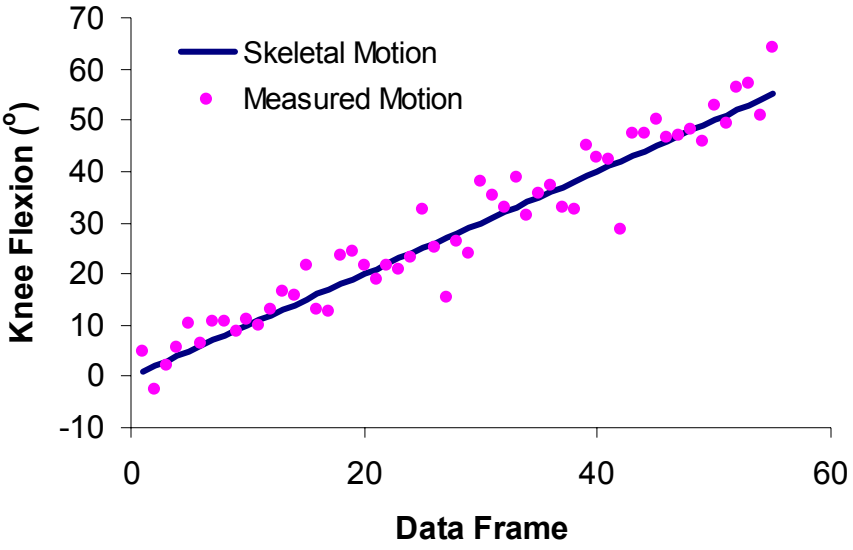

Figure 17: Skeletal flexion and flexion measured for random error in marker locations

5.3 RESULTS

The mean errors of measured knee rotations were 1 to 4° for the HH marker set, 2 to 12° for the triad marker set, and 1 to 6° for the PCT (Figure 18, Figure 19, Figure 20). For each marker set, rotational errors were similar in all 3 DOF. The error of knee rotations increased with the magnitude of error in marker locations for all 3 marker sets. For example, differences in the error of knee rotations were statistically significant between 5 and 20 mm of marker error for all marker sets and in all DOF ($p<0.05$). The errors of knee rotations calculated with the triad marker set were larger than those of both the HH and PCT marker sets ($p<0.05$). In most cases, the errors for the triad marker set were twice as large as the errors in knee rotations for the HH and PCT marker sets. No differences were found in the errors of knee flexion-extension or varus-valgus rotation between the HH and PCT marker sets ($p>0.05$). However, the errors of internal-external rotation were larger for the PCT than for the HH marker set ($p<0.05$).

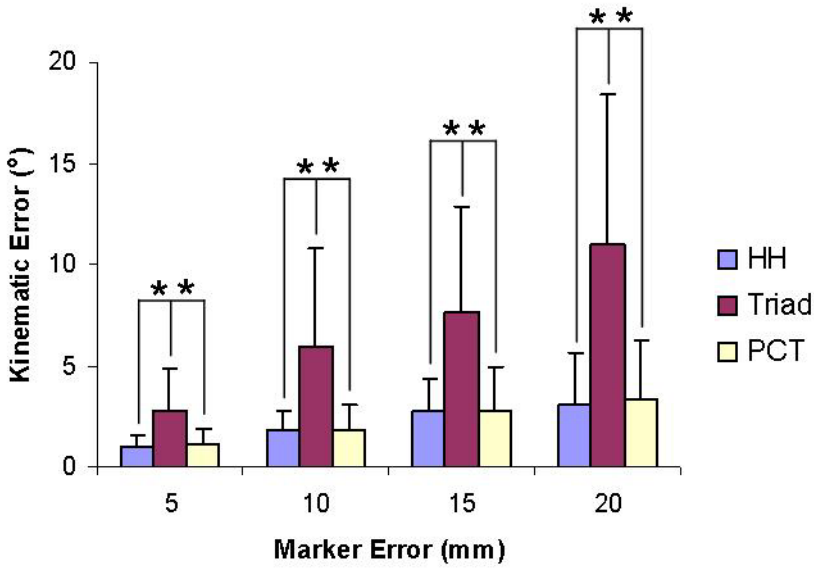

Figure 18: Error of knee flexion-extension measured with 3 marker sets, *p<0.05

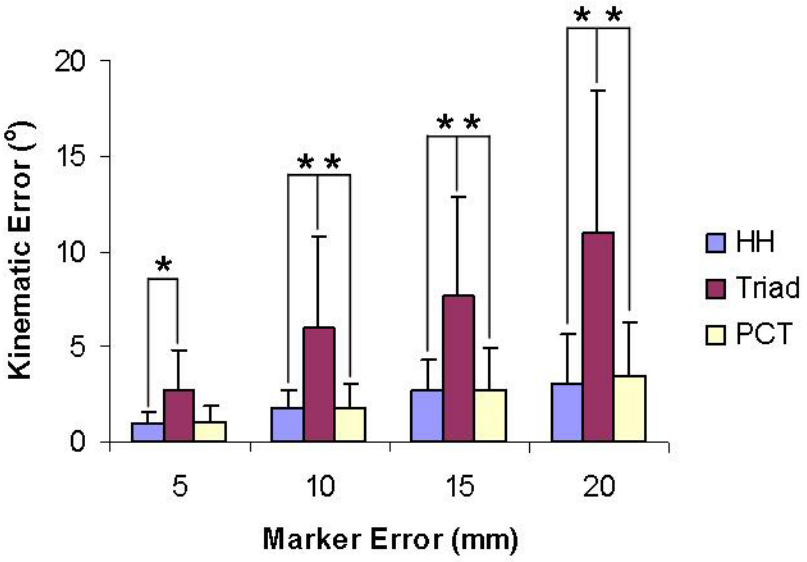

Figure 19: Error of varus-valgus knee rotation measured with 3 marker sets, *p<0.05

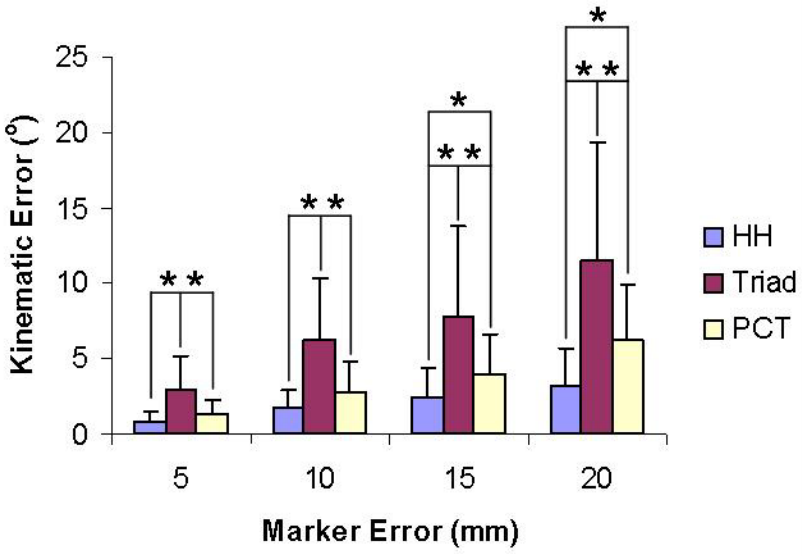

Figure 20: Error of internal-external tibial rotation measured with 3 marker sets, *p<0.05

The mean errors of measured knee translations were 5 to 35 mm for the triad marker set and 2 to 17 mm for the PCT (Figure 21, Figure 22, Figure 23). These errors increased with the magnitude of the errors in marker locations ($p<0.05$). In all but 2 of the 12 comparisons, the errors of knee translations were significantly smaller for the PCT compared to the triad marker set ($p<0.05$). The mean errors of knee translations were 46 to 69% lower for the PCT than for the triad marker set.

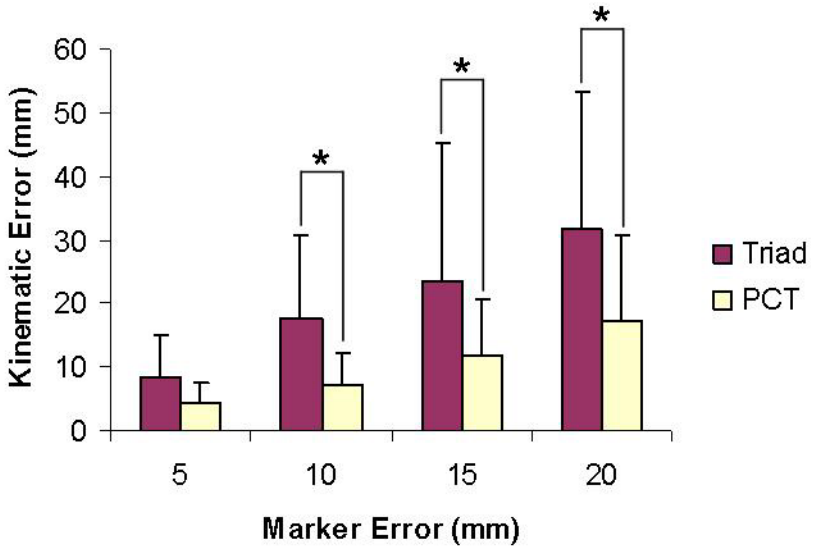

Figure 21: Error of medial-lateral tibial translation measured with 3 marker sets, *p<0.05

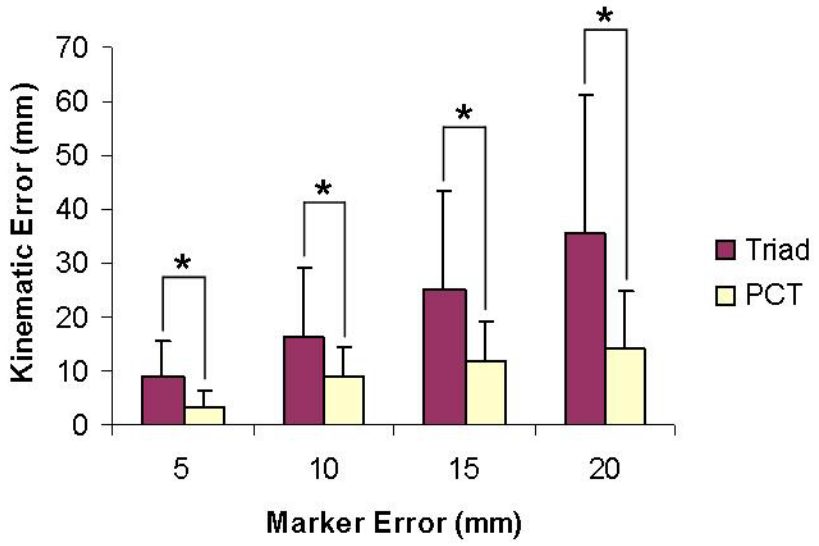

Figure 22: Error of anterior-posterior tibial translation measured with 3 marker sets, *p<0.05

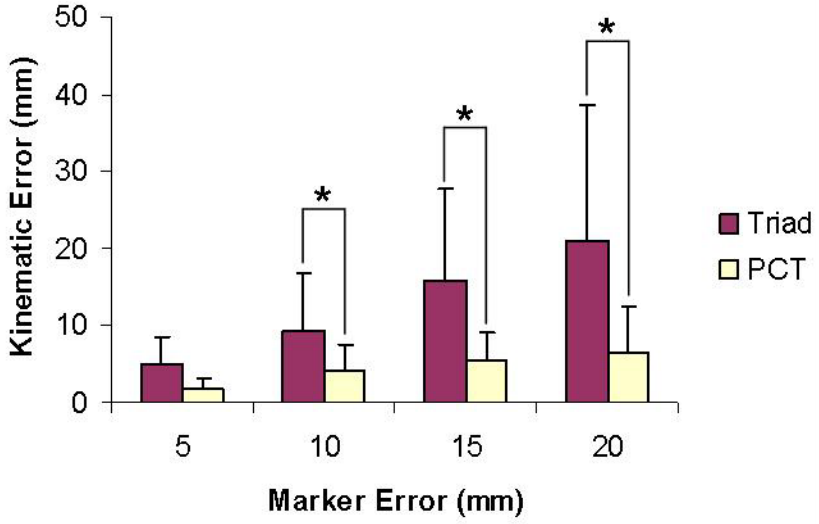

Figure 23: Error of proximal-distal tibial translation measured with 3 marker sets, *p<0.05

6.0 AIM 2: ACCURACY OF MOTION CAPTURE SYSTEM

6.1 INTRODUCTION

The PCT marker set was selected for further study based upon the results of the first aim. One source of error that contributes to errors of measured knee kinematics is inaccuracies of the motion capture system. The most common method for investigating the accuracy of these systems is measuring the distances between 2 markers or the angle formed by vectors between markers[241-247]. Studies utilizing these methods have shown large differences between systems[247] and it has been recommended that the reliability of each system be verified prior to clinical use[241]. Thus, the second specific aim of this thesis included examining the accuracy of a motion capture system for recording intermarker angles and distances. While these results would allow comparisons to be made with other motion capture systems, the errors of distances and angles measured between markers are difficult to interpret in a clinical context. Therefore, the accuracy of joint kinematics obtained using the PCT marker set were also determined. While many early studies using motion capture systems utilized 4 or less cameras, modern systems frequently use 6 or more. Therefore, motion capture configurations with 4 and 6 cameras were compared for this aim to determine if improved accuracy could be achieved by increasing the numbers of cameras. To investigate the reliability of the system, a model of a joint was constructed with rigidly attached markers. Intermarker angles and distances, in addition to 6 DOF joint kinematics, were measured using the motion capture system and compared to the actual values to determine error.

6.2 METHODS

6.2.1 Overview

A joint model was constructed by bolting 2 synthetic bones to a hinged base (Figure 24). Nine 19 mm diameter retroreflective markers (Peak Performance Technologies Inc., Centennial, CO) were rigidly attached to the femur to represent the thigh cluster and six were mounted to the tibia to simulate the shank cluster. Two additional markers were attached to the medial and lateral aspects of the femoral condyles. Plastic registration blocks were also fixed to the distal femur and proximal tibia. Brackets on the hinged base allowed the model to be fixed in 4 positions (Figure 25).

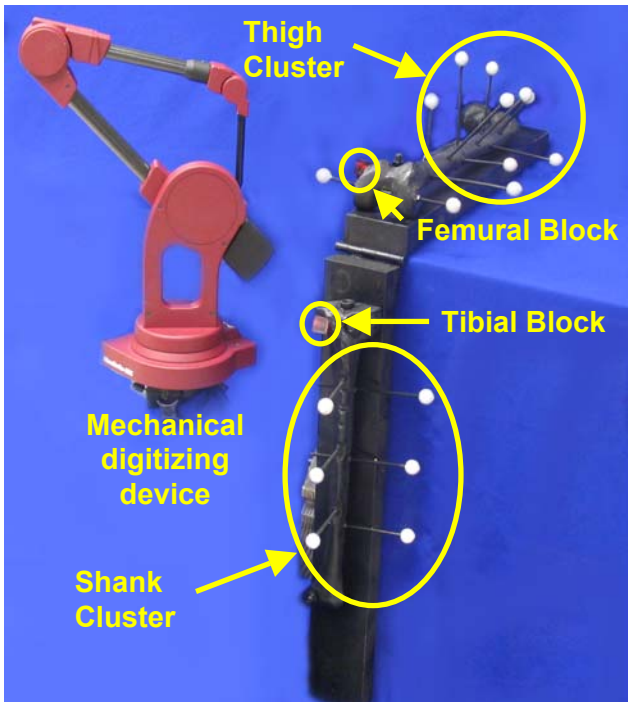

Figure 24: Joint model with reflective markers and registration blocks

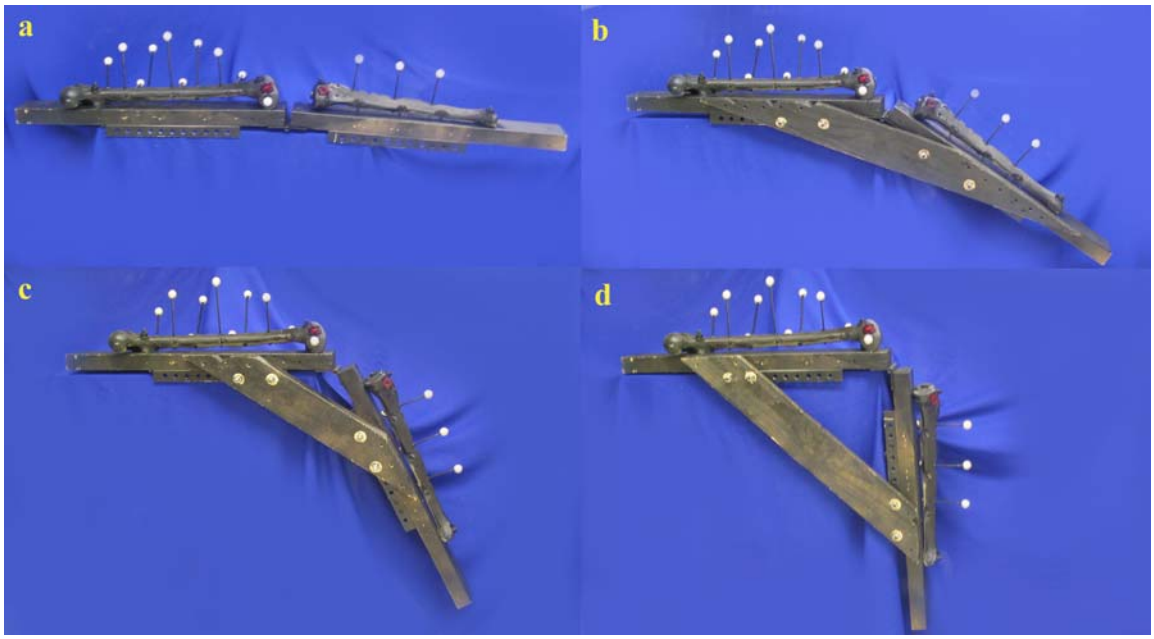

Figure 25: Knee model fixed in positions 1 to 4 (a-d, respectively)

The motion capture system was commercially obtained and utilized visible-red strobe lights (VICON 460 Datastation with M2 cameras, VICON Motion Systems, Inc., Lake Forest, CA). The reliability of 2 camera configurations were investigated: a 4 camera system and a 6 camera system. The latter system used cameras placed 1.6 to 2.3 m from the center of the measurement volume. These cameras were carefully arranged in an arc on the lateral side of the joint model such that each had an unobstructed view of all markers with the model in all 4 positions. The 4 camera system was obtained by disconnecting 2 cameras, leaving cameras placed 1.6 to 2.0 m from the center of the measurement volume.

Each trial began by calibrating the motion capture system using equipment supplied by the manufacturer. The mean calibration residual was recorded to quantify the quality of the calibration. The model was then placed in positions 1 to 4 in an order that was alternated between trials. At each position, the motion capture system was used to record the static marker locations for 4 s at 60 Hz. The first and last seconds of data were removed and the middle 2 s were used for analysis without being filtered. In each position, a mechanical digitizing device (Microscribe-3DX, Immersion Corp., San Jose, CA) was used to digitize 50 points on the surfaces of 3 orthogonal planes of both registration blocks. With the model at position 1, 20 points were digitized on the surface of markers FA1, FA3, TA1, and TA3 and also the markers over the medial and lateral condyles. This procedure of recording marker locations at each position and digitizing the model was repeated 20 times, alternating between the 4 and 6 camera configurations.

6.2.2 Intermarker Angles and Distances

The accuracy of intermarker angles and distances was investigated by defining 3 vectors between markers: V_1 between markers FA3 and FA1, V_2 between the lateral and medial condyle markers, and V_3 between markers TA1 and TA3 (Figure 26). The angle formed between V_1 and V_2 and the lengths of each vector were calculated for each data frame using the marker locations recorded by the motion capture system (MATLAB, The MathWorks, Natick, MA). The actual intermarker angle and distances for each trial were determined by fitting a sphere to the digitized marker locations obtained with the model in position 1[287].

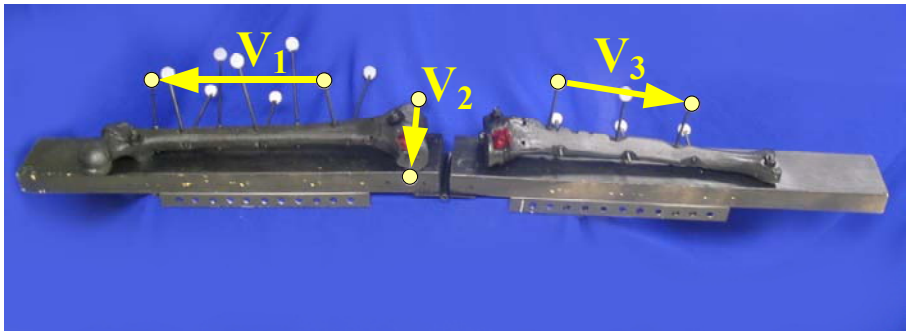

Figure 26: Vectors between markers to investigate accuracy of intermarker measurements

For each trial, the mean value and standard deviation of the 1 angle and 3 distances were calculated from the marker data for each position. Error was defined as the magnitude of the difference between the mean value recorded by the motion capture system and the actual value determined with the mechanical digitizing device. A 2 factor analysis of variance was used to compare error for the 2 camera configurations and the 4 joint positions (SuperANOVA, Abacus Concepts, Inc., Berkeley, CA). Multiple contrasts were performed to compare error for factors determined to be significant for $p < 0.05$.

6.2.3 Joint Kinematics

Joint kinematics are defined in 6 DOF by the relationship between 2 anatomic coordinate frames with origins near the joint. To allow the reliability of joint kinematics to be investigated, registration blocks were used to represent the anatomic coordinate frames (Figure 27). The actual positions of each block were measured directly using the mechanical digitizing device. Planes were fit to each set of 50 points[288] and coordinate frames were defined for the femoral and tibial blocks (Mathematica, Wolfram Research, Champaign, IL). The transformation describing the

position of the tibial block with respect to the femoral block was then calculated and decomposed to give the 3 Euler angles for an X-Y-Z rotation sequence (α, β, γ) and the 3 orthogonal translations (dx, dy, dz) (MathCAD, Mathsoft Engineering & Education, Inc. Cambridge, MA). These values were used to represent the actual joint rotations and translations, respectively.

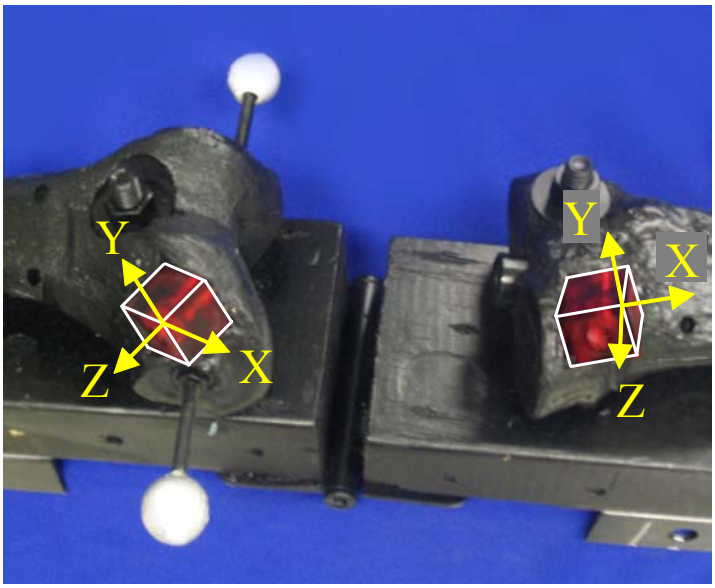

Figure 27: Registration blocks for calculating joint kinematics

To investigate the reliability of joint kinematics measured with the motion capture system, the block positions were also predicted from the recorded marker data. This required the transformations describing the positions of the femoral block with respect to the thigh cluster and the tibial block with respect to the shank cluster to be first determined. These fixed relationships between the clusters and blocks were obtained using the mechanical digitizing device. The joint model was fixed at position 1 and 20 points on the surface of each cluster marker were digitized. This allowed the position of the thigh and shank cluster coordinate frames to be obtained.

Without moving the joint model, 50 points on 3 orthogonal surfaces of each block were digitized to provide the positions of the block coordinate frames. The transformations describing the position of the femoral block with respect to the thigh cluster and the tibial block with respect to the shank cluster were then calculated and decomposed to 3 Euler angles and 3 translations (MathCAD, Mathsoft Engineering & Education, Inc. Cambridge, MA). This registration procedure was repeated 3 times and the average Euler angles and translations were calculated. The average transformation matrices were obtained using the average translations and orthogonal rotation matrices calculated using the averaged Euler angles.

Knowledge of the fixed relationships between the clusters and blocks allowed the positions of the registration blocks to be predicted from the recorded marker locations. This was performed by first determining the positions of the clusters from the recorded marker data, allowing the positions of the blocks to be predicted using the average cluster to block transformations from the registration. The 3 Euler angles and 3 orthogonal translations describing the position of the tibial block with respect to the femoral block were then calculated to provide the predicted joint kinematics. For each trial, the mean values and standard deviations of the predicted joint kinematics in each DOF were calculated from the marker data for each position (MATLAB, The MathWorks, Natick, MA). Error was defined as the magnitude of the difference between the mean value predicted from the motion capture system and the actual value determined with the mechanical digitizing device. A 2 factor analysis of variance was used to compare error for the 2 camera configurations and the 4 joint positions (SuperANOVA, Abacus Concepts, Inc., Berkeley, CA). Multiple contrasts were performed to compare error for factors determined to be significant for $p < 0.05$.

6.2.4 Reliability of Mechanical Digitizing Device

Three tests were performed to assess the reliability of the mechanical digitizing device. The first determined the accuracy and repeatability of the device for measuring known distances. Three small conical indentations were center drilled in a metal block along a single line using a milling machine (Enco, Chicago, IL) with an accuracy of 0.03 mm (Figure 28) These indentations were spaced at increments of 25.40 mm. The mechanical digitizing device was then used to record the locations of the indentations 6 times. The mean distances between the points were compared to the actual values to investigate accuracy while the standard deviations of the distances for the 6 trials were calculated to determine repeatability.

Figure 28: Three indentations used to assess accuracy of mechanical digitizing device

The repeatability of the device for measuring actual intermarker distances was also investigated. Two markers were attached to the ends of a 110 mm rigid bar. Twenty points were digitized on the surface of each marker, spheres were fit to the data to provide marker centers, and the intermarker distance was calculated. This procedure was repeated 5 times and the standard deviation of the distances were calculated.

The repeatability of the mechanical digitizing device for measuring actual joint kinematics was determined by digitizing each block 10 times with the model in each of the 4 positions. The 6 DOF joint kinematics were calculated and the standard deviations between the 10 trials were determined in each DOF.

6.2.5 Error Propagation from Cluster to Block Registrations

The accuracy of the predicted joint kinematics relies upon the correct registration of the clusters to the blocks. These transformations were calculated 3 times and averaged to predict the joint kinematics for the 20 trials, as previously explained. However, the Euler angles and translations for the cluster to block transformations ranged up to 1° and 1 mm between the 3 registrations. To investigate the amount of error in joint kinematics that could be attributed to this uncertainty in the registration, joint kinematics were calculated using cluster to block transformations with random errors of ± 0.5° and ± 0.5 mm for 1 of the 20 trials (MATLAB, The MathWorks, Natick, MA). This sensitivity analysis was repeated 1000 times and the average differences of the kinematics with and without the random registration error were determined in each DOF.

6.3 RESULTS

6.3.1 Intermarker Angles and Distances

The actual angle formed by V_1 and V_2 was 98.32 ± 0.09° (mean ± SD, n = 20). The mean errors of the motion capture system for measuring this angle ranged from 0.05 to 0.12° (Table 3). No significant differences were found between the different model positions while the 6 camera configuration more accurately measured this angle than the 4 camera configuration at position 3. However, the mean calibration residuals for the 4 and 6 camera configurations were 0.43 ± 0.06 mm and 0.42 ± 0.04 mm, respectively, suggesting similar calibration qualities. The maximum within trial standard deviation of the measured angle was 0.12°.

The actual intermarker distances for V_1, V_2, and V_3 measured with the digitizer were 217.9 ± 0.2 mm, 179.7 ± 0.2 mm, and 181.8 ± 0.2 mm, respectively (mean ± SD, n = 20). The mean errors of these distances measured by the motion capture system were 0.3 to 0.9 mm (Table 3). No significant differences were found for the different model positions or camera configurations. The within trial standard deviations of the measured distances were up to 0.6 mm but were generally less than 0.1 mm.

Table 3: Error of intermarker angle and lengths (mean±SD, n=10, *p<0.05 versus 4 cam.)

	Position 1		Position 2		Position 3		Position 4	
	4 cam.	6 cam.	4 cam.	6 cam.	4 cam.	6 cam.	4 cam.	6 cam.
$\Delta \angle V_1V_2$ (°)	0.08 ± 0.06	0.07 ± 0.07	0.08 ± 0.08	0.07 ± 0.05	0.12 ± 0.06	0.05 ± 0.05*	0.09 ± 0.06	0.07 ± 0.05
$\Delta \lvert V_1 \rvert$ (mm)	0.5 ± 0.3	0.5 ± 0.3	0.6 ± 0.3	0.6 ± 0.3	0.6 ± 0.3	0.6 ± 0.4	0.6 ± 0.3	0.6 ± 0.3
$\Delta \lvert V_2 \rvert$ (mm)	0.4 ± 0.3	0.5 ± 0.5	0.4 ± 0.3	0.5 ± 0.4	0.3 ± 0.3	0.5 ± 0.4	0.4 ± 0.3	0.6 ± 0.5
$\Delta \lvert V_3 \rvert$ (mm)	0.7 ± 0.3	0.8 ± 0.5	0.9 ± 0.3	0.9 ± 0.4	0.9 ± 0.3	0.9 ± 0.4	0.9 ± 0.3	0.7 ± 0.5

6.3.2 Joint Kinematics

The actual joint rotations determined by digitizing the registration blocks ranged from -6.9 ± 0.4°, 7.4 ± 0.4°, and 27.9 ± 0.4° for α, β, and γ respectively (mean ± SD, n = 20) at position 1 to -75.7 ± 0.5°, -43.9 ± 0.3°, and 86.4 ± 0.7° at position 4. The mean errors of the 4 camera motion capture system for predicting these rotations were 0.2 to 1.8° while those for the 6 camera configuration were 0.2 to 1.9° (Table 4). No significant differences were found between the 4 and 6 camera configurations ($p>0.05$). However, the error of joint rotations α and γ increased from position 1 to position 4 ($p<0.05$) (Figure 29).

Table 4: Error of joint kinematics (mean±SD, n=10, *p<0.05 versus position 1)

	Position 1		Position 2		Position 3		Position 4	
	4 cam.	6 cam.	4 cam.	6 cam.	4 cam.	6 cam.	4 cam.	6 cam.
Δ α (°)	0.4 ± 0.2	0.2 ± 0.2	0.3 ± 0.2	0.2 ± 0.1	0.6 ± 0.5	0.7 ± 0.2*	1.0 ± 0.5*	1.1 ± 0.5*
Δ β (°)	0.4 ± 0.3	0.6 ± 0.4	0.4 ± 0.3	0.4 ± 0.2	0.5 ± 0.3	0.5 ± 0.3	0.2 ± 0.2	0.4 ± 0.3
Δ γ (°)	0.4 ± 0.3	0.5 ± 0.3	0.7 ± 0.3	0.7 ± 0.4	1.2 ± 0.8*	1.5 ± 0.4*	1.8 ± 0.7*	1.9 ± 0.9*
Δ dx (mm)	1.4 ± 0.7	1.4 ± 0.7	0.8 ± 0.6	1.3 ± 1.0	2.0 ± 1.2	2.2 ± 0.9	1.4 ± 1.6	2.5 ± 1.7*
Δ dy (mm)	0.8 ± 0.5	1.0 ± 0.7	1.3 ± 0.7	0.6 ± 0.5	1.5 ± 0.6*	1.5 ± 0.7	2.6 ± 0.9*	2.8 ± 1.1*
Δ dz (mm)	2.0 ± 0.5	1.9 ± 0.5	2.0 ± 0.6	2.7 ± 0.6*	1.8 ± 0.8	1.7 ± 0.8	1.9 ± 0.7	1.8 ± 0.7

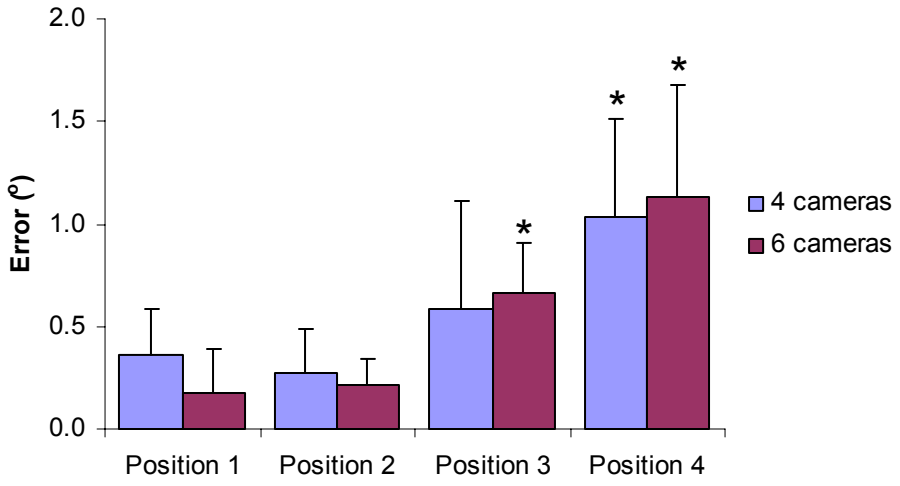

Figure 29: Error of joint rotation α (mean±SD, n=10, *p<0.05 compared to position 1)

The actual joint translations determined by digitizing the registration blocks ranged from 91.9 ± 0.5 mm, -37.4 ± 0.7 mm, and -77.7 ± 0.7 mm for dx, dy, and dz respectively (mean ± SD, n = 20) at position 1 to 53.8 ± 1.6 mm, -208.7 ± 0.4 mm, and -86.3 ± 0.7 mm at position 4. The mean errors of the 4 camera motion capture system for predicting these translations were 0.8 to 2.6 mm while those for the 6 camera configuration were 0.6 to 2.8 mm (Table 4). Similarly to the errors of joint rotations, no significant differences were found between the 4 and 6 camera configurations ($p>0.05$). However, the error of joint translations dx and dy increased from position 1 to position 4 ($p<0.05$)

6.3.3 Reliability of Mechanical Digitizing Device

The mean errors of 25.40 mm distances measured by digitizing individual points were 0.04 and 0.02 mm while the standard deviations of these distances were 0.13 and 0.15 mm, respectively. The device measured a 50.80 mm distance with a mean error of 0.06 mm and a standard deviation of 0.19 mm. The distance between 2 markers that was measured by digitizing 20 points on each marker had a smaller standard deviation of 0.06 mm.

The repeatability of the mechanical digitizing device for measuring actual joint kinematics was found to depend upon the position of the model. In position 1, the standard deviation of the Euler angles were 0.1 to 0.2°. However, in position 4, these standard deviations increased to 0.3 to 0.6°. The standard deviations of the measured locations of the tibial block with respect to the femoral block showed a similar trend; the standard deviations were 0.2 to 0.4 mm in position 1 while in position 4, the standard deviations were 0.3 to 0.8 mm.

6.3.4 Error Propagation from Cluster to Block Registrations

Introducing random errors of ± 0.5° and ± 0.5 mm into the cluster to block transformations also resulted in errors in predicted joint kinematics that increased from position 1 to position 4. The average errors of joint kinematics from uncertainty in the registration procedure were 0.3° and 0.5 mm at position 1 (Table 5). At position 4, these errors increased to 0.4° and 0.8 mm.

Table 5: Average error of predicted joint kinematics resulting from registration error

	Position 1	Position 2	Position 3	Position 4
Error of Rotations (°)	0.3	0.3	0.4	0.4
Error of Translations (mm)	0.5	0.6	0.7	0.8

7.0 AIM 3: EFFICACY OF INTERVAL DEFORMATION TECHNIQUE

7.1 INTRODUCTION

Skin movement is considered the main source of error for measuring human motion using surface markers[266], however, these errors may be reduced using various algorithms. The interval deformation technique (IDT) has recently been developed by Alexander and Andriacchi for improving the accuracy of knee kinematics calculated with the point cluster technique (PCT) marker set[285]. This method assumes that skin movement is systematic and can be mathematically modeled. The IDT uses optimization algorithms to determine the parameters describing skin movement thus allowing the true skeletal kinematics to be estimated.

The IDT method was validated by Alexander and Andriacchi using 2 methods. First, marker locations were mathematically generated for a single cluster. Skin movement following a Gaussian function with randomly generated parameters (amplitude, mean, SD) was then added and the IDT was used to calculate the cluster position. The second method investigated the accuracy of the position of the tibia determined with the IDT while a human subject performed a step-up activity. For both methods, the IDT reduced the errors of the calculated bone orientation and location by 70 to 80% compared to a method that assumed the clusters were rigid.

While Alexander and Andriacchi showed that significantly improved estimates of segmental positions can be obtained using the IDT, the overall errors in knee kinematics were not reported. Therefore, the third specific aim of this thesis was to determine the efficacy of the IDT for reducing errors of knee kinematics that result from systematic skin movement of the shank cluster. This was conducted for three types of skin movement that followed a Gaussian function over time. The first case used randomly chosen parameters to model skin movement during knee flexion-extension. The second case used parameters chosen to simulate muscle contraction during the stance phase of gait. Lastly, skin movement resulting from heel strike of gait was modeled. The efficacy of the IDT for correcting for these 3 types of skin movement was assessed by mathematically generating marker locations corresponding to known parameterized skin movement and then using the IDT to optimize the parameters.

7.2 METHODS

7.2.1 Generating Marker Locations

The relationships between the anatomic coordinate frames and the cluster markers were required to generate marker locations simulating knee motion. This geometry was obtained from the right extremity of a typical female subject (21 y, 1.7 m, 54 kg) using a protocol approved by the Institutional Review Board of the University of Pittsburgh. Nine markers were attached to the subject for the thigh cluster and 6 for the shank cluster (Appendix B). Two additional markers were placed on the medial and lateral femoral epicondyles and a motion capture system (Peak Performance Technologies Inc., Centennial, CO) was used to record marker locations while the

subject was supine. A single frame of data was selected to define marker locations in the reference position (Figure 30). The transformation matrices describing the global positions of the anatomic frames were obtained with Equations 28 – 34 using FA1 and FA3 as the proximal and distal femoral markers and TA1 and TA3 as the proximal and distal tibial markers, respectively. The positions of both cluster coordinate frames were calculated using Equations 35 - 38. The transformation matrices describing the position of the thigh cluster with respect to the femoral anatomy and the shank cluster with respect to the tibial anatomy were then calculated. Additionally, the locations of the femoral markers with respect to the thigh cluster and the tibial markers with respect to the shank cluster were determined ($Pb_{ij}(ref)$)

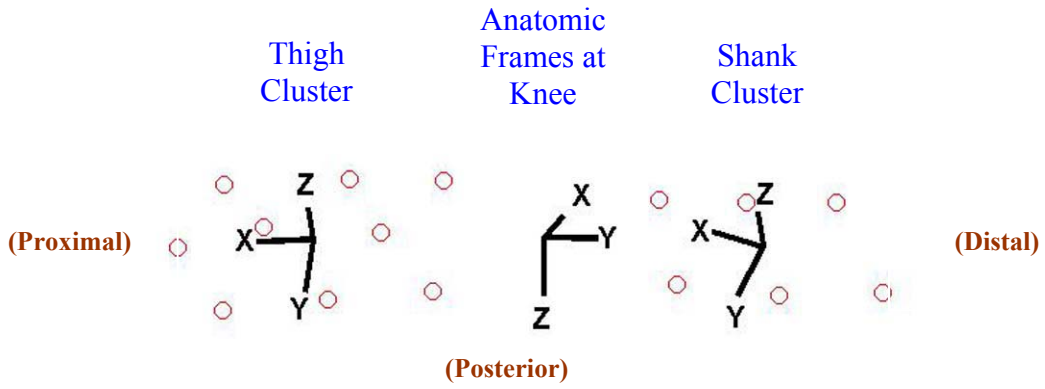

Figure 30: Marker locations with the knee fully extended in the reference position

Marker locations were then generated to simulate 3 types of knee motion (MATLAB, The MathWorks, Natick, MA). For case 1, 30 frames of data were used to model knee flexion-extension. Knee flexion increased linearly from 0 to 90° over the first 15 data frames and then decreased linearly to 0° over the last 15 data frames. The knee translations and also varus-valgus and internal-external tibial rotations were specified to be zero for all 30 data frames. The positions of the femoral anatomic frame over time were arbitrarily assumed to be constant and aligned with the global axes, such that the long axis of the femur was horizontal. The position of the tibial anatomic frame was determined for each data frame using the specified knee kinematics. The positions of both cluster coordinate systems could then be calculated based on the geometry of the subject in the reference position. Finally, the locations of each cluster marker in the global coordinate frame, $Pg_{ij}(t)$, were determined using the relationships between the cluster frames and the markers, $Pb_{ij}(ref)$, measured with the subject in the reference position.

Knee kinematics during the stance phase of gait were modeled for cases 2 and 3. The first 60% of the stance phase was simulated for case 2. Knee flexion increased linearly from 0 to 20° over the first 15 data frames and then decreased linearly to 0° at frame 30. This simulated a normal subject walking at 1.2 m/s recorded with a motion capture system at 60 Hz[183]. The knee translations and also varus-valgus and internal-external tibial rotations were specified to be zero for all 30 data frames. For case 3, the first 30% of stance phase was simulated. Knee flexion increased linearly from 0 to 20° over 15 data frames while the knee translations and also varus-valgus and internal-external tibial rotations were zero. The previously described methods were used to generate marker locations corresponding to these motions of the knee.

Marker locations were then generated to simulate the same 3 activities but including skin movement of the shank markers. This was performed by adding parameterized movement to the location of each tibial marker with respect to the shank cluster coordinate frames in the reference position (Equation 40) and recalculating the locations of the markers in the global coordinate frame. The parameterized skin movement, $\varepsilon_{ij}(t)$, was modeled by a Gaussian curve (Equation 43). Values for the amplitude, mean, and standard deviation were required to specify the skin movement for each of the 6 tibial markers in each orthogonal direction. Therefore, 54 parameters were necessary to completely describe the skin movement of the tibial markers for each activity.

For the first case, random values for the amplitude, mean and standard deviation were generated, similarly to the methods used by Alexander and Andriacchi[285]. Each of the 18 amplitude parameters were randomly chosen from a uniform distribution between -20 and 20 mm. Values for the mean and standard deviation were similarly chosen from ranges of 8 to 22 frames and 2 to 5 frames, respectively. The amount of skin movement, $\varepsilon_{ij}(t)$, for each marker i in each direction j with respect to the cluster could then be determined by evaluating Equation 44 for each of the 30 data frames. The locations of each marker in the global coordinate frame, $Pg_{ij}(t)$, were then calculated. This procedure of choosing random parameters and generating marker locations was repeated to generate 5 sets of marker data.

The second case that was considered used parameters selected to simulate skin movement of the shank resulting from muscle contraction during the stance phase of gait. Cappozzo and coworkers showed that a marker located on the anterior shank displaced anteriorly about 10 mm with respect to the tibia during the early stance phase of gait while skin movement in the proximal-distal and medial-lateral directions were small[266]. Contraction of the tibialis anterior, which has been shown to be activated in the early stance phase of gait[289], likely contributed to this skin movement. These observations were used to estimate reasonable ranges for the parameters describing skin movement for the anterior tibial markers (TA1, TA2, TA3). To model skin movement in the anterior direction during the beginning of stance phase, amplitudes in the y direction (posterolateral, Figure 30) were randomly chosen from a uniform distribution between -7 and -10 mm while amplitudes in the z direction (anterolateral) were between 7 and 10 mm. Amplitudes in the x direction (proximal) were -3 to +3 mm. The mean for the anterior shank markers in all directions were between 1 and 10 frames to correspond to tibialis anterior contraction and the standard deviations were 2 to 5 frames. The lateral tibial markers (TL1, TL2, TL3) are located over the anterior border of the lateral head of the gastrocnemius. This muscle contracts in mid and late stance phase of gait[289]. Surface markers placed on the lateral shank were observed to displace laterally with respect to the tibia during isometric gastrocnemius contraction. This skin movement was modeled by randomly generating amplitudes between 7 and 10 mm in the y and z directions and -3 to +3 mm in the x direction. The means were between 20 and 30 frames to correspond to the time periods of gastrocnemius contraction and the standard deviations were 2 to 5 frames. This procedure was repeated to generate 5 sets of marker data.

For case 3, skin movement resulting from impact of the foot at heel strike was simulated. Tashman and Anderst have shown that surface markers displace about 20 mm in the proximal-distal direction with respect to the skeleton within 0.1 s of landing from a hopping activity[269]. To model skin movement of the tibial markers at heel strike of gait, the amplitudes for all 6 markers in the x direction (proximal, Figure 30) were randomly chosen between -10 and -20 mm. The amplitudes in the y and z directions were -3 to 3 mm. To simulate this high frequency skin movement shortly after heel strike, the mean for all directions were 1 to 4 frames and the standard deviations were 1 to 2 frames. Five separate sets of data were generated using different parameters, randomly determined from these ranges.

7.2.2 Optimization

The efficacy of the IDT was then assessed using a custom program to optimize the parameters characterizing the skin movement of the shank and correct the calculated knee kinematics (MATLAB, The MathWorks, Natick, MA) (Appendix C). A simulated annealing method was used for this numerical optimization[290]. This algorithm generated initial guesses for each of the 54 parameters and then added random perturbations to the predicted parameters until the differences between the predicted and measured locations of the tibial markers with respect to the shank cluster were minimized (Equation 43). The inputs to this program were the marker locations during activity and the outputs were the kinematics calculated with and without the IDT (Appendix D).

The error function (Equation 42) was first evaluated for all $\varepsilon_{ij}(t) = 0$. This provided an indication of how much the shank cluster deformed during the activity compared to the cluster shape in the reference position. The initial guesses for each parameter were determined by fitting Gaussian curves to the differences between the measured locations of each marker with respect to the cluster coordinate frame during activity, ($Pc_{ij}(t)$), and the reference location of the same marker, ($Pb_{ij}(ref)$), in the j direction. The error function was then evaluated using the initial guesses.

To begin the optimization, the optimized parameters were set equal to the initial guesses. A random perturbation was then added to one of the 54 optimized parameter values. The magnitudes of the perturbations were specified as were constraints on the parameter values . The error function was then evaluated with the perturbed parameter value and the 53 other optimized parameter values. If the error decreased compared to the previous value for the optimized parameters, the new parameter value was accepted and replaced the previous optimized value for that parameter. However, if the error increased, the probability of the parameter value being accepted depended upon a value called "temperature". The probability, p, of the perturbed parameter being accepted was

$$p = e^{\frac{-\Delta E}{T}} \tag{44}$$

where ΔE is the change in the error function compared to error for the optimized parameter values and T is temperature. A random number between 0 and 1 was then generated and if this value was smaller than p, the new parameter was accepted. However, if the random number was greater than p, the perturbed parameter value was rejected. This process of generating a random perturbation to a parameter and deciding to accept or reject the value was sequentially repeated for each of the 54 parameters.

At high temperatures, many parameter values would be accepted despite large increases of the value of the error function. However, at low temperatures, the probability that parameter values that increased the error would be accepted decreased. Therefore, random perturbations were first generated at high temperatures and then the temperature was slowly decreased so fewer unfavorable perturbations would be accepted. For this study, the temperature was decreased linearly to 30% of the initial value over 500 temperature steps. At each temperature step, perturbations to each of the 54 parameters were made.

It has been shown that rather than simply decreasing temperature from a maximum to a minimum value, periodically increasing the temperature can be advantageous[290]. Therefore, after the temperature was decreased to 30% of the initial value over 500 steps, it was increased back to 80% and the procedure was repeated. This was performed 50 times (Figure 31). Therefore, perturbations were made to each of the 54 parameters at 25,000 temperatures.

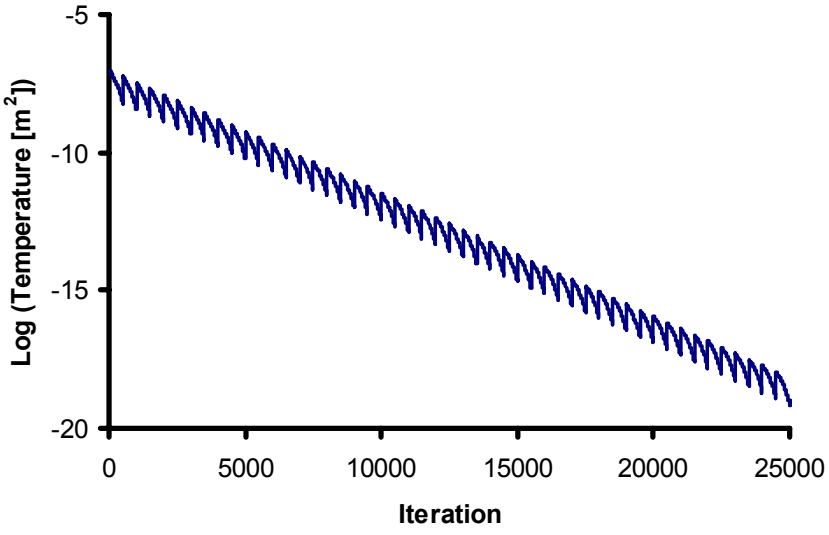

Figure 31: Typical temperature decreases for amplitude parameters

The parameter values were constrained to remain with specified ranges. For all 3 cases, the amplitude parameters were limited to the range between -20 and 20 mm. The ranges for the mean parameters were 1 to 30 frames for cases 1 and 2 and 1 to 15 frames for case 3. The standard deviation parameters were specified to remain between 2 and 5 frames for cases 1 and 2 and between 1 and 2 frames for case 3.

The magnitude of the parameter perturbations were decreased through the optimization. For the first 500 iterations, the perturbation magnitudes were half the range of the parameter constraints. For example, the perturbation magnitudes for cases 1 and 2 over the first 500 iterations were ± 20 mm, ± 14.5 frames, and ± 1.5 frames for the amplitude, mean, and standard deviation parameters, respectively. Every 500 iterations, these perturbation magnitudes were decreased by 5%, 3%, and 1%, respectively (Figure 32). For the final 500 iterations of the optimization, the perturbation magnitudes for the amplitude, mean, and standard deviation parameters had decreased to ± 2 mm, ± 2 frames, and ± 1 frame, respectively.

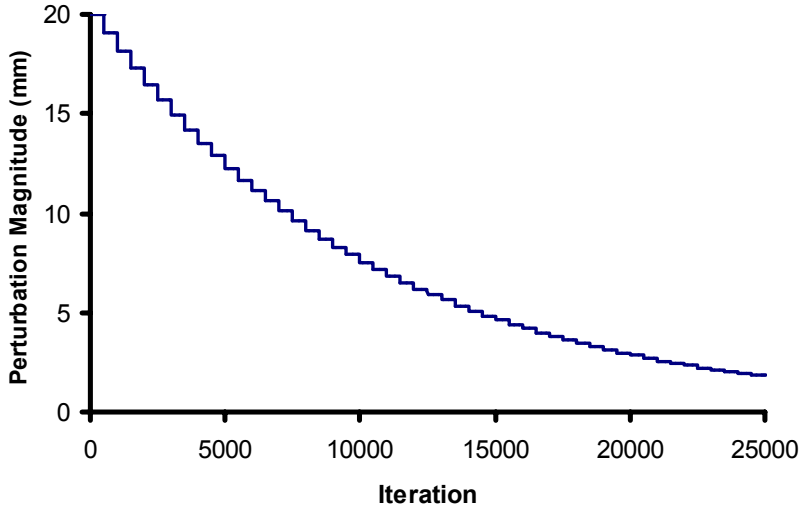

Figure 32: Decreases of perturbation magnitude for amplitude parameters

The value of temperature describes the probability that a parameter perturbation that increases the error function will be accepted. However, the error function changes different magnitudes for perturbations to the 3 different types of parameters (i.e., amplitude, mean, standard deviation). Therefore, different temperatures were used for perturbations to the amplitude, mean, and standard deviation parameters. The initial temperatures were determined by randomly perturbing each parameter individually and calculating the error function. The standard deviation of these errors was then calculated for each parameter type and used as the initial error. This resulted in about 60% of the parameter perturbations to be accepted for the first 500 iterations but only about 5% to be accepted for the last 500 iterations.

7.2.3 Assessment of Efficacy

The minimized value of the error function was used to assess the efficacy of the simulated annealing optimization. This value was recorded for all 5 trials for each case. The minimized values of the error function were also compared to the error function evaluated without IDT correction and also with the correct solutions for the 54 parameters to determine how well the optimization decreased the error function. The value of the error function and the optimized parameter values were also recorded every 500 iterations through each optimization to investigate convergence.

The efficacy of the IDT was investigated by calculating errors of the knee kinematics. Kinematic error was determined in each DOF as the absolute value of the difference between the kinematics calculated from marker data with skin movement and the true kinematics obtained from marker data without skin movement. The maximum kinematic error was defined as the largest kinematic

error over the 15 (case 3) or 30 (cases 1 and 2) data frames of each trial. The maximum kinematic error was first determined using the marker data with skin movement but without implementation of the IDT. This represented the errors that would be expected if the PCT marker set was used without IDT correction. The maximum kinematic error was then calculated after the IDT had estimated the skin movement of each marker. Finally, maximum kinematic error was determined when the correct solutions for the 54 parameters were used.

7.3 RESULTS

7.3.1 Random Parameters

The maximum errors of knee kinematics calculated from marker data having skin movement with random parameters were 3.3 ± 1.3° to 6.2 ± 4.5° and 3.7 ± 1.7 mm to 19.4 ± 10.3 mm (mean ± SD, n = 5) before the IDT was used. The error function evaluated without using the IDT was $1.1 \times 10^{-2} \pm 0.4 \times 10^{-2}$ m^2. When the correct solutions for the 54 parameters were used, the error function was reduced to 3.1×10^{-7} m^2 and the maximum kinematic errors were less than 0.01° and 0.02 mm This demonstrated the accuracy that could be obtained if the IDT successfully optimized all parameters.

The IDT was then used to optimize the 54 parameter values. The minimized value of the error function was $7.3 \times 10^{-7} \pm 8.5 \times 10^{-7}$ m^2 (Table 6). Trials 2, 3, and 4 minimized the error function to less than 3×10^{-7} m^2, the value corresponding to the correct solution (Figure 33). While the error function still appeared to be decreasing at the completion of the optimization for all 5 trials, the parameter values had converged (Figure 34).

Table 6: Error function for trials with random parameters (mean±SD, n=5)

	Error Function (m^2)
No correction	1.1×10^{-2} $\pm 0.4 \times 10^{-2}$
Minimized by IDT	7.3×10^{-7} $\pm 8.5 \times 10^{-7}$
Correct solution	3.1×10^{-7} $\pm 0.0 \times 10^{-7}$

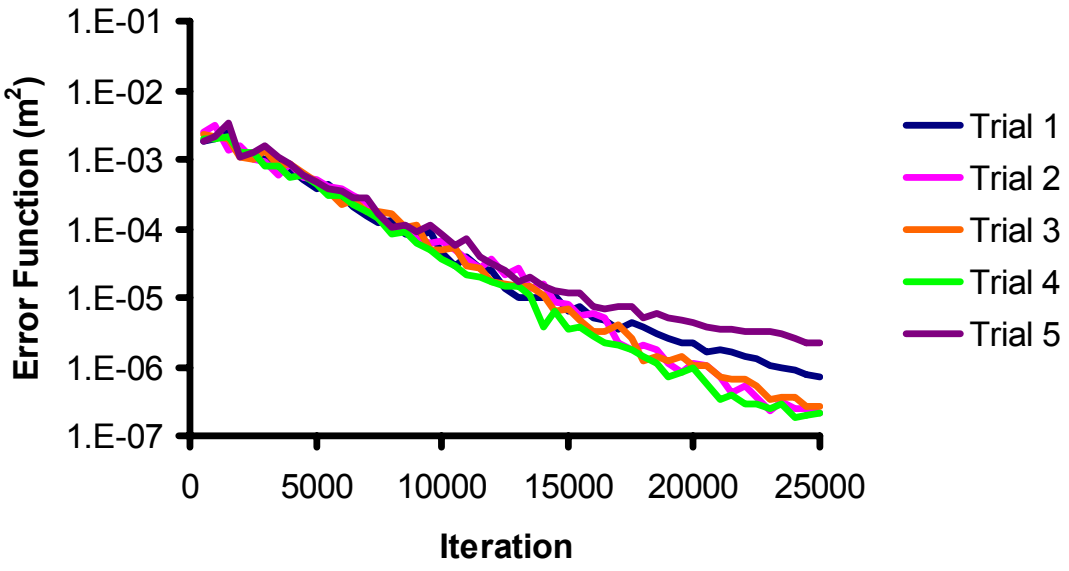

Figure 33: Error function for 5 trials with random parameters

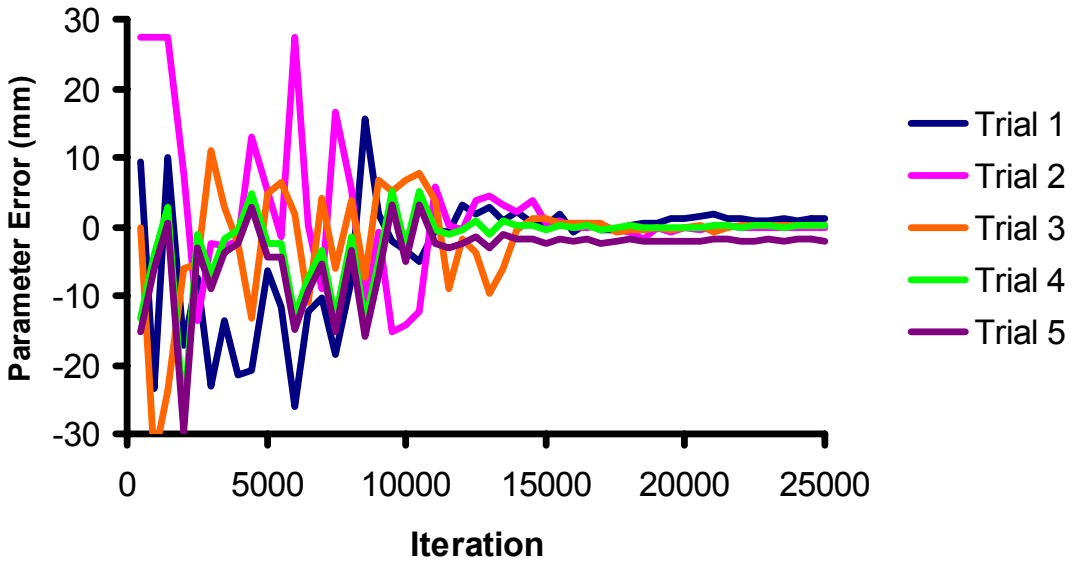

Figure 34: Error of amplitude for TA1 in z direction for random parameters

The maximum errors of knee kinematics after the IDT was used to correct for skin movement were 0.5 ± 0.5° to 1.3 ± 1.7° and 0.8 ± 1.1 mm to 1.6 ± 1.6 mm (mean ± SD, n = 5) (Table 7). Trials 2, 3, and 4, having the smallest values of the optimized error function, had average maximum errors of knee kinematics of 0.3° and 0.5 mm. However, the average maximum errors were 1.7° and 2.2 mm for trials 1 and 5. On average, the maximum errors of knee kinematics were reduced 78 to 94% with the IDT.

Table 7: Maximum kinematic errors from random parameters (mean±SD, n=5)

	Flexion-Extension (°)	Varus-Valgus (°)	Internal-External (°)	Medial-Lateral (mm)	Anterior-Posterior (mm)	Proximal-Distal (mm)
No Correction	3.3 ± 1.3	4.6 ± 2.0	6.2 ± 4.5	19.4 ± 10.3	12.1 ± 6.2	3.7 ± 1.7
With IDT	0.7 ± 0.7	0.5 ± 0.5	1.3 ± 1.7	1.2 ± 1.3	1.6 ± 1.6	0.8 ± 1.1
Average Improvement	**79%**	**89%**	**79%**	**94%**	**87%**	**78%**

7.3.2 Simulated Muscle Contraction during Stance Phase of Gait

The maximum errors of knee kinematics that were calculated from marker data with simulated muscle contraction ranged from 2.1 ± 0.4° to 4.5 ± 0.7° and from 1.8 ± 0.4 mm to 14.4 ± 2.3 mm (mean ± SD, n = 5) before the IDT was used. The error function evaluated without using the IDT was $2.0 \times 10^{-3} \pm 0.2 \times 10^{-3}$ m^2. When the correct solutions for the 54 parameters were used, the error function was decreased to 3.0×10^{-7} m^2 and the maximum kinematic errors were again less than 0.01° and 0.02 mm.

The minimized value of the error function after the IDT was used to optimize the 54 parameter values was $5.0 \times 10^{-6} \pm 6.3 \times 10^{-6}$ m^2 (Table 8). There was some variability between the 5 trials with only trials 1 and 5 reducing the error function to less than 3×10^{-7} m^2 (Figure 35). The error function for trials 1 and 5 still appeared to be decreasing at the end of this optimization however the parameters had converged for all trials (Figure 36). The optimized parameters for trials 1 and 5 approached the correct solution while the parameters for trails 2, 3, and 4 converged incorrectly in the z direction.

Table 8: Error function for trials with simulated muscle contraction (mean±SD, n=5)

	Error Function (m^2)
No correction	2.0×10^{-3} $\pm 0.2 \times 10^{-3}$
Minimized by IDT	5.0×10^{-6} $\pm 6.3 \times 10^{-6}$
Correct solution	3.0×10^{-7} $\pm 0.0 \times 10^{-7}$

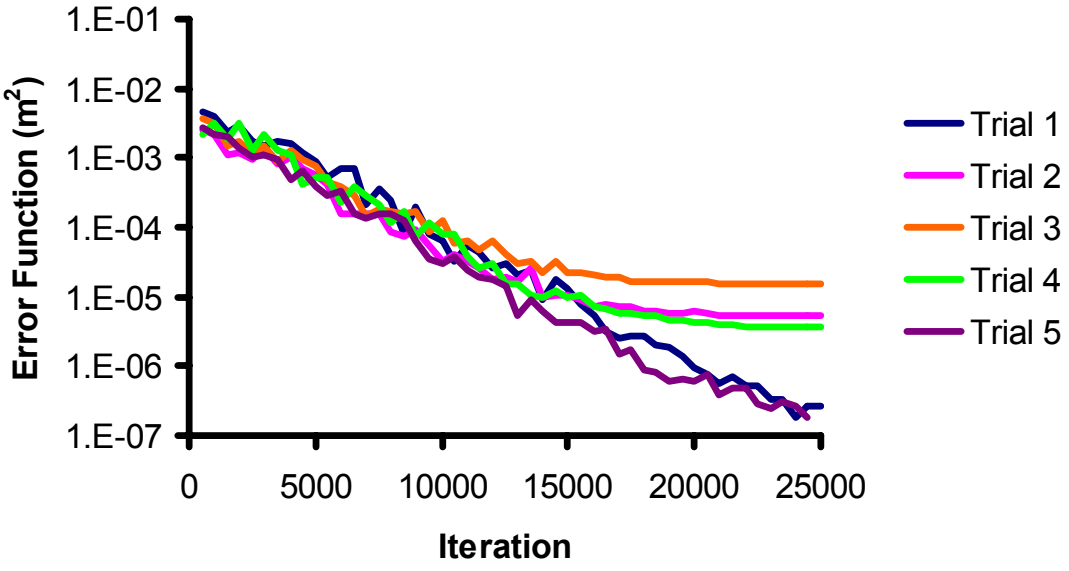

Figure 35: Error function for 5 trials of simulated muscle contraction

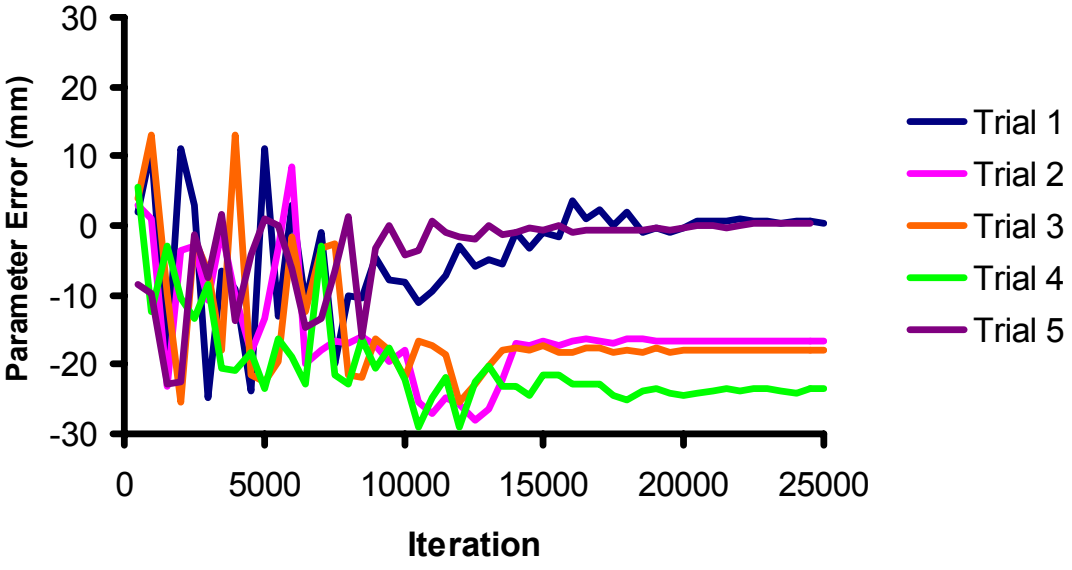

Figure 36: Error of amplitude for TL1 in z direction for simulated muscle contraction

The maximum errors of knee kinematics corrected by the IDT were 0.2 ± 0.2° to 4.5 ± 4.0° and 0.1 ± 0.0 mm to 2.7 ± 3.8 mm (mean ± SD, n = 5) (Table 9). The maximum kinematics errors for trials 1 and 5, having the smallest values of the optimized error function, averaged 0.1° and 0.3 mm. The IDT reduced the maximum errors of knee kinematics 93 to 99% for these 2 trials. However, the maximum errors of the calculated kinematics averaged 2.7° and 2.4 mm for trials 2, 3, and 4. Overall, the IDT did not decrease the errors of internal-external rotation, however, the maximum kinematic errors in the other 5 DOFs were improved by 79 to 94%.

Table 9: Maximum kinematic errors from simulated muscle contraction (mean±SD, n=5)

	Flexion-Extension (°)	Varus-Valgus (°)	Internal-External (°)	Medial-Lateral (mm)	Anterior-Posterior (mm)	Proximal-Distal (mm)
No Correction	2.1 ± 0.4	2.3 ± 0.3	4.5 ± 0.7	9.0 ± 1.6	14.4 ± 2.3	1.8 ± 0.4
With IDT	0.3 ± 0.4	0.2 ± 0.2	4.5 ± 4.0	1.9 ± 2.5	2.7 ± 3.8	0.1 ± 0.0
Average Improvement	**86%**	**91%**	**0%**	**79%**	**81%**	**94%**

7.3.3 Simulated Skin Movement at Heel Strike of Gait

The maximum errors of knee kinematics calculated from marker data simulating skin movement at heel strike of gait were 0.9 ± 0.4° to 2.1 ± 1.0° and 4.7 ± 1.1 mm to 12.3 ± 1.4 mm (mean ± SD, n = 5) before the IDT was implemented. The error function evaluated without using the IDT was $9.3 \times 10^{-4} \pm 3.8 \times 10^{-4}$ m^2. The maximum kinematic errors were less than 0.01° and 0.02 mm and the error function was 1.5×10^{-7} m^2 when the correct solutions for the 54 parameters were used.

The minimized value of the error function was $5.6 \times 10^{-6} \pm 6.9 \times 10^{-6}$ m^2 (Table 10). Trials 1 and 2 decreased the error function to less than 5×10^{-7} m^2 while the minimized error functions for the remaining 3 trials were greater than 2×10^{-6} m^2 (Figure 37). Both the error function and parameter values had converged by the end of the optimization (Figure 38).

Table 10: Error function for trials with simulated heel strike (mean±SD, n=5)

	Error Function (m^2)
No correction	9.3×10^{-4} $\pm 3.8 \times 10^{-4}$
Minimized by IDT	5.6×10^{-6} $\pm 6.9 \times 10^{-6}$
Correct solution	1.5×10^{-7} $\pm 0.0 \times 10^{-7}$

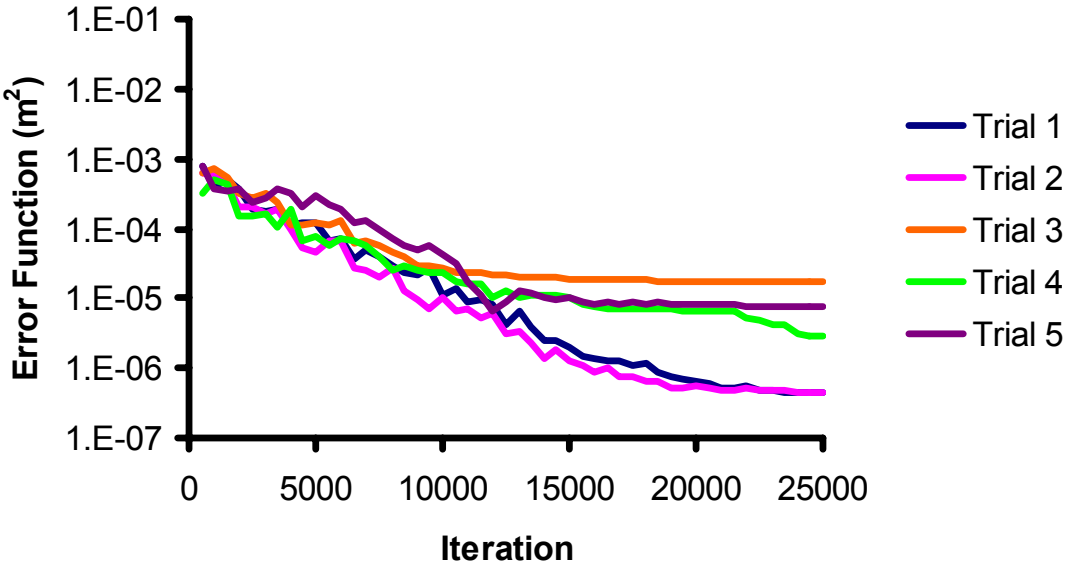

Figure 37: Error function for 5 trials simulating heel strike of gait

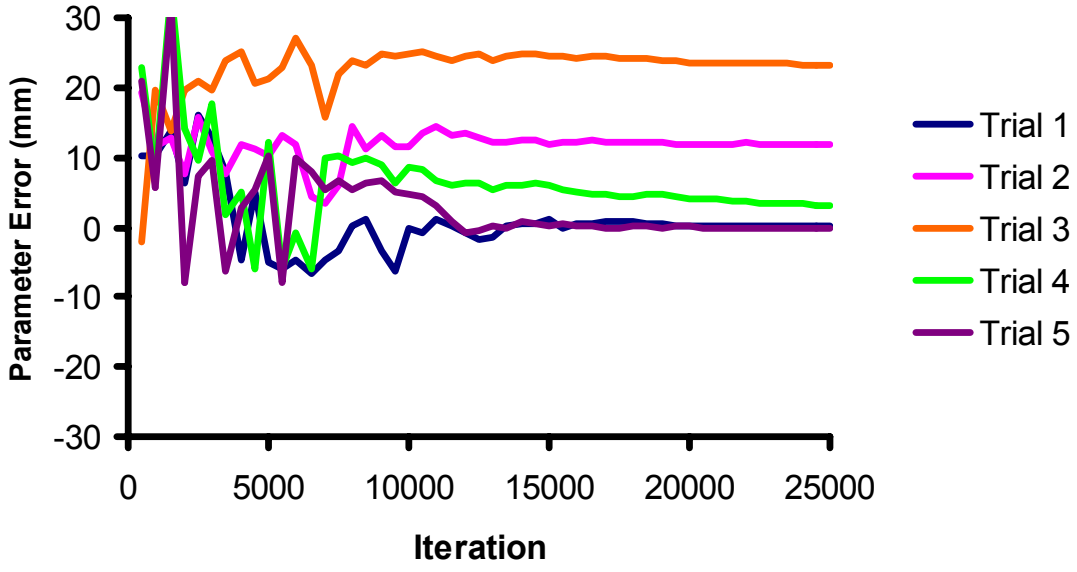

Figure 38: Error of amplitude for TA1 in x direction for heel strike of gait

The maximum errors of knee kinematics corrected by the IDT were 1.3 ± 0.5° to 3.4 ± 3.3° and 7.9 ± 7.9 mm to 12.7 ± 12.7 mm (mean ± SD, n = 5) (Table 11). Despite most effectively minimizing the error function, the maximum errors of the corrected kinematics for trials 1 and 2 averaged 2.8° and 10.9 mm. Overall, the IDT only improved the estimate of proximal-distal translation. In the other 5 DOFs, the IDT actually increased the maximum error of knee kinematics 44 to 100%.

Table 11: Maximum kinematic errors from simulated heel strike (mean±SD, n=5)

	Flexion-Extension (°)	Varus-Valgus (°)	Internal-External (°)	Medial-Lateral (mm)	Anterior-Posterior (mm)	Proximal-Distal (mm)
No Correction	1.0 ± 0.7	2.1 ± 1.0	0.9 ± 0.4	7.4 ± 3.4	4.7 ± 1.1	12.3 ± 1.4
With IDT	2.0 ± 1.9	3.4 ± 3.3	1.3 ± 0.5	12.7 ± 12.7	7.9 ± 7.9	7.9 ± 9.5
Average Improvement	**-100%**	**-62%**	**-44%**	**-72%**	**-68%**	**36%**

8.0 DISCUSSION

The objective of this thesis was to evaluate the accuracy of knee kinematics measured non-invasively using a motion capture system and surface markers. The results were used to judge the suitability of this method for measuring the changes in dynamic knee stability that are associated with ACL injury and reconstruction. The first aim investigated how various marker sets were affected by random errors in marker locations and was used to choose a marker set. The second and third aims investigated sources of error from inaccuracies of the motion capture system and from skin movement, respectively.

The first specific aim showed that kinematics calculated with the triad marker set were drastically affected by errors in marker locations while the HH and PCT were affected to a lesser extent. While random errors in marker locations had a statistically smaller effect on the accuracy of internal-external tibial rotation calculated with the HH marker set than with the PCT, it is important to note that these comparisons were for the same amount of errors in marker locations. Cappozzo and coworkers have shown that markers placed above anatomical landmarks experience greater amounts of skin movement than those placed mid-segment[266]. Therefore, markers for the PCT likely have smaller skin movement than those for the HH marker set and provide more accurate kinematics. Additionally, the PCT marker set is capable of providing knee translations, which may be an important indicator of knee function after ACL injury, while the HH marker set does not provide translational results.

The random errors in marker locations investigated in the first aim were intended to represent both inaccuracies of motion capture systems and skin movement. While it may be reasonable to model system inaccuracies as random error, Cappozzo and colleagues have clearly shown that skin movement of markers on the thigh and shank is systematic[266]. However, data describing the motion of markers attached to wands and on the pelvis were not available so it was not possible to more accurately model skin movement. Therefore, these results were not intended to predict errors of knee kinematics measured *in vivo*; rather they demonstrate how error propagation affects various marker sets differently.

Based on the first specific aim, the PCT marker set was chosen for further study. The purposes of the second and third aims were to investigate how the accuracy of kinematics calculated with the PCT marker set were affected by specific sources of error. The second specific aim quantified the errors of a motion capture system and elucidated how the accuracy of joint kinematics and intermarker measurements were affected. While this was ultimately achieved, several preliminary investigations were necessary to implement the PCT marker set. Preliminary studies showed that a motion capture system (Peak Motus 7, Peak Performance Technologies Inc., Centennial, CO) with 6 cameras placed 5 to 10 m from the measurement volume was not successful at even recording the closely spaced cluster markers. When 2 additional cameras were added to this system 2 m from the measurement volume, markers could be recorded, however the mean errors of intermarker distances were 1.5 to 3 mm. To investigate if these errors could be improved by decreasing the fields of view of the cameras, another test using only 4 of these cameras that were placed 2 m from the model was conducted. However, mean errors of intermarker distances remained to be 1 to 3 mm. It was not until the VICON motion capture

system was used that sub-millimeter errors of intermarker distances could consistently be obtained. These improvements can likely be attributed to the higher resolution of the optical capture board and also the algorithm for finding marker centers in the 2D camera views by fitting ellipses to the images.

The mean errors of intermarker angles and distances determined for the second specific aim using the VICON system were 0.1° and 1 mm. Results from other studies using similar methods have generally shown mean errors of 0.1 to 1° and 1 to 4 mm[242-247]. In a recent comparison of commercial motion capture systems, only 2 of 8 systems had mean errors of 0.3° or less for measuring intermarker angles and 2 mm or less for intermarker distances[248]. The most accurate system of the 8 had mean errors of 0.2° and 0.4 mm (Table 1). These past studies support the choice of the motion capture system utilized for this thesis.

The mean errors of joint kinematics determined in the second aim were up to 2° and 3 mm. Andriacchi and coworkers used similar methods to investigate the accuracy of joint kinematics determined with a motion capture system using the PCT marker set and found errors up to 1.0° and 1.5 mm[262]. The inferior accuracy of the motion capture system used in this thesis can likely be attributed to 2 factors; uncertainty in digitizing the registration blocks to determine the actual kinematics and error in the registration of the clusters to the blocks. Both explanations are supported by the trends of increasing error as the joint was moved from position 1 to position 4.

It is interesting to note that no differences in the accuracy of joint kinematics were found between the 4 and 6 camera configurations. While only 2 cameras are required to calculate the 3D positions of markers, additional cameras improve the redundancy of the system and theoretically improve accuracy. However, the most significant benefit of increasing the number of cameras is improving the ability of the system to continuously record the markers during dynamic activities. For example, when markers overlap in the 2D camera images or are lost from view, a small number of cameras are unable to reconstruct the 3D marker locations. In this study, the cameras were carefully placed so each had a full view of all markers with the model in each position. While no apparent benefits of using a larger number of cameras were shown by this study, utilizing more cameras may be justified when complicated activities are recorded.

The joint model and methods used for this study were designed to simulate *in vivo* testing conditions. Markers were attached using the same cluster arrangements that would be used with human subjects and the cameras were set up as they would be for human testing. However, it was difficult to define anatomic coordinate frames that could be measured directly to provide actual joint kinematics with high accuracy. Therefore, the joint kinematics were defined using registration blocks that were not aligned with the anatomy and it was not possible to determine if the accuracy of joint kinematics varied between different DOF. Additionally, the registration blocks were attached close to the joint, however, they were not coincident at full extension, resulting in large, unphysiologic joint translations. Knee joint translations during *in vivo* activities are an order of magnitude smaller therefore the accuracy of joint kinematics reported here may represent a conservative estimate. In this study, the accuracy of the motion capture system was determined with static markers. While some have suggested that error may increase

with the velocity of the subject[245], the results of this study might apply to dynamic activities as well if the cameras are accurately synchronized and sampling rates high enough to prevent marker distortion are used.

The second specific aim showed that the motion capture system used for this thesis could accurately measure intermarker angles and distances compared to other commercial systems. While the error of joint kinematics were up to 2° and 3 mm, these values could likely be reduced to under 1° and 2 mm if uncertainty in the actual joint kinematics and error in the cluster to block registrations are eliminated.

The objective of this third aim was to investigate the affect of skin movement on the accuracy of knee kinematics measured using surface markers. Specifically, errors of knee kinematics were determined before and after the IDT was used to account for skin movement of the shank cluster. The first case used skin movement simulated with randomly generated parameters. For this type of skin movement, the IDT reduced the maximum errors of knee kinematics by approximately 80 to 90%. Alexander and Andriacchi validated the IDT using a similar method that also simulated skin movement by a Gaussian curve with random parameters[285]. These authors reported that the IDT could improve the accuracy of estimated cluster orientations and locations by 70 to 80%, however, these comparisons were with respect to a least-squares method and are difficult to compare to the results of this study. While the IDT program developed for this thesis did not solve for the skin movement parameters exactly, these results showed that improvements in the accuracy of knee kinematics approaching an order of magnitude may be possible with this method.

Two cases were also considered that attempted to model *in vivo* skin movement and determine the efficacy of the IDT for more realistic activities. For the 2 trials that best minimized the error function for simulated muscle contraction, the maximum errors of knee kinematics were reduced from 5° and 17 mm to 0.5° and 1 mm (90% improvement). However, the IDT was totally unsuccessful at improving the estimates of knee kinematics during heel strike of gait and, unlike the previous case with simulated muscle contraction, no relationship was observed between the minimized value of the error function and the accuracy of knee kinematics.

This variability in the efficacy of the IDT for different types of skin movement can be explained. The IDT optimizes parameters that characterize skin movement based on the deformed shape of the cluster over a certain interval of time. However, for the case that simulated heel strike, all the markers moved in the same direction simultaneously causing the shape of the cluster to remain relatively constant. This demonstrates that the IDT is unable to predict skin movement during activities when the cluster experiences uniform skin movement. Therefore, the IDT may not be appropriate for activities when skin movement primarily results from rapid deceleration and inertial effects[269]. The IDT more successfully determined the parameters that described skin movement for simulated muscle contraction in the stance phase of gait. During this activity, the shape of the cluster changed over time with the anterior markers experiencing skin movement as the tibialis anterior contracted in early stance phase and the lateral markers moving as the gastrocnemius was activated in mid stance. Therefore, the IDT may be useful for activities when skin movement results from muscle contraction that affects the cluster markers non-uniformly. An example of this may be active knee-flexion extension with hamstring and gastrocnemius contraction during flexion and quadriceps contraction during extension.

The overall objective of this thesis was to evaluate the accuracy of knee kinematics measured with a motion capture system and surface markers. The accuracy of the motion capture system for recording joint kinematics was about 1° and 2 mm after uncertainty in the actual kinematics and error of the registration were accounted for. Under ideal conditions with the functional form of skin movement being known, the IDT was shown to be capable of reducing errors of knee kinematics resulting from skin movement of the shank to approximately 0.5° and 1 mm. Skin movement of the thigh would likely contribute at least another 0.5° and 1 mm. Therefore, a best case estimate for the accuracy of knee kinematics measured using this method is 2° and 4 mm. While this accuracy may be sufficient for comparing the knee kinematics of ACL intact and deficient subjects[230, 264], it is unlikely that reliable estimates of the *in situ* force of the ligament may be obtained with these errors.

9.0 FUTURE DIRECTIONS

Several recommendations for future research can be made based upon the results of this thesis. The first specific aim showed that random errors in marker locations could result in large errors in knee kinematics measured with the triad marker set. This can likely be attributed to the close spacing of the markers[259, 291]. Researchers utilizing triad marker sets to investigate many types of lower extremity disorders may consider increasing the size of the triads to reduce these errors.

Three recommendations may be made from the second specific aim. First, future studies for validating motion capture systems should ensure that an accurate method of determining the actual joint kinematics is available. Secondly, reducing errors in the measured transformations between the clusters and anatomic coordinate systems is crucial for improving the accuracy of knee kinematics measured with the PCT. The accuracy of registration methods using specialized MR opaque markers or reflective markers placed over anatomical landmarks of subjects should be verified in the future. Lastly, while these results did not show a significant difference between the reliability of 4 and 6 camera configurations, changing the relative camera orientations or camera to measurement volume distances[241] could be investigated in the future to determine the optimal system configuration.

For the third specific aim, the optimization did not converge correctly for several of the trials of simulated muscle contraction. While improvements in the accuracy of knee kinematics were still obtained, the simulated annealing algorithm described in this thesis should be improved. For example, most parameters converged between iterations 10,000 and 15,000. Increasing the number of perturbations within the temperature range corresponding to this interval may be beneficial. Similarly, the iterations at higher and lower temperatures may not be needed. The current optimization required over 2 days for a single trial with 30 data frames and considered only skin movement of the shank cluster. It is reasonable to predict that optimizations taking up to a week may be required for longer trials where the skin movement of the thigh is also determined. The parameters for this simulated annealing algorithm should be investigated to provide a more effective yet efficient optimization.

The results of the third aim are not sufficient for fully validating the IDT for *in vivo* activities since the functional form of the skin movement in these simulations was known. While modeling skin movement with a Gaussian function during activities where the subject performs a simple motion and begins or ends in the reference position may be reasonable, this should be confirmed *in vivo*. Stagni and coworkers have shown that using various mathematical functions to model skin movement with the IDT results in different solutions for knee kinematics[286]. While the results of this aim show that the IDT is a promising method for improving the accuracy of knee kinematics for certain types of activities, further research utilizing fluoroscopy[223] or dynamic MRI[292] is needed to elucidate *in vivo* patterns of skin movement. These data will be valuable for better understanding the capabilities of algorithms such as the IDT and for improving the efficacy of these methods.

Further research is also needed to clarify the accuracy that motion capture systems must achieve to measure the differences in knee kinematics between normal and ACL deficient or reconstructed subjects. While some literature is available to estimate the required accuracy, future studies utilizing radiographic techniques will be useful. Additionally, the accuracy required for reproducing knee kinematics to provide useful estimates of ACL *in situ* forces will be needed. This thesis successfully determined how several sources of error affect the accuracy of knee kinematics measured with a motion capture system. Future research will decrease these sources of error and ideally allow the *in vivo* knee kinematics of patients with ACL injuries to be measured non-invasively yet accurately during a variety of activities.

APPENDIX A: DERIVATION OF TRANSFORMATION MATRIX FOR JCS

1. Transformations for individual rotations and translations

$$R_X(\theta) := \begin{pmatrix} 1 & 0 & 0 & 0 \\ 0 & \cos(\theta) & -\sin(\theta) & 0 \\ 0 & \sin(\theta) & \cos(\theta) & 0 \\ 0 & 0 & 0 & 1 \end{pmatrix} \qquad R_Y(\theta) := \begin{pmatrix} \cos(\theta) & 0 & \sin(\theta) & 0 \\ 0 & 1 & 0 & 0 \\ -\sin(\theta) & 0 & \cos(\theta) & 0 \\ 0 & 0 & 0 & 1 \end{pmatrix} \qquad R_Z(\theta) := \begin{pmatrix} \cos(\theta) & -\sin(\theta) & 0 & 0 \\ \sin(\theta) & \cos(\theta) & 0 & 0 \\ 0 & 0 & 1 & 0 \\ 0 & 0 & 0 & 1 \end{pmatrix}$$

$$T_X(x) := \begin{pmatrix} 1 & 0 & 0 & x \\ 0 & 1 & 0 & 0 \\ 0 & 0 & 1 & 0 \\ 0 & 0 & 0 & 1 \end{pmatrix} \qquad T_Y(y) := \begin{pmatrix} 1 & 0 & 0 & 0 \\ 0 & 1 & 0 & y \\ 0 & 0 & 1 & 0 \\ 0 & 0 & 0 & 1 \end{pmatrix} \qquad T_Z(z) := \begin{pmatrix} 1 & 0 & 0 & 0 \\ 0 & 1 & 0 & 0 \\ 0 & 0 & 1 & z \\ 0 & 0 & 0 & 1 \end{pmatrix}$$

2. Overall transformation of tibia with respect to femur (right knee)

$$T(\alpha, \beta, \gamma, d_m, d_p, d_d) := R_X(\alpha) \cdot T_X(d_m) \cdot R_Z(\beta) \cdot T_Z(d_p) \cdot R_Y(\gamma) \cdot T_Y(d_d)$$

$$T(\alpha, \beta, \gamma, d_m, d_p, d_d) \rightarrow \begin{pmatrix} \cos(\beta)\cdot\cos(\gamma) & -\sin(\beta) & \cos(\beta)\cdot\sin(\gamma) & -\sin(\beta)\cdot d_d + d_m \\ \cos(\alpha)\cdot\sin(\beta)\cdot\cos(\gamma) + \sin(\alpha)\cdot\sin(\gamma) & \cos(\alpha)\cdot\cos(\beta) & \cos(\alpha)\cdot\sin(\beta)\cdot\sin(\gamma) - \sin(\alpha)\cdot\cos(\gamma) & \cos(\alpha)\cdot\cos(\beta)\cdot d_d - \sin(\alpha)\cdot d_p \\ \sin(\alpha)\cdot\sin(\beta)\cdot\cos(\gamma) - \cos(\alpha)\cdot\sin(\gamma) & \sin(\alpha)\cdot\cos(\beta) & \sin(\alpha)\cdot\sin(\beta)\cdot\sin(\gamma) + \cos(\alpha)\cdot\cos(\gamma) & \sin(\alpha)\cdot\cos(\beta)\cdot d_d + \cos(\alpha)\cdot d_p \\ 0 & 0 & 0 & 1 \end{pmatrix}$$

3. Solution for rotations and translations

$$\operatorname{atan}\left(\frac{T(\alpha,\beta,\gamma,d_m,d_p,d_d)_{3,2}}{T(\alpha,\beta,\gamma,d_m,d_p,d_d)_{2,2}}\right) \rightarrow \operatorname{atan}\left(\frac{\sin(\alpha)}{\cos(\alpha)}\right)$$

$$\operatorname{atan}\left(\frac{-T(\alpha,\beta,\gamma,d_m,d_p,d_d)_{1,2}}{\cos(\alpha)\cdot T(\alpha,\beta,\gamma,d_m,d_p,d_d)_{2,2} + \sin(\alpha)\, T(\alpha,\beta,\gamma,d_m,d_p,d_d)_{3,2}}\right) \rightarrow \operatorname{atan}\left(\frac{\sin(\beta)}{\cos(\alpha)^2\cdot\cos(\beta) + \sin(\alpha)^2\cdot\cos(\beta)}\right)$$

$$\operatorname{atan}\left(\frac{T(\alpha,\beta,\gamma,d_m,d_p,d_d)_{1,3}}{T(\alpha,\beta,\gamma,d_m,d_p,d_d)_{1,1}}\right) \rightarrow \operatorname{atan}\left(\frac{\sin(\gamma)}{\cos(\gamma)}\right)$$

Given

$$-\sin(\beta)\cdot d_d + d_m = dx$$

$$\cos(\alpha)\cdot\cos(\beta)\cdot d_d - \sin(\alpha)\cdot d_p = dy$$

$$\sin(\alpha)\cdot\cos(\beta)\cdot d_d + \cos(\alpha)\cdot d_p = dz$$

$$\operatorname{Find}(d_m,d_p,d_d) \rightarrow \begin{pmatrix} \dfrac{\sin(\beta)\cdot\cos(\alpha)\cdot dy + \sin(\beta)\cdot dz\cdot\sin(\alpha) + dx\cdot\cos(\beta)}{\cos(\beta)} \\ -dy\cdot\sin(\alpha) + \cos(\alpha)\cdot dz \\ \dfrac{\cos(\alpha)\cdot dy + dz\cdot\sin(\alpha)}{\cos(\beta)} \end{pmatrix}$$

APPENDIX B: PROTOCOL OF ATTACHMENT OF PCT MARKERS

1. Place LM on distal apex of the lateral malleolus
2. Place LP on most lateral point of the ridge of lateral tibial plateau
3. Place TL1-3 on LM-LP line, evenly spaced between LP and LM
4. Place TA1 on distal aspect of tibial tuberosity
5. Place TA3 on anterior-medial border of the tibia at a level 2-3 cm proximal to TL3
6. Place TA2 on anterior shank, centered between TA1 and TA3
7. Place MM on distal apex of the medial malleolus
8. Place MP on most medial point of the ridge of medial tibial plateau
9. Place GT over prominence of greater trochanter external surface
10. Place FP1-3 on GT-LP line, evenly spaced between GT and LP
11. Measure distance from anterior superior iliac spine to proximal aspect of patella
12. Place FA3 on ASIS-PT line, 20% of total distance from patella
13. Place FA2 on ASIS-PT line, 40% of total distance from patella
14. Place FA1 on ASIS-PT line, 65% of total distance from patella
15. Place FL1 centered between FA1 and GT
16. Place FL2 centered between FA2 and FP1
17. Place FL3 centered between FA3 and FP2
18. Place MC and LC over medial and lateral femoral epicondyles

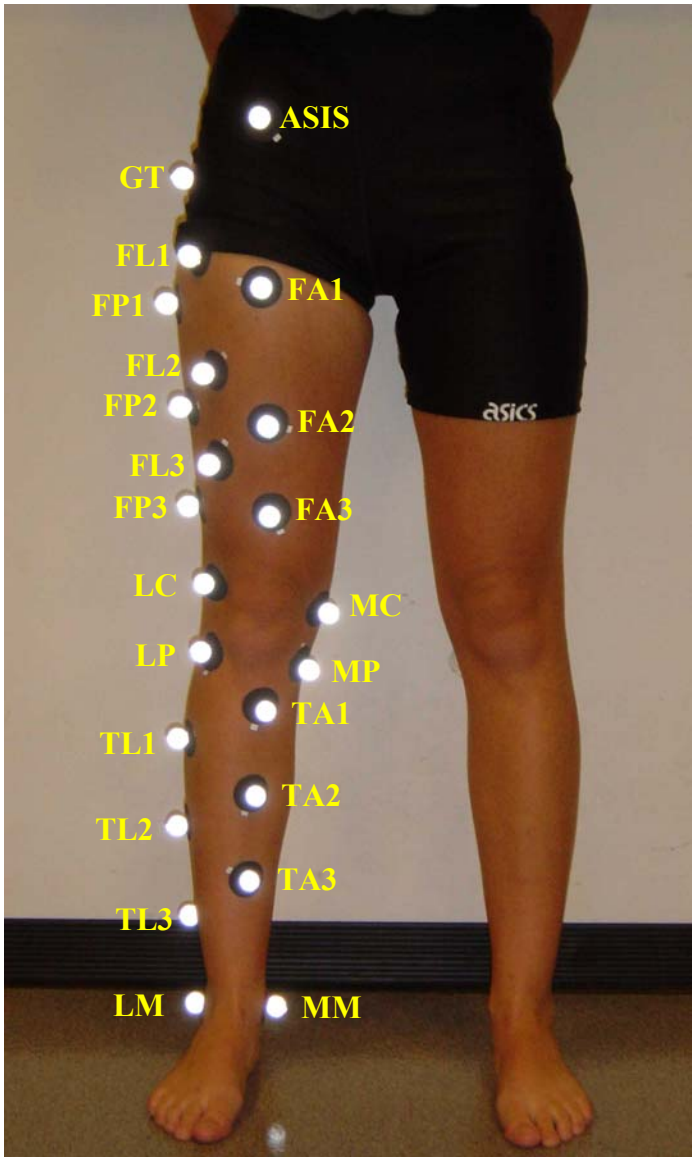

Figure 39: Subject with markers attached for the point cluster technique

APPENDIX C: PSEUDOCODE FOR INTERVAL DEFORMATION TECHNIQUE

Set variables
Load clusterdata.txt (marker locations during activity)
Load refdata.txt (marker locations in reference position)

PART 1: REGISTRATION OF CLUSTERS TO ANATOMY (~Line 150)
(use refdata)
Display time

For t = 1 : max
    Calculate tibial anatomy wrt shank cluster (Tsc_ta)
    Decompose to translations and Euler angles
    Save tibial anatomy wrt shank cluster translations and rotations (alp(t)…dz(t))
Plot dx, dy, dz for each frame
Plot alpha, beta, gamma for each frame
Average alpha, beta, gamma, dx, dy, dz (m_alp…m_dz)
Display standard deviations of alpha, beta, gamma, dx, dy, dz
Calculate orthogonal transformation matrix of anatomy wrt cluster from
    m_alp…m_dz (Tsc_ta)

For t = 1 : max
    Calculate femural anatomy wrt thigh cluster (Ttc_fa)
    Decompose to translations and Euler angles
    Save femural anatomy wrt thigh cluster translations and rotations (alp(t)…dz(t))
Plot dx, dy, dz for each frame
Plot alpha, beta, gamma for each frame
Average alpha, beta, gamma, dx, dy, dz (m_alp…m_dz)
Display standard deviations of alpha, beta, gamma, dx, dy, dz
Calculate orthogonal transformation matrix of anatomy wrt cluster from
    m_alp…m_dz (Ttc_fa)

Plot femural anatomical axes and markers and thigh axes and markers
Plot tibial anatomical axes and markers and shank axes and markers
Pause

Optional:

Calculate locations of markers wrt cluster
Calculate locations of markers wrt anatomy

PART II: NORMAL ANALYSIS, NO SKIN MOVEMENT CORRECTION (~Line 600)
(use clusterdata)
Display time
For (t = 1)
    Save eigenvalues of thigh cluster inertia tensor (tc_eval(t))
    Calculate thigh cluster inertia (t_inertia)
    Calculate principal axes of thigh cluster, frame 1 (tc_ev1…tc_ev3)
    Calculate thigh cluster COM (tc_x_com…tc_z_com)
    Save thigh cluster COM (tc_xyz_COM(t))
    Calculate transformation matrix from global to thigh cluster from principal axes
        and COM (Tg_tc)
    Calculate transformation matrix from global to femoral anatomy:
        (Tg_fa=Tg_tc*Ttc_fa)
    Calculate femoral axes wrt global (fx_g…fz_g)
    Calculate femoral CS COM (fa_com)
    Save eigenvalue of shank cluster inertia tensor (sc_eval(t))
    Calculate shank cluster inertia (s_inertia)
    Calculate principal axes of shank cluster, frame 1 (sc_ev1…sc_ev3)
    Calculate shank cluster COM (sc_x_com…sc_z_com)
    Save shank cluster COM (sc_xyz_COM(t))
    Calculate transformation matrix from global to shank cluster from principal axes
        and COM (Tg_sc)
    Calculate transformation matrix from global to tibial anatomy:
        Tg_ta=Tg_sc*Tsc_ta
    Calculate tibial axes wrt global (tx_g…tz_g)
    Calculate tibial CS COM (ta_com)

    Plot markers, cluster axes, and calculated anatomical axes
    While cluster axis directions do not match frame 1 of registration
        Input which cluster axes are incorrect
        Change axis directions (e.g. tc_e1 = -tc_ev1)
        Recalculate transformation matrix from global to thigh cluster using
            corrected cluster axes (Tg_tc)
        Calculate transformation from global to femoral anatomy:
            Tg_fa= Tg_tc * Ttc_fa
        Calculate femoral axes wrt global (fx_g…fz_g)
        Calculate femoral CS COM (fa_com)
        Recalculate transformation matrix from global to shank cluster using
            corrected cluster axes (Tg_sc)
        Calculate transformation from global to tibial anatomy:

Tg_ta= Tg_sc * Tsc_ta
Calculate tibial axes wrt global (tx_g…tz_g)
Calculate tibia CS COM (ta_com)
Replot markers, cluster axes, and recalculated anatomical axes
Specify if directions are still incorrect
Save corrected axis directions (t_evec(t), s_evec(t))
Save cluster inertia (t_in(t), s_in(t))
Save individual thigh cluster axes (t11(t), t12(t)..t33(t)
Save individual shank cluster axes (s11(t), s12(t)..s33(t)
Save Euler angles of thigh cluster wrt global (t_alp(t)…t_gam(t))
Save Euler angles of shank cluster wrt global (s_alp(t)…s_gam(t))
Calculate relative transformation from femur to tibia:
Tfa_ta=Tg_fa^{-1}*Tg_ta
Save relative translations of tibia wrt femur (rel_x(t)…rel_z(t))
Save relative rotations of tibia wrt femur (rel_alp(t)…rel_gam(t))
If knee is from left side
Calculate and save JMD kinematics (FE(t)…PD(t))
Calculate and save orthogonal translations (del_x(t)…del_z(t))
If knee is from right side
Calculate and save JMD kinematics (FE(t)…PD(t))
Calculate and save orthogonal translations (del_x(t)…del_z(t))
Optional:
Plot markers and axes in frame 1 and save for movie

Initialize count of corrected cluster axes (count = 0)
For t = 2 : max
Save eigenvalue of thigh cluster inertia tensor (tc_eval(t))
Calculate thigh cluster inertia (t_inertia)
Calculate principal axes of thigh cluster, frame 1 (tc_ev1…tc_ev3)
Calculate thigh cluster COM (tc_x_com…tc_z_com)
Save thigh cluster COM (tc_xyz_COM(t))
Save eigenvalue of shank cluster inertia tensor (sc_eval(t))
Calculate shank cluster inertia (s_inertia)
Calculate principal axes of shank cluster, frame 1 (sc_ev1…sc_ev3)
Calculate shank cluster COM (sc_x_com…sc_z_com)
Save shank cluster COM (sc_xyz_COM(t))
If direction of cluster eigenvectors switched from previous frame
Correct axis (e.g. tc_ev1 = -tc_ev1)
Increment count
Save corrected axis directions (t_evec(t), s_evec(t))
Save cluster inertia (t_in(t), s_in(t))
Save individual thigh cluster axes (t11(t), t12(t)..t33(t)
Save individual shank cluster axes (s11(t), s12(t)..s33(t)
Save Euler angles of thigh cluster wrt global (t_alp(t)…t_gam(t))
Save Euler angles of shank cluster wrt global (s_alp(t)…s_gam(t))
Calculate transformation from global to thigh cluster (Tg_tc)

Calculate transformation from global to shank cluster (Tg_sc)
Calculate transformation from global to femoral anatomy:
Tg_fa= Tg_tc * Ttc_fa
Calculate femur anatomy axes (fx_g…fz_g)
Calculate femur anatomy COM (fa_com)
Save femural anatomy COM (fa_x(t)…fa_x(t))
Save Euler angles of femur wrt global (fa_alp(t)…fa_gam(t))
Calculate transformation from global to tibial anatomy:
Tg_ta= Tg_sc * Tsc_ta
Calculate tibial anatomy axes (tx_g…tz_g)
Calculate tibial anatomy COM (ta_com)
Save tibial anatomy COM (ta_x(t)…ta_x(t))
Save Euler angles of tibia wrt global (ta_alp(t)…ta_gam(t))

Calculate relative transformation from femur to tibia:
Tfa_ta=Tg_fa^{-1}*Tg_ta
Save relative translations of tibia wrt femur (rel_x(t)…rel_z(t))
Save relative rotations of tibia wrt femur (rel_alp(t)…rel_gam(t))
If knee is from left side
Calculate and save JMD kinematics (FE(t)…PD(t))
Calculate and save orthogonal translations (del_x(t)…del_z(t))
If knee is from right side
Calculate and save JMD kinematics (FE(t)…PD(t))
Calculate and save orthogonal translations (del_x(t)…del_z(t))
Optional:
Plot markers and axes in frame 1 and save for movie
Play movie

Rename kinematics variables (flex(t)…med(t))
Display mean and standard deviation of knee kinematics through activity
Display mean and standard deviation of cluster eigenvalues norms through activity
Display number of corrected cluster axes
Plot rotations for each frame
Plot JMD translations for each frame
Plot orthogonal translations for each frame
Plot components of thigh axes wrt global for each frame
Plot components of shank axes wrt global for each frame
Plot cluster eigenvalues norms for each frame
Optional:
Plot global x, y, z of desired marker
Plot global x, y, z of thigh cluster COM
Plot global Euler angles of thigh cluster COM
Plot global x, y, z of shank cluster COM
Plot global Euler angles of shank cluster COM
Plot global x, y, z of femural CS COM
Plot global Euler angles of femural CS

Plot global x, y, z of tibial CS COM
Plot global Euler angles of tibial CS
Plot x, y, z of tibia wrt femur
Plot Euler angles of tibia wrt femur
Save normal kinematics (kin_normal.txt)
Pause

PART III: DETERMINE PARAMETERS FOR SHANK CLUSTER (~Line 1900)
(using notation from Alexander, 2001)

Display time

1) Calculate observed markers wrt cluster during activity:
(use clusterdata)
Save global shank marker locations as G
For t = 1 : max
Calculate shank cluster orientation using sc_evec (E)
Calculate shank cluster COM using sc_xyz_com (C)
Calculate local marker locations wrt observed cluster: $Lob(t) = E^{-1}*(G - C)$
Optional:
Save observed local marker locations (Lob_Shank.txt)
Save observed marker locations using Stanford format (Locdata_Alex.txt)

2) Calculate markers wrt cluster in reference position:
(use refdata)
Initialize count of corrected cluster axes (count = 0)
For t = 1 : max
Calculate shank cluster axes (sc_ev1(t), sc_ev2(t), sc_ev3(t))
Calculate shank cluster COM (sc_x_com, sc_y_com…)
By definition, axis directions are correct in frame 1 of refdata
If t > 1
Correct axis directions if switched from previous frame and increment count
Let P = shank cluster COM
Let Q = corrected cluster axis directions
Calculate local marker locations wrt bone: $Rob(t) = Q^{-1}*(Gref - P)$
Calculate mean Rob of each marker (Rmean)
Save marker locations in reference position using Stanford format (Reference_Alex.txt)
Optional:
On same axes:
Plot observed marker locations wrt bone (Rmean)
Plot observed marker locations wrt cluster for specified frame (Lob)
Calculate standard deviation of each marker location wrt bone in each direction over time
Display mean and maximum marker location standard deviation
Display number of axis directions automatically corrected
Optional:

Save marker locations wrt bone of each frame (Rob_Shank.txt)
Save mean marker locations wrt bone (Rob_shank.txt)

3) Calculate error for no correction:
(use clusterdata)
For each marker and in each direction and for each time, sum error of difference between actual marker locations wrt bone (Rmean) and observed marker locations wrt cluster: er_last = Σ (Lob(t)- Rmean)^2
Optional:
Plot error over time
Display error for no correction

4) Determine parameter limits:
Find and display maximum difference between observed and actual local marker locations: delta = max[abs(Rmean – Lob(t))]
Set constraints on parameters using program inputs
Calculate initial parameter perturbation magnitudes

5) Determine initial guesses:
calculate Lob-Rmean for each marker in each direction over time
fit Gaussian curve to these data
For t = 1: max
Calculate markers wrt bone using initial guesses (Rhat(t)=Rmean +f(guesses,t))
Calculate cluster COM and axes (Ecb, Ccb), making sure axis directions didn't switch
Calculate predicted markers wrt cluster: $Lhat(t)=Ecb^{-1}(Rhat-Ccb)$
Determine and display error for initial guesses: Σ (Lob(t)- Lhat(t))^2

6) Determine initial temperatures for each parameter type:
add random perturbation to each of the 54 parameters
calculate corresponding errors (same process as above)
calculate SD of error for perturbations to each type of parameter
Ti amp=multiple of SD(amp perturbations)
Ti mean=multiple of SD(mean perturbations)
Ti sd=multiple of SD(sd perturbations)

7) Optimize parameters
Display optimization settings
For restarts = 1:max
Display restart number
Reset number of accepted sets
Decrease perturbation magnitudes
Calculate initial temperatures for restart
Calculate minimum temperatures for restart

Check for amplitude shift

Change all amplitude parameters in one direction uniformly
Use shift that best reduces error

For temperature steps = 1 : max, perturb parameters and calculate error
Calculate temp
For each parameter
parnew= pars + (random(0,1)-0.5)*2*perturbation magnitude
check that parnew is within limits
Optional:
parnew = correct solution
For t = 1:max, determine error
Rhat(t) = Rmean + f(parnew,t)
Check axis directions
Calculate orientation of proposed cluster axes wrt bone (Ecb)
Calculate COM of proposed cluster wrt bone (Ccb)
Calculate marker locations wrt proposed cluster:
Lhat(t)=Ecb^{-1}(Rhat-Ccb)
Sum error er = Σ (Lob(t)- Lhat(t))^2)
Calculate probability of changing states from last successful state:
W=exp(er_last/temp – er/temp)
Generate random number between 0 and 1 (R)
If W > R, proposed state is accepted
Save parameters (par = parnew)
Save error (er_last = er)
If W < R, proposed state is unfavorable
Do nothing
(repeat for all 54 parameters)
(decrease temperature)
At end of each restart
Display percentages of accepted parameters
Display temperature ranges
Display perturbation magnitudes
Display final error
Display optimized amplitude parameters of TA1
Save error and parameter values (kin_corrected.txt)

8) Save transformations between cluster and bone for optimized parameters
For t = 1 : max, calculate local marker locations of optimized parameters
Rhat(t) = Rmean+f(pars,t)
For t = 1 : max
Calculate orientation of cluster axes wrt bone (Ecb_opt(t))
Calculate COM of cluster wrt bone (Ccb_opt(t))
Optional:
Plot locations of predicted and observed marker wrt cluster
Display error for optimized parameters

Pause

PART IV: DETERMINE PARAMETERS FOR THIGH CLUSTER (~Line 3000)
Display time

(not used)

PART V: INTERVAL DEFORMATION TECHNIQUE RESULTS (~Line 3000)
Display time

For t = 1 : max
    Calculate shank cluster COM (C(t))
    Calculate cluster axes (E(t))
    Calculate orientation of tibia: $Q = E*Ecb^{-1}$
    Calculate location of tibia: P=C-Q*Ccb
    Calculate transformation from global to tibia using Q, P, Tsc_ta

    Calculate transformation from global to thigh cluster using t_evec(t) and
        tc_xyz_com(t)
    Calculate transformation from global to femur using registration Ttc_fa
    Calculate JMD and orthogonal kinematics
    Optional:
        Plot markers and axes and save for movie
Optional:
    Play movie
Rename kinematic variables (flex_postIDT…med_postIDT)
Display mean and std of knee kinematics in each DOF
Plot rotations for each frame
Plot translations for each frame
Save corrected knee kinematics (kin_corrected.txt)
Display final time
(~Line 3500)

APPENDIX D: SAMPLE PROGRAM OUTPUT FOR AIM 3

(Trial 5 of Case 2)

```
>> int_def_3
********** Interval Deformation: Ver. 3 **********
Press Ctrl-C at any time to abort

Enter run identification: Trial 10
Enter knee side (l/r): r

Clusterdata.txt has 30 frames
Ref_data.txt has 1 frames

PART I: REGISTRATION OF CLUSTERS TO ANATOMY
Beginning on 01-Mar-2004 at 21:18:13
Standard Deviations of Transformation for Shank in Reference Position Are
0 deg,  0 deg,  0 deg,  0 mm, 0 mm,  0 mm

Standard Deviations of Transformation for Thigh in Reference Position Are
0 deg,  0 deg,  0 deg,  0 mm,  0 mm,  0 mm

Print figures if registration is satisfactory and press any key to continue

PART II: NORMAL ANALYSIS, NO SKIN MOVEMENT CORRECTION
Beginning on 01-Mar-2004 at 21:18:16
All markers in frame 1 of Trial 10:
Does direction of T1 match registration (y/n)? n
Does direction of T2 match registration (y/n)? n
Does direction of T3 match registration (y/n)? y
Does direction of S1 match registration (y/n)? n
Does direction of S2 match registration (y/n)? y
Does direction of S3 match registration (y/n)? n
Are axis directions now correct (y/n)? y

Flexion = 10.5116 +/- 5.2167 deg
Valgus = 0.73976 +/- 0.77225 deg
```

Internal = 0.90881 +/- 2.6086 deg
Anterior = 2.8423 +/- 5.666 mm
Medial = 1.5822 +/- 4.9018 mm
Proximal = -0.43066 +/- 0.72187 mm
Dx = 1.5683 +/- 4.8805 mm
Dy = 0.7089 +/- 1.4543 mm
Dz = -2.7598 +/- 5.5371 mm

Eigenvalues of shank cluster = 0.058303 +/- 0.00051104
Eigenvalues of thigh cluster = 0.09811 +/- 1.4115e-017
110 eigenvectors were corrected automatically

Successfully saved kin_normal.txt
Press any key to begin interval deformation of shank

PART III: DETERMINE PARAMETERS FOR SHANK CLUSTER
Beginning on 01-Mar-2004 at 21:18:31

Successfully saved Locdata_Alex.txt
Successfully saved Reference_Alex.txt

Mean Stdev of Local Marker Locations in Reference Position Is 0 m
Max Stdev of Local Marker Locations in Reference Position Is 0 m
0 eigenvectors were automatically corrected

For parameters = 0, error is 0.0017832 m^2 or 1.8172 mm /marker/direction/frame
Maximum difference between observed and actual local marker location is 6.3895 mm
Parameter Limits:
  Amplitude: -20 mm to 20 mm
  Mean: 1 frames to 30 frames
  STD: 2 frames to 5 frames
Getting initial parameter guesses...
For initial parameters, error is 0.00052016 m^2 or 0.98146 mm /marker/direction/frame

Changes to each parameter will be attempted at 500 temperature steps for each of 50 restarts

Initial perturbation magnitudes are 0.5 times parmax-parmin
Perturbation magnitudes are decreased by [0.9523, 0.9748, 0.992] each restart
Initial temperature is 1 times SD
Minimum temperature of each restart is 0.3 of initial
Initial temperature for next restart is 0.8 of previous initial

Restart 1:
  Shift number 2 was used, 65.8347 percent improvement
   [68.5111   56.2667   64.8333] percent accepted

Temperature decreased from [0.00079641 3.3179e-005 9.3116e-006] to [0.00023892 9.9538e-006 2.7935e-006] m^2 in 500 steps
Perturbation magnitude was 20 mm and 14.5/1.5 frames
Final error was 0.0026585
TA1 amplitudes are -1.4812, 0.029278, 9.0194 mm
Restart 2:
Shift number 4 was used, 4.7498 percent improvement
[64.5778 55.3889 64.6889] percent accepted
Temperature decreased from [0.00063713 2.6543e-005 7.4493e-006] to [0.00019114 7.963e-006 2.2348e-006] m^2 in 500 steps
Perturbation magnitude was 19.046 mm and 14.1346/1.488 frames
Final error was 0.002202
TA1 amplitudes are -11.1329, -0.209, 9.9793 mm
Restart 3:
No shift
[59.2222 52.4556 63.3] percent accepted
Temperature decreased from [0.0005097 2.1235e-005 5.9595e-006] to [0.00015291 6.3704e-006 1.7878e-006] m^2 in 500 steps
Perturbation magnitude was 18.1375 mm and 13.7784/1.4761 frames
Final error was 0.0019646
TA1 amplitudes are 6.6196, -4.6266, 0.11275 mm
Restart 4:
Shift number 1 was used, 18.9584 percent improvement
[56.5 49.5 62.6] percent accepted
Temperature decreased from [0.00040776 1.6988e-005 4.7676e-006] to [0.00012233 5.0963e-006 1.4303e-006] m^2 in 500 steps
Perturbation magnitude was 17.2723 mm and 13.4312/1.4643 frames
Final error was 0.0013794
TA1 amplitudes are 1.4475, -4.4128, 6.5247 mm

…

Restart 48:
No shift
[3.4556 2.7111 8.1667] percent accepted
Temperature decreased from [2.2201e-008 9.249e-010 2.5957e-010] to [6.6602e-009 2.7747e-010 7.7871e-011] m^2 in 500 steps
Perturbation magnitude was 2.0109 mm and 4.3692/1.0283 frames
Final error was 2.5934e-007
TA1 amplitudes are 2.0162, -9.0376, 7.3693 mm
Restart 49:
No shift
[3.15556 4.45556 10.9] percent accepted
Temperature decreased from [1.776e-008 7.3992e-010 2.0766e-010] to [5.3281e-009 2.2198e-010 6.2297e-011] m^2 in 500 steps
Perturbation magnitude was 1.915 mm and 4.2591/1.0201 frames

Final error was 1.8852e-007
TA1 amplitudes are 1.991, -9.0615, 7.3359 mm
Restart 50:
No shift
[3.0778 3.1556 8.5556] percent accepted
Temperature decreased from [1.4208e-008 5.9194e-010 1.6613e-010] to [4.2625e-009 1.7758e-010 4.9838e-011] m^2 in 500 steps
Perturbation magnitude was 1.8237 mm and 4.1517/1.012 frames
Final error was 1.7397e-007
TA1 amplitudes are 2.0456, -9.0693, 7.5571 mm
After 1350000 iterations:
Final error is 1.7397e-007m^2
(Average error is 0.017949 mm /marker/direction/frame)

PART IV: DETERMINE PARAMETERS FOR THIGH CLUSTER
Beginning on 03-Mar-2004 at 11:19:10

Press any key to calculate kinematics corrected for skin movement

PART V: INTERVAL DEFORMATION TECHNIQUE RESULTS
Beginning on 03-Mar-2004 at 11:19:10

Flexion = 9.9939 +/- 5.906 deg
Valgus = -0.02391 +/- 0.01001 deg
Internal = 0.066115 +/- 0.087128 deg
Anterior = -0.14516 +/- 0.1849 mm
Medial = -0.062225 +/- 0.024336 mm
Proximal = -0.064311 +/- 0.018852 mm
Dx = -0.062201 +/- 0.02433 mm
Dy = 0.044184 +/- 0.029661 mm
Dz = 0.15623 +/- 0.18021 mm

Successfully saved kin_corrected.txt
Ending on 03-Mar-2004 at 11:19:11

********** END **********

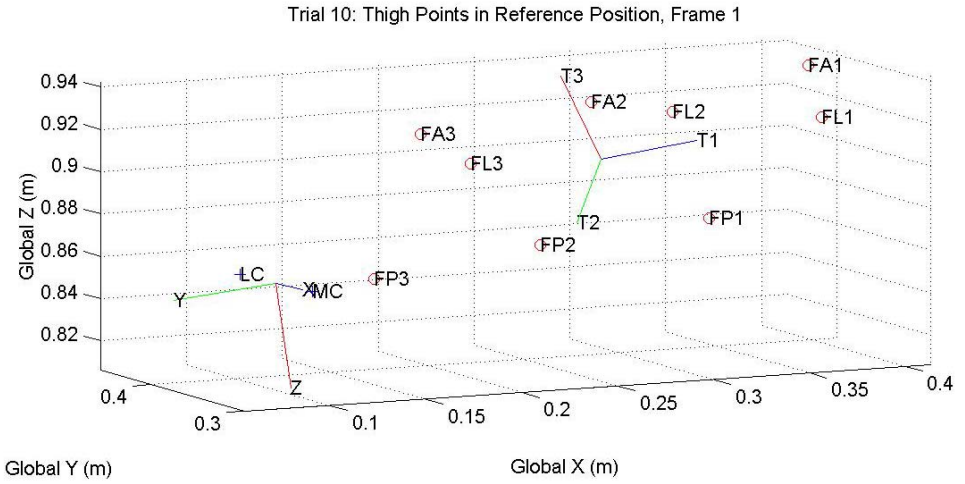

Figure 40: Sample output, thigh axes in reference position

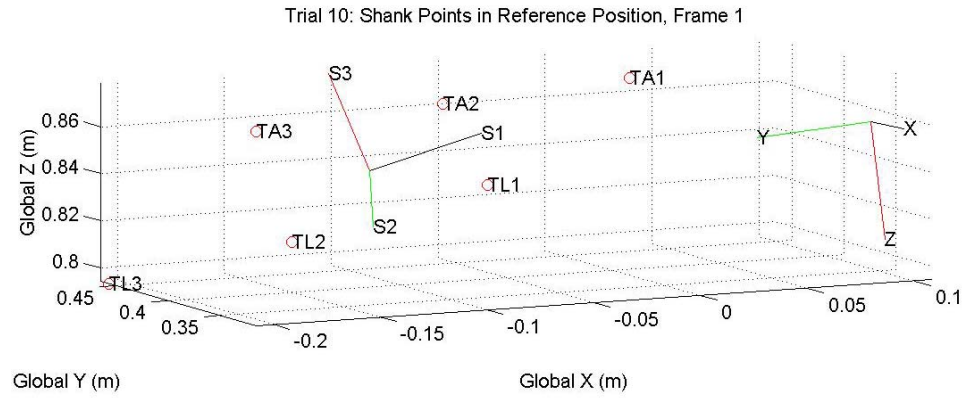

Figure 41: Sample output, shank axes in reference position

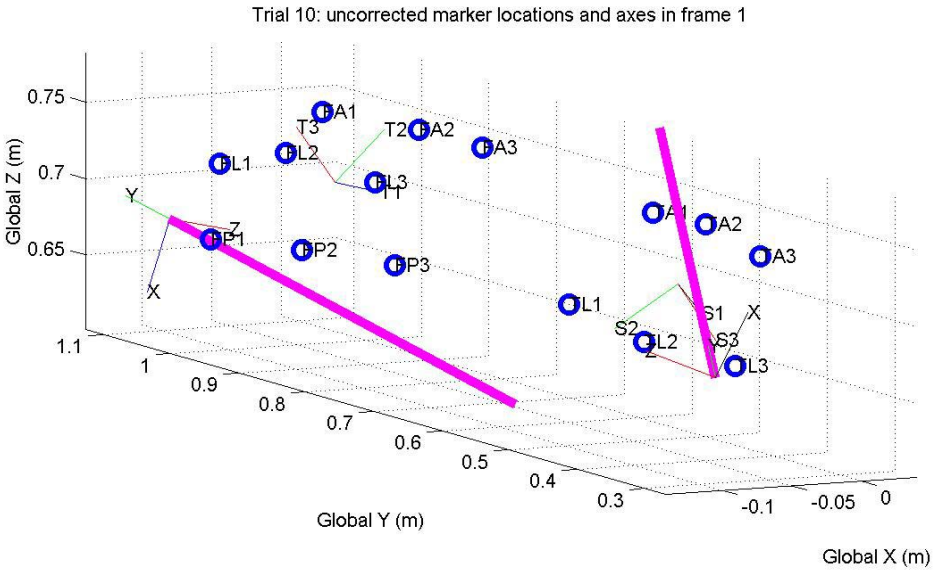

Figure 42: Sample output, uncorrected axes for first frame of activity

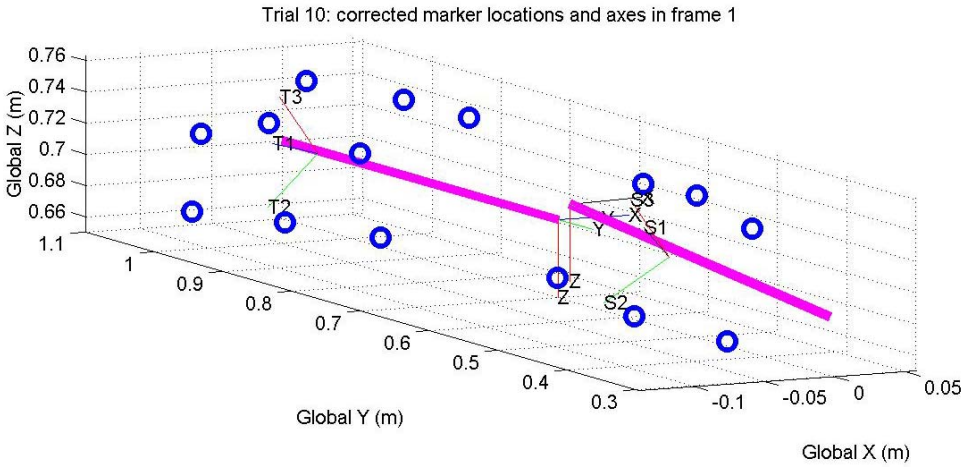

Figure 43: Sample output, corrected axes for first frame of activity

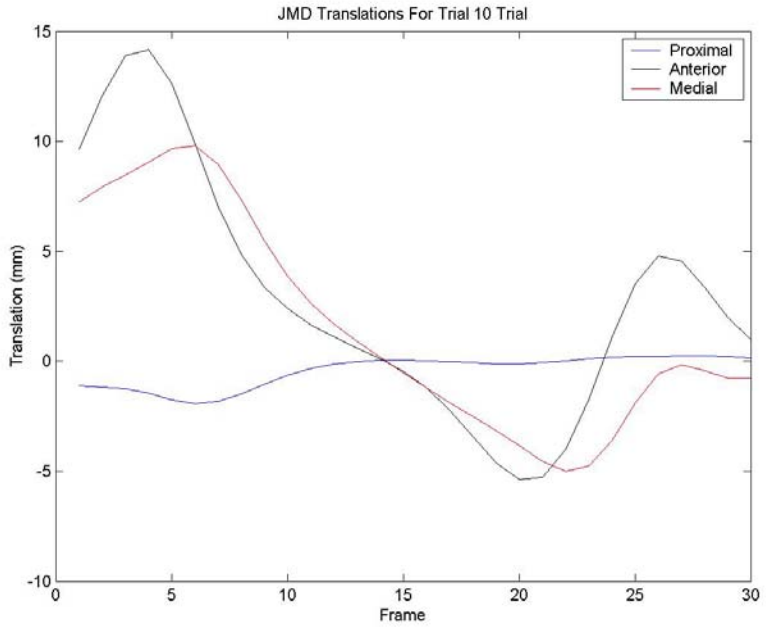

Figure 44: Sample output, translations in JCS before IDT correction

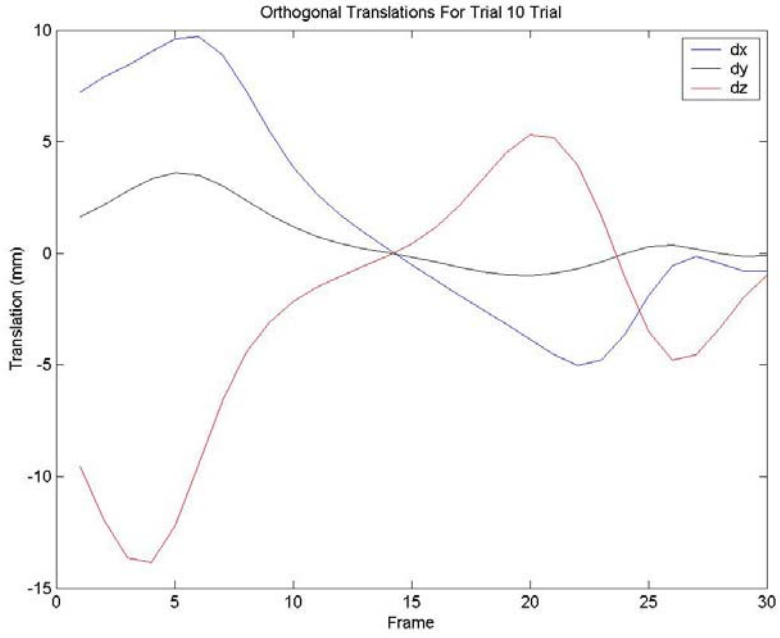

Figure 45: Sample output, orthogonal translations before IDT correction

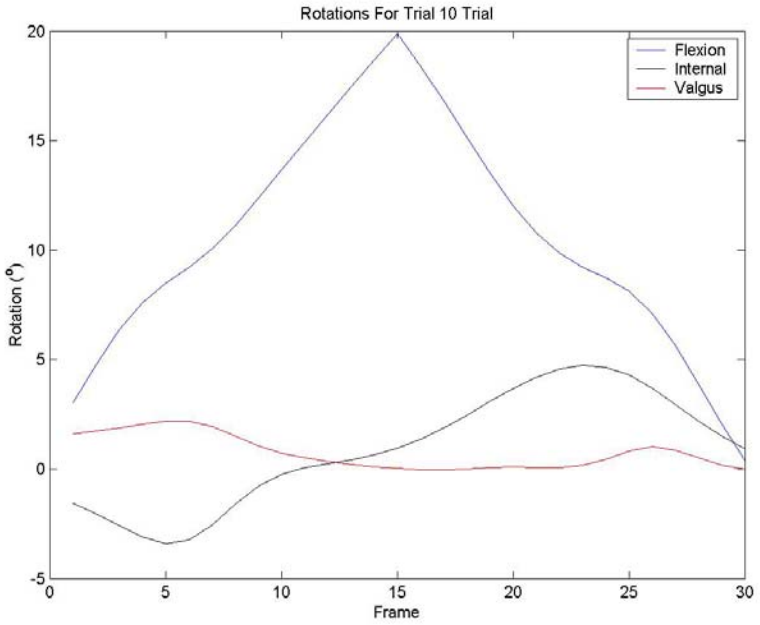

Figure 46: Sample output, rotations before IDT correction

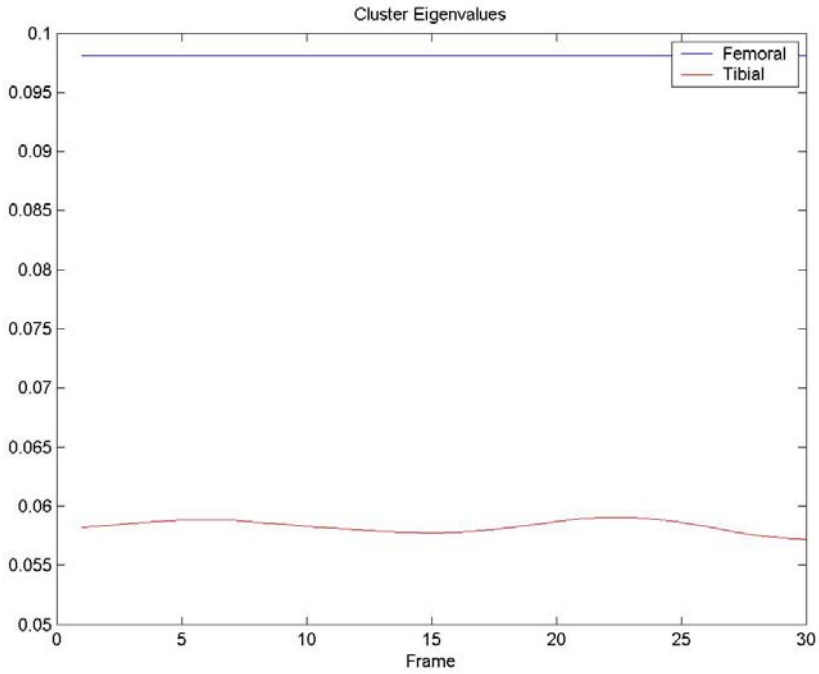

Figure 47: Sample output, cluster eigenvalue norms during activity

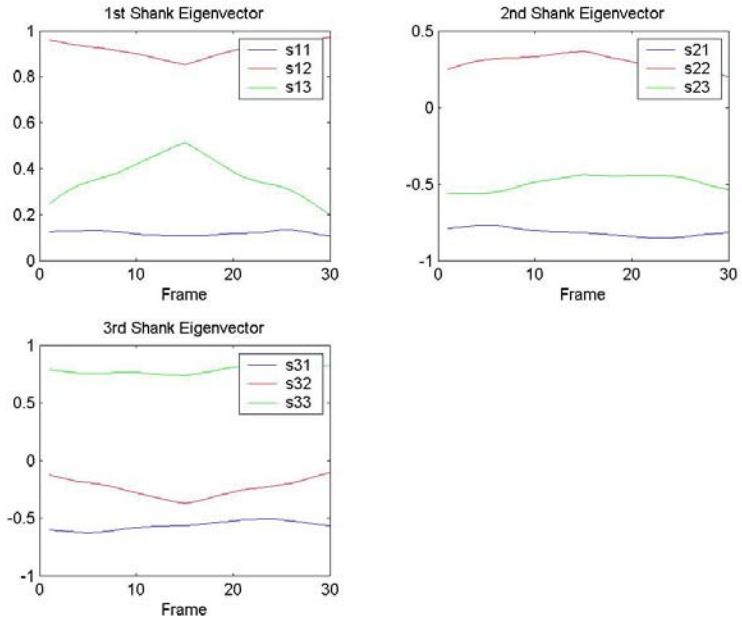

Figure 48: Sample output, eigenvectors of shank cluster during activity

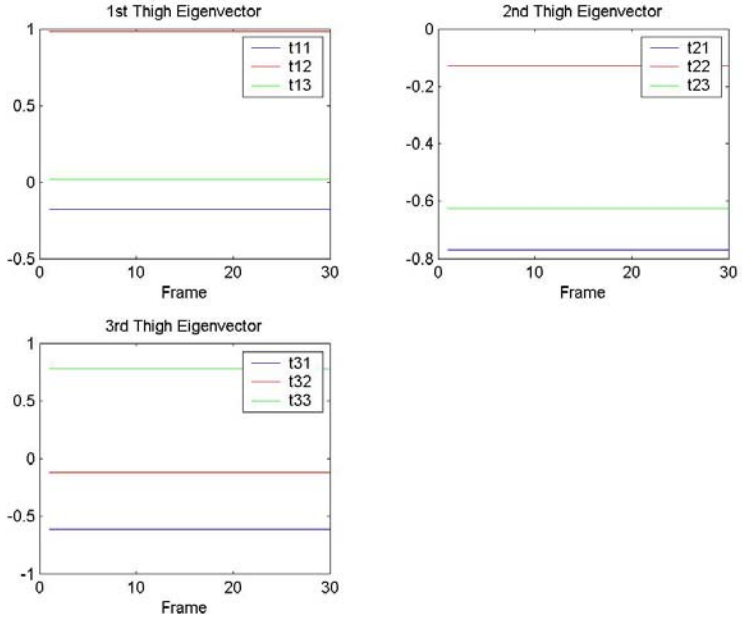

Figure 49: Sample output, eigenvectors of thigh cluster during activity

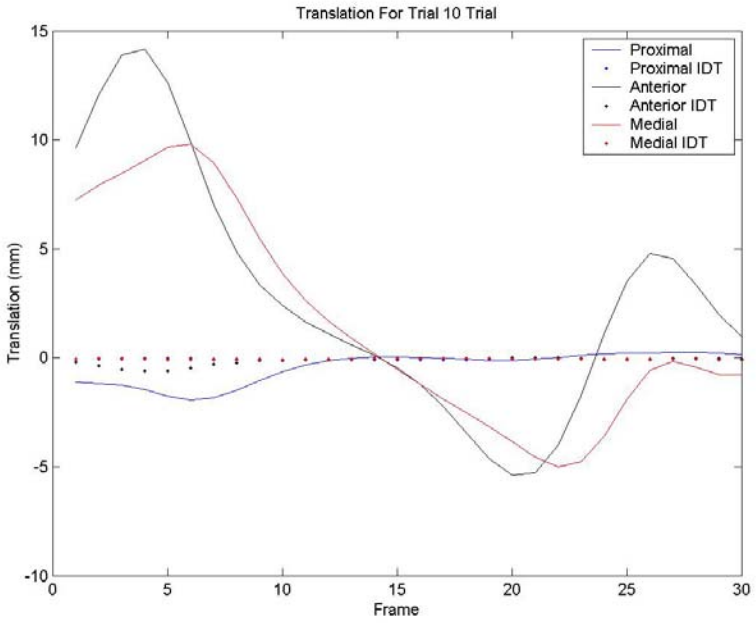

Figure 50: Sample output, translations in JCS before and after IDT correction

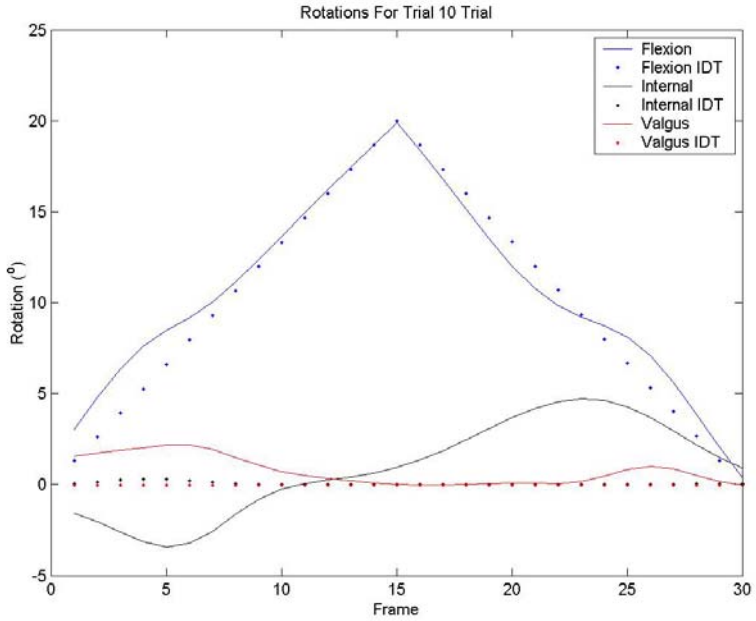

Figure 51: Sample output, rotations before and after IDT correction

BIBLIOGRAPHY

1. Miyasaka, K.C., et al., *The incidence of knee ligament injuries in the general population.* American Journal of Knee Surgery, 1991. **4**(1): p. 3-8.

2. Griffin, L.Y., et al., *Noncontact anterior cruciate ligament injuries: risk factors and prevention strategies.* J Am Acad Orthop Surg, 2000. **8**(3): p. 141-50.

3. Urabe, Y., et al., *Anterior cruciate ligament injury in recreational alpine skiers: analysis of mechanisms and strategy for prevention.* J Orthop Sci, 2002. **7**(1): p. 1-5.

4. Pressman, A. and D.H. Johnson, *A review of ski injuries resulting in combined injury to the anterior cruciate ligament and medial collateral ligaments.* Arthroscopy, 2003. **19**(2): p. 194-202.

5. Viola, R.W., et al., *Anterior cruciate ligament injury incidence among male and female professional alpine skiers.* Am J Sports Med, 1999. **27**(6): p. 792-5.

6. Warme, W.J., et al., *Ski injury statistics, 1982 to 1993, Jackson Hole Ski Resort.* Am J Sports Med, 1995. **23**(5): p. 597-600.

7. Bradley, J.P., et al., *Anterior cruciate ligament injuries in the National Football League: epidemiology and current treatment trends among team physicians.* Arthroscopy, 2002. **18**(5): p. 502-9.

8. Emerson, R.J., *Basketball knee injuries and the anterior cruciate ligament.* Clin Sports Med, 1993. **12**(2): p. 317-28.

9. Gomez, E., J.C. DeLee, and W.C. Farney, *Incidence of injury in Texas girls' high school basketball.* Am J Sports Med, 1996. **24**(5): p. 684-7.

10. Micheli, L.J., et al., *Anterior cruciate ligament reconstructive surgery in adolescent soccer and basketball players.* Clin J Sport Med, 1999. **9**(3): p. 138-41.

11. Soderman, K., et al., *Anterior cruciate ligament injuries in young females playing soccer at senior levels.* Scand J Med Sci Sports, 2002. **12**(2): p. 65-8.

12. Bjordal, J.M., et al., *Epidemiology of anterior cruciate ligament injuries in soccer.* Am J Sports Med, 1997. **25**(3): p. 341-5.

13. McClay Davis, I. and M.L. Ireland, *ACL research retreat: the gender bias. April 6-7, 2001. Meeting report and abstracts.* Clin Biomech (Bristol, Avon), 2001. **16**(10): p. 937-59.

14. Arendt, E. and R. Dick, *Knee injury patterns among men and women in collegiate basketball and soccer. NCAA data and review of literature.* Am J Sports Med, 1995. **23**(6): p. 694-701.

15. Rudolph, K.S., M.J. Axe, and L. Snyder-Mackler, *Dynamic stability after ACL injury: who can hop?* Knee Surg Sports Traumatol Arthrosc, 2000. **8**(5): p. 262-9.

16. Lewek, M.D., et al., *Dynamic knee stability after anterior cruciate ligament rupture.* Exerc Sport Sci Rev, 2003. **31**(4): p. 195-200.

17. Fu, F.H., et al., *Current trends in anterior cruciate ligament reconstruction. Part 1: Biology and biomechanics of reconstruction.* Am J Sports Med, 1999. **27**(6): p. 821-30.

18. McDaniel, W.J., Jr. and T.B. Dameron, Jr., *Untreated ruptures of the anterior cruciate ligament. A follow-up study.* J Bone Joint Surg Am, 1980. **62**(5): p. 696-705.

19. Bonamo, J.J., C. Fay, and T. Firestone, *The conservative treatment of the anterior cruciate deficient knee.* Am J Sports Med, 1990. **18**(6): p. 618-23.

20. Shelton, W.R., G.R. Barrett, and A. Dukes, *Early season anterior cruciate ligament tears. A treatment dilemma.* Am J Sports Med, 1997. **25**(5): p. 656-8.

21. de Roeck, N.J. and A. Lang-Stevenson, *Meniscal tears sustained awaiting anterior cruciate ligament reconstruction.* Injury, 2003. **34**(5): p. 343-5.

22. Cipolla, M., et al., *Different patterns of meniscal tears in acute anterior cruciate ligament (ACL) ruptures and in chronic ACL-deficient knees. Classification, staging and timing of treatment.* Knee Surg Sports Traumatol Arthrosc, 1995. **3**(3): p. 130-4.

23. Finsterbush, A., et al., *Secondary damage to the knee after isolated injury of the anterior cruciate ligament.* Am J Sports Med, 1990. **18**(5): p. 475-9.

24. Pattee, G.A., et al., *Four to ten year followup of unreconstructed anterior cruciate ligament tears.* Am J Sports Med, 1989. **17**(3): p. 430-5.

25. Kannus, P. and M. Jarvinen, *Conservatively treated tears of the anterior cruciate ligament. Long-term results.* J Bone Joint Surg Am, 1987. **69**(7): p. 1007-12.

26. Woo, S.L., S.S. Chan, and T. Yamaji, *Biomechanics of knee ligament healing, repair and reconstruction.* J Biomech, 1997. **30**(5): p. 431-9.

27. Bray, R.C., C.A. Leonard, and P.T. Salo, *Correlation of healing capacity with vascular response in the anterior cruciate and medial collateral ligaments of the rabbit.* J Orthop Res, 2003. **21**(6): p. 1118-23.

28. Frank, C.B. and D.W. Jackson, *The science of reconstruction of the anterior cruciate ligament.* J Bone Joint Surg Am, 1997. **79**(10): p. 1556-76.

29. Clancy, W.G., Jr., J.M. Ray, and D.J. Zoltan, *Acute tears of the anterior cruciate ligament. Surgical versus conservative treatment.* J Bone Joint Surg Am, 1988. **70**(10): p. 1483-8.

30. Fu, F.H., et al., *Current trends in anterior cruciate ligament reconstruction. Part II. Operative procedures and clinical correlations.* Am J Sports Med, 2000. **28**(1): p. 124-30.

31. Fu, F.H. and C.B. Ma, *Anterior cruciate ligament reconstruction using quadruple hamstring.* Operative Techniques in Orthopaedics, 1999. **9**(4): p. 264-272.

32. Aglietti, P., et al., *A comparison between patellar tendon and doubled semitendinosus/gracilis tendon for anterior cruciate ligament reconstruction. A minimum five-year follow-up.* J. Sports Traumatol. rel. res., 1997. **19**: p. 57-68.

33. Woo, S.L., et al., *The effectiveness of reconstruction of the anterior cruciate ligament with hamstrings and patellar tendon . A cadaveric study comparing anterior tibial and rotational loads.* J Bone Joint Surg Am, 2002. **84-A**(6): p. 907-14.

34. Scheffler, S.U., et al., *Biomechanical comparison of hamstring and patellar tendon graft anterior cruciate ligament reconstruction techniques: The impact of fixation level and fixation method under cyclic loading.* Arthroscopy, 2002. **18**(3): p. 304-15.

35. Tis, J.E., et al., *Braided hamstring tendons for reconstruction of the anterior cruciate ligament. A biomechanical analysis.* Am J Sports Med, 2002. **30**(5): p. 684-8.

36. Takeuchi, R., et al., *Double-bundle anatomic anterior cruciate ligament reconstruction using bone-hamstring-bone composite graft.* Arthroscopy, 2002. **18**(5): p. 550-5.

37. Cunningham, R., et al., *A survey of the tension applied to a doubled hamstring tendon graft for reconstruction of the anterior cruciate ligament.* Arthroscopy, 2002. **18**(9): p. 983-8.

38. Feller, J.A., K.E. Webster, and B. Gavin, *Early post-operative morbidity following anterior cruciate ligament reconstruction: patellar tendon versus hamstring graft.* Knee Surg Sports Traumatol Arthrosc, 2001. **9**(5): p. 260-6.

39. Marcacci, M., et al., *Anatomic double-bundle anterior cruciate ligament reconstruction with hamstrings.* Arthroscopy, 2003. **19**(5): p. 540-6.

40. Barrett, G.R., et al., *Reconstruction of the anterior cruciate ligament in females: A comparison of hamstring versus patellar tendon autograft.* Arthroscopy, 2002. **18**(1): p. 46-54.

41. Pinczewski, L.A., et al., *A five-year comparison of patellar tendon versus four-strand hamstring tendon autograft for arthroscopic reconstruction of the anterior cruciate ligament.* Am J Sports Med, 2002. **30**(4): p. 523-36.

42. Bach, B.R., Jr., et al., *Arthroscopically assisted anterior cruciate ligament reconstruction using patellar tendon autograft. Five- to nine-year follow-up evaluation.* Am J Sports Med, 1998. **26**(1): p. 20-9.

43. Ritchie, J.R. and R.D. Parker, *Graft selection in anterior cruciate ligament revision surgery.* Clin Orthop, 1996(325): p. 65-77.

44. Jorgensen, U., et al., *Reconstruction of the anterior cruciate ligament with the iliotibial band autograft in patients with chronic knee instability.* Knee Surg Sports Traumatol Arthrosc, 2001. **9**(3): p. 137-45.

45. Charlick, D.A. and D.N. Caborn, *Technical note: alternative soft-tissue graft preparation technique for cruciate ligament reconstruction.* Arthroscopy, 2000. **16**(8): p. E20.

46. Haut Donahue, T.L., et al., *A biomechanical evaluation of anterior and posterior tibialis tendons as suitable single-loop anterior cruciate ligament grafts.* Arthroscopy, 2002. **18**(6): p. 589-97.

47. Siebold, R., et al., *Primary ACL reconstruction with fresh-frozen patellar versus Achilles tendon allografts.* Arch Orthop Trauma Surg, 2003. **123**(4): p. 180-5.

48. Guidoin, M.F., et al., *Analysis of retrieved polymer fiber based replacements for the ACL.* Biomaterials, 2000. **21**(23): p. 2461-74.

49. Kumar, K. and N. Maffulli, *The ligament augmentation device: an historical perspective.* Arthroscopy, 1999. **15**(4): p. 422-32.

50. Richmond, J.C., et al., *Anterior cruciate reconstruction using a Dacron ligament prosthesis. A long-term study.* Am J Sports Med, 1992. **20**(1): p. 24-8.

51. Mae, T., et al., *Single- versus two-femoral socket anterior cruciate ligament reconstruction technique: Biomechanical analysis using a robotic simulator.* Arthroscopy, 2001. **17**(7): p. 708-16.

52. Sapega, A.A., et al., *Testing for isometry during reconstruction of the anterior cruciate ligament. Anatomical and biomechanical considerations.* J Bone Joint Surg Am, 1990. **72**(2): p. 259-67.

53. Sidles, J.A., et al., *Ligament length relationships in the moving knee.* J Orthop Res, 1988. **6**(4): p. 593-610.

54. Loh, J.C., et al., *Knee stability and graft function following anterior cruciate ligament reconstruction: Comparison between 11 o'clock and 10 o'clock femoral tunnel placement.* Arthroscopy, 2003. **19**(3): p. 297-304.

55. Hame, S.L., et al., *Effects of notchplasty and femoral tunnel position on excursion patterns of an anterior cruciate ligament graft.* Arthroscopy, 2003. **19**(4): p. 340-5.

56. Howell, S.M., *Principles for placing the tibial tunnel and avoiding roof impingement during reconstruction of a torn anterior cruciate ligament.* Knee Surg Sports Traumatol Arthrosc, 1998. **6 Suppl 1**: p. S49-55.

57. Numazaki, H., et al., *The effect of initial graft tension in anterior cruciate ligament reconstruction on the mechanical behaviors of the femur-graft-tibia complex during cyclic loading.* Am J Sports Med, 2002. **30**(6): p. 800-5.

58. Cuppone, M. and B.B. Seedhom, *Effect of implant lengthening and mode of fixation on knee laxity after ACL reconstruction with an artificial ligament: a cadaveric study.* J Orthop Sci, 2001. **6**(3): p. 253-61.

59. Hamner, D.L., et al., *Hamstring tendon grafts for reconstruction of the anterior cruciate ligament: biomechanical evaluation of the use of multiple strands and tensioning techniques.* J Bone Joint Surg Am, 1999. **81**(4): p. 549-57.

60. Fleming, B.C., et al., *The relationship between graft tensioning and the anterior-posterior laxity in the anterior cruciate ligament reconstructed goat knee.* J Orthop Res, 2001. **19**(5): p. 841-4.

61. Tohyama, H. and K. Yasuda, *Significance of graft tension in anterior cruciate ligament reconstruction. Basic background and clinical outcome.* Knee Surg Sports Traumatol Arthrosc, 1998. **6 Suppl 1**: p. S30-7.

62. Abramowitch, S.D., et al., *The effect of initial graft tension on the biomechanical properties of a healing ACL replacement graft: a study in goats.* J Orthop Res, 2003. **21**(4): p. 708-15.

63. Lundberg, W.R., et al., *In vivo forces during remodeling of a two-segment anterior cruciate ligament graft in a goat model.* J Orthop Res, 1997. **15**(5): p. 645-51.

64. Segawa, H., et al., *Influence of the femoral tunnel location and angle on the contact pressure in the femoral tunnel in anterior cruciate ligament reconstruction.* Am J Sports Med, 2003. **31**(3): p. 444-8.

65. Simmons, R., S.M. Howell, and M.L. Hull, *Effect of the angle of the femoral and tibial tunnels in the coronal plane and incremental excision of the posterior cruciate ligament on tension of an anterior cruciate ligament graft: an in vitro study.* J Bone Joint Surg Am, 2003. **85-A**(6): p. 1018-29.

66. Kousa, P., et al., *The fixation strength of six hamstring tendon graft fixation devices in anterior cruciate ligament reconstruction. Part II: tibial site.* Am J Sports Med, 2003. **31**(2): p. 182-8.

67. Kousa, P., et al., *The fixation strength of six hamstring tendon graft fixation devices in anterior cruciate ligament reconstruction. Part I: femoral site.* Am J Sports Med, 2003. **31**(2): p. 174-81.

68. Aglietti, P., et al., *Anatomic versus non-anatomic tibial fixation in anterior cruciate ligament reconstruction with bone-patellar tendon-bone graft.* Knee Surg Sports Traumatol Arthrosc, 1998. **6 Suppl 1**: p. S43-8.

69. Lee, M.C., et al., *Analysis of initial fixation strength of press-fit fixation technique in anterior cruciate ligament reconstruction. A comparative study with titanium and bioabsorbable interference screw using porcine lower limb.* Knee Surg Sports Traumatol Arthrosc, 2003. **11**(2): p. 91-8.

70. Singhatat, W., et al., *How four weeks of implantation affect the strength and stiffness of a tendon graft in a bone tunnel: a study of two fixation devices in an extraarticular model in ovine.* Am J Sports Med, 2002. **30**(4): p. 506-13.

71. Ishibashi, Y., et al., *The effect of anterior cruciate ligament graft fixation site at the tibia on knee stability: evaluation using a robotic testing system.* Arthroscopy, 1997. **13**(2): p. 177-82.

72. Honl, M., et al., *Bone-patellar tendon-bone grafts for anterior cruciate ligament reconstruction: an in vitro comparison of mechanical behavior under failure tensile loading and cyclic submaximal tensile loading.* Am J Sports Med, 2002. **30**(4): p. 549-57.

73. Costi, J.J., et al., *Comparison of torsional strengths of bioabsorbable screws for anterior cruciate ligament reconstruction.* Am J Sports Med, 2001. **29**(5): p. 575-80.

74. Amis, A.A. and R.P. Jakob, *Anterior cruciate ligament graft positioning, tensioning and twisting.* Knee Surg Sports Traumatol Arthrosc, 1998. **6 Suppl 1**: p. S2-12.

75. Paulos, L., et al., *Knee rehabilitation after anterior cruciate ligament reconstruction and repair.* Am J Sports Med, 1981. **9**(3): p. 140-9.

76. Glasgow, S.G., et al., *The effect of early versus late return to vigorous activities on the outcome of anterior cruciate ligament reconstruction.* Am J Sports Med, 1993. **21**(2): p. 243-8.

77. Shelbourne, K.D. and P. Nitz, *Accelerated rehabilitation after anterior cruciate ligament reconstruction.* Am J Sports Med, 1990. **18**(3): p. 292-9.

78. Fu, F.H., S.-Y. Woo, and J. Irrgang, *Current concepts for rehabilitation following anterior cruciate ligament reconstruction.* JOSPT, 1992. **15**(6): p. 270-278.

79. MacDonald, P.B., et al., *Effects of an accelerated rehabilitation program after anterior cruciate ligament reconstruction with combined semitendinosus-gracilis autograft and a ligament augmentation device.* Am J Sports Med, 1995. **23**(5): p. 588-92.

80. Howell, S.M. and M.A. Taylor, *Brace-free rehabilitation, with early return to activity, for knees reconstructed with a double-looped semitendinosus and gracilis graft.* J Bone Joint Surg Am, 1996. **78**(6): p. 814-25.

81. Hardin, J.A., et al., *The effects of "decelerated" rehabilitation following anterior cruciate ligament reconstruction on a hyperelastic female adolescent: a case study.* J Orthop Sports Phys Ther, 1997. **26**(1): p. 29-34.

82. Beynnon, B.D., et al., *The effect of functional knee bracing on the anterior cruciate ligament in the weightbearing and nonweightbearing knee.* Am J Sports Med, 1997. **25**(3): p. 353-9.

83. Colville, M.R., C.L. Lee, and J.V. Ciullo, *The Lenox Hill brace. An evaluation of effectiveness in treating knee instability.* Am J Sports Med, 1986. **14**(4): p. 257-61.

84. Wu, G.K., G.Y. Ng, and A.F. Mak, *Effects of knee bracing on the sensorimotor function of subjects with anterior cruciate ligament reconstruction.* Am J Sports Med, 2001. **29**(5): p. 641-5.

85. Cook, F.F., J.E. Tibone, and F.C. Redfern, *A dynamic analysis of a functional brace for anterior cruciate ligament insufficiency.* Am J Sports Med, 1989. **17**(4): p. 519-24.

86. Risberg, M.A., et al., *Proprioception after anterior cruciate ligament reconstruction with and without bracing.* Knee Surg Sports Traumatol Arthrosc, 1999. **7**(5): p. 303-9.

87. Henriksson, M., P. Rockborn, and L. Good, *Range of motion training in brace vs. plaster immobilization after anterior cruciate ligament reconstruction: a prospective randomized comparison with a 2-year follow-up.* Scand J Med Sci Sports, 2002. **12**(2): p. 73-80.

88. Birmingham, T.B., J.F. Kramer, and A. Kirkley, *Effect of a functional knee brace on knee flexion and extension strength after anterior cruciate ligament reconstruction.* Arch Phys Med Rehabil, 2002. **83**(10): p. 1472-5.

89. Mikkelsen, C., S. Werner, and E. Eriksson, *Closed kinetic chain alone compared to combined open and closed kinetic chain exercises for quadriceps strengthening after anterior cruciate ligament reconstruction with respect to return to sports: a prospective matched follow-up study.* Knee Surg Sports Traumatol Arthrosc, 2000. **8**(6): p. 337-42.

90. Morrissey, M.C., et al., *Effects of open versus closed kinetic chain training on knee laxity in the early period after anterior cruciate ligament reconstruction.* Knee Surg Sports Traumatol Arthrosc, 2000. **8**(6): p. 343-8.

91. Escamilla, R.F., et al., *Biomechanics of the knee during closed kinetic chain and open kinetic chain exercises.* Med Sci Sports Exerc, 1998. **30**(4): p. 556-69.

92. Yack, H.J., C.E. Collins, and T.J. Whieldon, *Comparison of closed and open kinetic chain exercise in the anterior cruciate ligament-deficient knee.* Am J Sports Med, 1993. **21**(1): p. 49-54.

93. Hollman, J.H., et al., *Knee joint movements in subjects without knee pathology and subjects with injured anterior cruciate ligaments.* Phys Ther, 2002. **82**(10): p. 960-72.

94. Cerulli, G., A. Caraffa, and F. Ponteggia, *Rehabilitation issues in women with anterior cruciate ligament deficiency.* Sports Medicine and Arthroscopy Review, 2002. **10**(1): p. 76-82.

95. Marx, R.G., et al., *Beliefs and attitudes of members of the American Academy of Orthopaedic Surgeons regarding the treatment of anterior cruciate ligament injury.* Arthroscopy, 2003. **19**(7): p. 762-70.

96. Irrgang, J.J., et al., *Use of the International Knee Documentation Committee guidelines to assess outcome following anterior cruciate ligament reconstruction.* Knee Surg Sports Traumatol Arthrosc, 1998. **6**(2): p. 107-14.

97. Clancy, W.G., Jr., et al., *Anterior cruciate ligament reconstruction using one-third of the patellar ligament, augmented by extra-articular tendon transfers.* J Bone Joint Surg Am, 1982. **64**(3): p. 352-9.

98. Kocher, M.S., et al., *Determinants of patient satisfaction with outcome after anterior cruciate ligament reconstruction.* J Bone Joint Surg Am, 2002. **84-A**(9): p. 1560-72.

99. Brandsson, S., et al., *A comparison of results in middle-aged and young patients after anterior cruciate ligament reconstruction.* Arthroscopy, 2000. **16**(2): p. 178-82.

100. Cross, M.J., et al., *Acute repair of injury to the anterior cruciate ligament. A long-term followup.* Am J Sports Med, 1993. **21**(1): p. 128-31.

101. Aglietti, P., et al., *Long-term study of anterior cruciate ligament reconstruction for chronic instability using the central one-third patellar tendon and a lateral extraarticular tenodesis.* Am J Sports Med, 1992. **20**(1): p. 38-45.

102. Yagi, M., et al., *Biomechanical analysis of an anatomic anterior cruciate ligament reconstruction.* Am J Sports Med, 2002. **30**(5): p. 660-6.

103. Abramowitch, S.D., et al., *The healing medial collateral ligament following a combined anterior cruciate and medial collateral ligament injury--a biomechanical study in a goat model.* J Orthop Res, 2003. **21**(6): p. 1124-30.

104. Georgoulis, A.D., et al., *The presence of proprioceptive mechanoreceptors in the remnants of the ruptured ACL as a possible source of re-innervation of the ACL autograft.* Knee Surg Sports Traumatol Arthrosc, 2001. **9**(6): p. 364-8.

105. Bonfim, T.R., C.A. Jansen Paccola, and J.A. Barela, *Proprioceptive and behavior impairments in individuals with anterior cruciate ligament reconstructed knees.* Arch Phys Med Rehabil, 2003. **84**(8): p. 1217-23.

106. Fremerey, R.W., et al., *Proprioception after rehabilitation and reconstruction in knees with deficiency of the anterior cruciate ligament: a prospective, longitudinal study.* J Bone Joint Surg Br, 2000. **82**(6): p. 801-6.

107. Urbach, D., et al., *Effects of reconstruction of the anterior cruciate ligament on voluntary activation of quadriceps femoris a prospective twitch interpolation study.* J Bone Joint Surg Br, 2001. **83**(8): p. 1104-10.

108. Ernst, G.P., et al., *Lower extremity compensations following anterior cruciate ligament reconstruction.* Phys Ther, 2000. **80**(3): p. 251-60.

109. Natri, A., et al., *Isokinetic muscle performance after anterior cruciate ligament surgery. Long-term results and outcome predicting factors after primary surgery and late-phase reconstruction.* Int J Sports Med, 1996. **17**(3): p. 223-8.

110. Keays, S.L., et al., *The relationship between knee strength and functional stability before and after anterior cruciate ligament reconstruction.* J Orthop Res, 2003. **21**(2): p. 231-7.

111. Fu, F.H., et al., *Biomechanics of knee ligaments.* J Bone Joint Surg Am, 1993. **75-A**(11): p. 1716-1727.

112. Jonsson, T., et al., *Clinical diagnosis of ruptures of the anterior cruciate ligament: a comparative study of the Lachman test and the anterior drawer sign.* Am J Sports Med, 1982. **10**(2): p. 100-2.

113. Katz, J.W. and R.J. Fingeroth, *The diagnostic accuracy of ruptures of the anterior cruciate ligament comparing the Lachman test, the anterior drawer sign, and the pivot shift test in acute and chronic knee injuries.* Am J Sports Med, 1986. **14**(1): p. 88-91.

114. Malcom, L.L., et al., *The measurement of anterior knee laxity after ACL reconstructive surgery.* Clin Orthop, 1985(196): p. 35-41.

115. Bach, B.R., Jr., et al., *Arthrometric evaluation of knees that have a torn anterior cruciate ligament.* J Bone Joint Surg Am, 1990. **72**(9): p. 1299-306.

116. Daniel, D.M., et al., *Instrumented measurement of anterior knee laxity in patients with acute anterior cruciate ligament disruption.* Am J Sports Med, 1985. **13**(6): p. 401-7.

117. Howell, S.M., *Anterior tibial translation during a maximum quadriceps contraction: is it clinically significant?* Am J Sports Med, 1990. **18**(6): p. 573-8.

118. Markolf, K.L., et al., *Biomechanical effects of femoral notchplasty in anterior cruciate ligament reconstruction.* Am J Sports Med, 2002. **30**(1): p. 83-9.

119. Beynnon, B.D., et al., *Anterior cruciate ligament replacement: comparison of bone-patellar tendon-bone grafts with two-strand hamstring grafts. A prospective, randomized study.* J Bone Joint Surg Am, 2002. **84-A**(9): p. 1503-13.

120. Markolf, K.L., et al., *Biomechanical consequences of replacement of the anterior cruciate ligament with a patellar ligament allograft. Part I: insertion of the graft and anterior-posterior testing.* J Bone Joint Surg Am, 1996. **78**(11): p. 1720-7.

121. Markolf, K.L., et al., *Reconstruction of knees with combined cruciate deficiencies: a biomechanical study.* J Bone Joint Surg Am, 2003. **85-A**(9): p. 1768-74.

122. Snyder-Mackler, L., et al., *The relationship between passive joint laxity and functional outcome after anterior cruciate ligament injury.* Am J Sports Med, 1997. **25**(2): p. 191-5.

123. Lephart, S., et al., *Relationship between selected physical characteristics and functional capacity in the anterior cruciate ligament -insufficient athlete.* J Orthop Sports Phys Ther, 1992. **16**(4): p. 174-181.

124. Patel, R.R., et al. *Clinical measures of knee instability are not reflective of dynamic function in ACL deficient patients*. in *ORS*. 1998. New Orleans, LA.

125. Harter, R.A., et al., *Long-term evaluation of knee stability and function following surgical reconstruction for anterior cruciate ligament insufficiency.* Am J Sports Med, 1988. **16**(5): p. 434-43.

126. Seto, J.L., et al., *Assessment of quadriceps/hamstring strength, knee ligament stability, functional and sports activity levels five years after anterior cruciate ligament reconstruction.* Am J Sports Med, 1988. **16**(2): p. 170-80.

127. Miyasaka, T., et al., *Coordination of the anterior and posterior cruciate ligaments in constraining the varus-valgus and internal-external rotatory instability of the knee.* J Orthop Sci, 2002. **7**(3): p. 348-53.

128. Berchuck, M., et al., *Gait adaptations by patients who have a deficient anterior cruciate ligament.* J Bone Joint Surg Am, 1990. **72**(6): p. 871-7.

129. Zhang, L.Q., et al., *Six degrees-of-freedom kinematics of ACL deficient knees during locomotion-compensatory mechanism.* Gait Posture, 2003. **17**(1): p. 34-42.

130. Lloyd, D.G. and T.S. Buchanan, *Strategies of muscular support of varus and valgus isometric loads at the human knee.* J Biomech, 2001. **34**(10): p. 1257-67.

131. Rudolph, K.S., et al., *Dynamic stability in the anterior cruciate ligament deficient knee.* Knee Surg Sports Traumatol Arthrosc, 2001. **9**(2): p. 62-71.

132. Torzilli, P.A., X. Deng, and R.F. Warren, *The effect of joint-compressive load and quadriceps muscle force on knee motion in the intact and anterior cruciate ligament-sectioned knee.* Am J Sports Med, 1994. **22**(1): p. 105-12.

133. More, R.C., et al., *Hamstrings--an anterior cruciate ligament protagonist. An in vitro study.* Am J Sports Med, 1993. **21**(2): p. 231-7.

134. Elias, J.J., et al., *The soleus muscle acts as an agonist for the anterior cruciate ligament. An in vitro experimental study.* Am J Sports Med, 2003. **31**(2): p. 241-6.

135. Woo, S.L., et al., *Use of robotic technology for diathrodial joint research.* J Sci Med Sport, 1999. **2**(4): p. 283-97.

136. Darcy, S., *Estimation of ACL forces by reproducing average knee kinematics.* Masters Thesis, University of Pittsburgh, http://etd.library.pitt.edu:80/ETD/available/etd-07162003-072424/, 2003.

137. Song, Y., et al., *A three-dimensional finite element model of the human anterior cruciate ligament: a computational analysis with experimental validation.* J Biomech, 2004. **37**(3): p. 383-90.

138. Rudy, T.W., et al., *A combined robotic/universal force sensor approach to determine in situ forces of knee ligaments.* J Biomech, 1996. **29**(10): p. 1357-60.

139. Fujie, H., et al., *The use of a universal force-moment sensor to determine in-situ forces in ligaments: a new methodology.* J Biomech Eng, 1995. **117**(1): p. 1-7.

140. Woo, S.L., et al., *Force and force distribution in the anterior cruciate ligament and its clinical implications.* Sportorthopadic-Sporttraumatologie, 1997. **13**(1): p. 37-48.

141. Jobe, C.M. and M. Wright, *Anatomy of the Knee*, in *Knee Surgery*, K.G. Vince, Editor. 1994, Williams & Wilkins: Philadelphia, PA. p. 1-53.

142. Matsumoto, H., *Mechanism of the pivot shift.* J Bone Joint Surg Br, 1990. **72**(5): p. 816-21.

143. Moore, K.L., *Clinically oriented anatomy*. 2 ed, ed. J.N. Gardner. 1984, Baltimore, MD: Williams & Wilkins. 1101.

144. Weiss, J.A., et al., *Evaluation of a new injury model to study medial collateral ligament healing: primary repair versus nonoperative treatment.* J Orthop Res, 1991. **9**(4): p. 516-28.

145. Wadia, F.D., et al., *An anatomic study of the popliteofibular ligament.* Int Orthop, 2003. **27**(3): p. 172-4.

146. Odensten, M. and J. Gillquist, *Functional anatomy of the anterior cruciate ligament and a rationale for reconstruction.* J Bone Joint Surg Am, 1985. **67**(2): p. 257-62.

147. Sakane, M., et al., *In situ forces in the anterior cruciate ligament and its bundles in response to anterior tibial loads.* J Orthop Res, 1997. **15**(2): p. 285-93.

148. Harner, C.D., et al., *Comparative study of the size and shape of human anterior and posterior cruciate ligaments.* J Orthop Res, 1995. **13**(3): p. 429-34.

149. Matsumoto, H. and B. Seedhom, *Tension characteristics of the iliotibial tract and role of its superficial layer.* Clin Orthop, 1995(313): p. 253-5.

150. Kaplan, E.B., *The iliotibial tract; clinical and morphological significance.* J Bone Joint Surg Am, 1958. **40-A**(4): p. 817-32.

151. Terry, G.C., J.C. Hughston, and L.A. Norwood, *The anatomy of the iliopatellar band and iliotibial tract.* Am J Sports Med, 1986. **14**(1): p. 39-45.

152. Pandy, M.G. and K.B. Shelburne, *Dependence of cruciate-ligament loading on muscle forces and external load.* J Biomech, 1997. **30**(10): p. 1015-24.

153. Markolf, K.L., et al., *Direct measurement of resultant forces in the anterior cruciate ligament. An in vitro study performed with a new experimental technique.* J Bone Joint Surg Am, 1990. **72**(4): p. 557-67.

154. Lloyd, D.G. and T.S. Buchanan, *A model of load sharing between muscles and soft tissues at the human knee during static tasks.* J Biomech Eng, 1996. **118**(3): p. 367-76.

155. Woo, S.L., G.A. Livesay, and B.A. Smith, *Kinematics*, in *Knee Surgery*, K.G. Vince, Editor. 1994, Williams & Wilkins: Philadelphia, PA. p. 173-187.

156. Markolf, K.L., J.S. Mensch, and H.C. Amstutz, *Stiffness and laxity of the knee--the contributions of the supporting structures. A quantitative in vitro study.* J Bone Joint Surg Am, 1976. **58**(5): p. 583-94.

157. Ahmed, A.M., et al., *In-vitro ligament tension pattern in the flexed knee in passive loading.* J Orthop Res, 1987. **5**(2): p. 217-30.

158. Hame, S.L., D.A. Oakes, and K.L. Markolf, *Injury to the anterior cruciate ligament during alpine skiing: a biomechanical analysis of tibial torque and knee flexion angle.* Am J Sports Med, 2002. **30**(4): p. 537-40.

159. Markolf, K.L., et al., *In situ calibration of miniature sensors implanted into the anterior cruciate ligament part I: strain measurements.* J Orthop Res, 1998. **16**(4): p. 455-63.

160. Fujie, H., et al., *The use of robotics technology to study human joint kinematics: a new methodology.* J Biomech Eng, 1993. **115**(3): p. 211-7.

161. Li, G., et al., *In situ forces of the anterior and posterior cruciate ligaments in high knee flexion: an in vitro investigation.* J Orthop Res, 2004. **22**(2): p. 293-7.

162. Fujie, H., T. Sekito, and A. Orita, *A novel robotic system for joint biomechanical testing: application to the human knee joint.* J Biomech Eng, 2004. **126**: p. 54-61.

163. Shapiro, M.S., et al., *The effect of section of the medial collateral ligament on force generated in the anterior cruciate ligament.* J Bone Joint Surg Am, 1991. **73**(2): p. 248-56.

164. Gill, T.J., et al., *The biomechanical effect of posterior cruciate ligament reconstruction on knee joint function. Kinematic response to simulated muscle loads.* Am J Sports Med, 2003. **31**(4): p. 530-6.

165. Fox, R.J., et al., *Determination of the in situ forces in the human posterior cruciate ligament using robotic technology. A cadaveric study.* Am J Sports Med, 1998. **26**(3): p. 395-401.

166. Haimes, J.L., et al., *Role of the medial structures in the intact and anterior cruciate ligament-deficient knee. Limits of motion in the human knee.* Am J Sports Med, 1994. **22**(3): p. 402-9.

167. Shoemaker, S.C. and K.L. Markolf, *The role of the meniscus in the anterior-posterior stability of the loaded anterior cruciate-deficient knee. Effects of partial versus total excision.* J Bone Joint Surg Am, 1986. **68**(1): p. 71-9.

168. Fleming, B.C., et al., *The gastrocnemius muscle is an antagonist of the anterior cruciate ligament.* J Orthop Res, 2001. **19**(6): p. 1178-84.

169. Kwak, S.D., et al., *Hamstrings and iliotibial band forces affect knee kinematics and contact pattern.* J Orthop Res, 2000. **18**(1): p. 101-8.

170. Zatsiorsky, V.M., *Kinematics of Human Motion*, ed. L.M. Hooper-Davenport. 1998, Champaign, IL: Human Kinetics.

171. Craig, J.J., *Introduction to robotics: mechanics and control*. 2 ed. 1989, Reading, MA: Addison-Wesley.

172. Li, Z.M., J.A. Fisk, and S.L. Woo, *The use of the matrix method for the study of human motion: theory and applications.* Sheng Wu Yi Xue Gong Cheng Xue Za Zhi, 2003. **20**(3): p. 375-83.

173. An, K.N. and E.Y. Chao, *Kinematic analysis of human movement.* Ann Biomed Eng, 1984. **12**(6): p. 585-97.

174. Bull, A.M. and A.A. Amis, *Knee joint motion: description and measurement.* Proc Inst Mech Eng [H], 1998. **212**(5): p. 357-72.

175. Chao, E.Y., *Justification of triaxial goniometer for the measurement of joint rotation.* J Biomech, 1980. **13**(12): p. 989-1006.

176. Tupling, S.J. and M.R. Pierrynowski, *Use of cardan angles to locate rigid bodies in three-dimensional space.* Med Biol Eng Comput, 1987. **25**(5): p. 527-32.

177. Gil, J.E., *Development of a biomechanical testing platform for the study of the human knee joint.* Masters Thesis, University of Pittsburgh, http://etd.library.pitt.edu/ETD/available/etd-11172003-121731/, 2003.

178. Grood, E.S. and W.J. Suntay, *A joint coordinate system for the clinical description of three-dimensional motions: application to the knee.* J Biomech Eng, 1983. **105**(2): p. 136-44.

179. Pennock, G.R. and K.J. Clark, *An anatomy-based coordinate system for the description of the kinematic displacements in the human knee.* J Biomech, 1990. **23**(12): p. 1209-18.

180. Cappozzo, A., et al., *Position and orientation in space of bones during movement: anatomical frame definition and determination.* Clin Biomech (Bristol, Avon), 1995. **10**(4): p. 171-178.

181. Wu, G. and P.R. Cavanagh, *ISB recommendations for standardization in the reporting of kinematic data.* J Biomech, 1995. **28**(10): p. 1257-61.

182. Sheehan, F.T. and P. Mitiguy, *In regards to the "ISB recommendations for standardization in the reporting of kinematic data".* J Biomech, 1999. **32**(10): p. 1135-6.

183. Lafortune, M.A., et al., *Three-dimensional kinematics of the human knee during walking.* J Biomech, 1992. **25**(4): p. 347-57.

184. Hollis, J.M., et al., *The effects of knee motion and external loading on the length of the anterior cruciate ligament (ACL): a kinematic study.* J Biomech Eng, 1991. **113**(2): p. 208-14.

185. Kirstukas, S.J., J.L. Lewis, and A.G. Erdman, *6R instrumented spatial linkages for anatomical joint motion measurement--Part 1: Design.* J Biomech Eng, 1992. **114**(1): p. 92-100.

186. Kirstukas, S.J., J.L. Lewis, and A.G. Erdman, *6R instrumented spatial linkages for anatomical joint motion measurement--Part 2: Calibration.* J Biomech Eng, 1992. **114**(1): p. 101-10.

187. Johnston, R.C. and G.L. Smidt, *Measurement of hip-joint motion during walking. Evaluation of an electrogoniometric method.* J Bone Joint Surg Am, 1969. **51**(6): p. 1082-94.

188. Kettelkamp, D.B., et al., *An electrogoniometric study of knee motion in normal gait.* J Bone Joint Surg Am, 1970. **52**(4): p. 775-90.

189. Kinzel, G.L., A.S. Hall, Jr., and B.M. Hillberry, *Measurement of the total motion between two body segments. I. Analytical development.* J Biomech, 1972. **5**(1): p. 93-105.

190. Kinzel, G.L., et al., *Measurement of the total motion between two body segments. II. Description of application.* J Biomech, 1972. **5**(3): p. 283-93.

191. Vergis, A., S. Hammarby, and J. Gillquist, *Fluoroscopic validation of electrogoniometrically measured femorotibial translation in healthy and ACL deficient subjects.* Scand J Med Sci Sports, 2002. **12**(4): p. 223-9.

192. Kvist, J. and J. Gillquist, *Sagittal plane knee translation and electromyographic activity during closed and open kinetic chain exercises in anterior cruciate ligament-deficient patients and control subjects.* Am J Sports Med, 2001. **29**(1): p. 72-82.

193. Higuchi, H., et al., *Characteristics of anterior tibial translation with active and isokinetic knee extension exercise before and after ACL reconstruction.* J Orthop Sci, 2002. **7**(3): p. 341-7.

194. Vergis, A. and J. Gillquist, *Sagittal plane translation of the knee during stair walking. Comparison of healthy and anterior cruciate ligament--deficient subjects.* Am J Sports Med, 1998. **26**(6): p. 841-6.

195. Ishii, Y., et al., *Gait analysis after total knee arthroplasty. Comparison of posterior cruciate retention and substitution.* J Orthop Sci, 1998. **3**(6): p. 310-7.

196. Ishii, Y., et al., *Screw home motion after total knee replacement.* Clin Orthop, 1999(358): p. 181-7.

197. Suntay, W.J., et al., *Error analysis of a system for measuring three-dimensional joint motion.* J Biomech Eng, 1983. **105**(2): p. 127-35.

198. Sutherland, D.H., *The evolution of clinical gait analysis. Part II kinematics.* Gait Posture, 2002. **16**(2): p. 159-79.

199. Andriacchi, T.P. and E.J. Alexander, *Studies of human locomotion: past, present and future.* J Biomech, 2000. **33**(10): p. 1217-24.

200. Sutherland, D.H., et al., *Measurement of movements and timing of muscle contraction from movie film.* J Bone Joint Surg Am, 1967. **49A**: p. 1248-9.

201. Zeller, B.L., et al., *Differences in kinematics and electromyographic activity between men and women during the single-legged squat.* Am J Sports Med, 2003. **31**(3): p. 449-56.

202. Georgoulis, A.D., et al., *Three-dimensional tibiofemoral kinematics of the anterior cruciate ligament-deficient and reconstructed knee during walking.* Am J Sports Med, 2003. **31**(1): p. 75-9.

203. Karrholm, J., *Roentgen stereophotogrammetry. Review of orthopedic applications.* Acta Orthop Scand, 1989. **60**(4): p. 491-503.

204. Lysell, E., *Motion in the cervical spine. An experimental study on autopsy specimens.* Acta Orthop Scand, 1969: p. Suppl 123:1+.

205. Selvik, G., P. Alberius, and A.S. Aronson, *A roentgen stereophotogrammetric system. Construction, calibration and technical accuracy.* Acta Radiol Diagn (Stockh), 1983. **24**(4): p. 343-52.

206. Selvik, G., *A stereophotogrammetric system for the study of human movements.* Scand J Rehabil Med Suppl, 1978. **6**: p. 16-20.

207. van Dijk, R., R. Huiskes, and G. Selvik, *Roentgen stereophotogrammetric methods for the evaluation of the three dimensional kinematic behaviour and cruciate ligament length patterns of the human knee joint.* J Biomech, 1979. **12**(9): p. 727-31.

208. Karrholm, J., et al., *Active knee motion after cruciate ligament rupture. Stereoradiography.* Acta Orthop Scand, 1988. **59**(2): p. 158-64.

209. Karrholm, J., et al., *Three-dimensional instability of the anterior cruciate deficient knee.* J Bone Joint Surg Br, 1988. **70**(5): p. 777-83.

210. Jonsson, H., J. Karrholm, and L.G. Elmqvist, *Kinematics of active knee extension after tear of the anterior cruciate ligament.* Am J Sports Med, 1989. **17**(6): p. 796-802.

211. Brandsson, S., et al., *Kinematics and laxity of the knee joint after anterior cruciate ligament reconstruction: pre- and postoperative radiostereometric studies.* Am J Sports Med, 2002. **30**(3): p. 361-7.

212. Brandsson, S., et al., *Kinematics after tear in the anterior cruciate ligament: dynamic bilateral radiostereometric studies in 11 patients.* Acta Orthop Scand, 2001. **72**(4): p. 372-8.

213. Karrholm, J., S. Brandsson, and M.A. Freeman, *Tibiofemoral movement 4: changes of axial tibial rotation caused by forced rotation at the weight-bearing knee studied by RSA.* J Bone Joint Surg Br, 2000. **82**(8): p. 1201-3.

214. Fleming, B.C., et al., *Accuracy and repeatability of Roentgen stereophotogrammetric analysis (RSA) for measuring knee laxity in longitudinal studies.* J Biomech, 2001. **34**(10): p. 1355-9.

215. Fleming, B.C., et al., *Measurement of anterior-posterior knee laxity: a comparison of three techniques.* J Orthop Res, 2002. **20**(3): p. 421-6.

216. Almquist, P.O., et al., *Evaluation of an external device measuring knee joint rotation: an in vivo study with simultaneous Roentgen stereometric analysis.* J Orthop Res, 2002. **20**(3): p. 427-32.

217. Alexander, E.J. and T.P. Andriacchi. *Improving the analysis of human movement using markerless motion capture*. in *Proceedings of ASME Summer Bioengineering Conference*. 2003. Key Biscayne, FL.

218. Chaudhari, A.M., et al. *A video-based, markerless motion tracking system for biomechanical analysis in an arrbitrary environment*. in *Proceedings of the ASME Bioengineering Conference*. 2001. Snowbird, UT.

219. Banks, S.A. and W.A. Hodge, *Accurate measurement of three-dimensional knee replacement kinematics using single-plane fluoroscopy.* IEEE Trans Biomed Eng, 1996. **43**(6): p. 638-49.

220. Banks, S.A., G.D. Markovich, and W.A. Hodge, *In vivo kinematics of cruciate-retaining and -substituting knee arthroplasties.* J Arthroplasty, 1997. **12**(3): p. 297-304.

221. Banks, S., et al., *Knee motions during maximum flexion in fixed and mobile-bearing arthroplasties.* Clin Orthop, 2003(410): p. 131-8.

222. Komistek, R.D., D.A. Dennis, and M. Mahfouz, *In vivo fluoroscopic analysis of the normal human knee.* Clin Orthop, 2003(410): p. 69-81.

223. Tashman, S. and W. Anderst, *In-vivo measurement of dynamic joint motion using high speed biplane radiography and CT: application to canine ACL deficiency.* J Biomech Eng, 2003. **125**(2): p. 238-45.

224. Anderst, W. and S. Tashman. *In vivo bone motion from high frame rate stereo radiography*. in *Proceedings of IMECE'03*. 2003. Washington D.C.

225. Anderst, W.J. and S. Tashman, *A method to estimate in vivo dynamic articular surface interaction.* J Biomech, 2003. **36**(9): p. 1291-9.

226. Tashman, S. and W. Anderst. *Abnormal internal/external and varus/valgus rotations in ACL-reconstructed knees during running; analysis by high speed stereo radiography*. in *Proceedings of IMECE'03, ASME*. 2003. Washington D.C.

227. You, B.M., et al., *In vivo measurement of 3-D skeletal kinematics from sequences of biplane radiographs: application to knee kinematics.* IEEE Trans Med Imaging, 2001. **20**(6): p. 514-25.

228. Rebmann, A.J. and F.T. Sheehan, *Precise 3D skeletal kinematics using fast phase contrast magnetic resonance imaging.* J Magn Reson Imaging, 2003. **17**(2): p. 206-13.

229. Sheehan, F.T., F.E. Zajac, and J.E. Drace, *Using cine phase contrast magnetic resonance imaging to non-invasively study in vivo knee dynamics.* J Biomech, 1998. **31**(1): p. 21-6.

230. Tashman, S. and W. Anderst. *Dynamic instability of canine knees after ACL transection*. in *XVIIth ISB Congress*. 1999. Calgary.

231. Woo, S.L., et al., *Tensile properties of the human femur-anterior cruciate ligament-tibia complex. The effects of specimen age and orientation.* Am J Sports Med, 1991. **19**(3): p. 217-25.

232. Abdel-Aziz, Y.I. and H.M. Karara. *Direct linear transform from comparator coordinates into object space coordinates in close-range photogrammetry*. in *ASP Symposium on Close-Range Photogrammetry*. 1971. Urbana, IL: American Society of Photogrammetry.

233. Das, G.B., *A mathematical approach to problems in photogrammetry.* Empire Survey Review, 1949. **X**(73): p. 131-137.

234. Woltring, H.J., *Calibration and measurement in 3-dimensional monitoring of human motion by optoelectronic means. I. Preliminaries and theoretical aspects.* Biotelemetry, 1975. **2**(3-4): p. 169-96.

235. Miller, N.R., R. Shapiro, and T.M. McLaughlin, *A technique for obtaining spatial kinematic parameters of segments of biomechanical systems from cinematographic data.* J Biomech, 1980. **13**(7): p. 535-47.

236. Woltring, H.J., *Planar control in multi-camera calibration for 3-D gait studies.* J Biomech, 1980. **13**(1): p. 39-48.

237. Andriacchi, T.P., et al., *Three-dimensional coordinate data processing in human motion analysis.* J Biomech Eng, 1979. **101**: p. 279-283.

238. Gruen, A., *Fundamentals of videogrammetry - a review.* Human Movement Science, 1997. **16**: p. 155-187.

239. Gazzani, F., *Comparative assessment of two algorithms for calibrating stereophotogrammetric systems.* J Biomech, 1993. **26**(12): p. 1449-54.

240. Maas, H.-G., *Concepts of real time photogrammetry.* Human Movement Science, 1997. **16**: p. 189-199.

241. Scholz, J., *Reliability and validity of the WATSMART three-dimensional optoelectriv motion analysis system.* Phys Ther, 1989. **69**(8): p. 679-686.

242. Vander Linden, D.W., S.J. Carlson, and R.L. Hubbard, *Reproducibility and accuracy of angle measurements obtained under static conditions with the Motion Analysis video system.* Phys Ther, 1992. **72**(4): p. 300-5.

243. Scholz, J. and J. Millford, *Accuracy and precision of the PEAK performance technologies motion measurement system.* J Motor Behav, 1993. **25**(1): p. 2-7.

244. Klein, P.J. and J.J. DeHaven, *Accuracy of three-dimensional linear and angular estimates obtained with the Ariel Performance Analysis System.* Arch Phys Med Rehabil, 1995. **76**(2): p. 183-9.

245. Wilson, D.J., B.K. Smith, and J.K. Gibson, *Accuracy of reconstructed angular estimates obtained with the Ariel Performance Analysis System.* Phys Ther, 1997. **77**(12): p. 1741-6.

246. Haggard, P. and A. Wing, *Assessing and reporting the accuracy of position measurements made with optical tracking systems.* J Motor Behav, 1990. **22**(2): p. 315-321.

247. Ehara, Y., et al., *Comparison of the performance of 3D camera systems II.* Gait Posture, 1997. **5**: p. 251-255.

248. *Clinical Gait Analysis Forum of Japan-Comparison Meeting of Motion Analysis Systems, http://www.ne.jp/asahi/gait/analysis/comparison2002/index-eng.html, accessed 4/7/2004*. 2002.

249. Kadaba, M.P., et al. *Assessment of human motion with VICON*. in *ASME Biomech Symp*. 1987. Cincinnati, OH.

250. Kadaba, M.P., et al., *Repeatability of kinematic, kinetic, and electromyographic data in normal adult gait.* J Orthop Res, 1989. **7**(6): p. 849-60.

251. Kadaba, M.P., H.K. Ramakrishnan, and M.E. Wootten, *Measurement of lower extremity kinematics during level walking.* J Orthop Res, 1990. **8**(3): p. 383-92.

252. Vaughan, C.L., B.L. Davis, and J.C. O'Connor, *Dynamics of human gait*. Second ed. 1999, Cape Town, South Africa: Kiboho Publishers.

253. Cappozzo, A., *Gait analysis methodology.* Human Movement Science, 1984. **3**: p. 27-50.

254. Piazza, S.J., N. Okita, and P.R. Cavanagh, *Accuracy of the functional method of hip joint center location: effects of limited motion and varied implementation.* J Biomech, 2001. **34**(7): p. 967-73.

255. Mun, J.H., J.S. Freeman, and K. Rim, *Averaged coordinate reference system method for human motion analysis.* SAE Paper 1999-01-1910, 1999.

256. Crowninshield, R.D., et al., *A biomechanical investigation of the human hip.* J Biomech, 1978. **11**(1-2): p. 75-85.

257. Alexander, M.J. and J. Colbourne, *A method of determination of the angular velocity vector of a limb segment.* J Biomech, 1980. **13**(12): p. 1089-93.

258. Chao, E.Y. and B.F. Morrey, *Three-dimensional rotation of the elbow.* J Biomech, 1978. **11**(1-2): p. 57-73.

259. Cappozzo, A., et al., *Surface-marker cluster design criteria for 3-D bone movement reconstruction.* IEEE Trans Biomed Eng, 1997. **44**(12): p. 1165-74.

260. Lu, T.W. and J.J. O'Connor, *Bone position estimation from skin marker co-ordinates using global optimisation with joint constraints.* J Biomech, 1999. **32**(2): p. 129-34.

261. Andriacchi, T.P. and M.K. Toney. *In vivo measurement of six-degrees-of-freedom knee movement during functional testing*. in *Trans Orth Res Soc*. 1995. Orlando, FL.

262. Andriacchi, T.P., et al., *A point cluster method for in vivo motion analysis: applied to a study of knee kinematics.* J Biomech Eng, 1998. **120**(6): p. 743-9.

263. Andriacchi, T.P., C.O. Dyrby, and T.S. Johnson, *The use of functional analysis in evaluating knee kinematics.* Clin Orthop, 2003(410): p. 44-53.

264. Andriacchi, T., C. Darby, and M. Dillingham. *ACL injury causes rotational abnormalities at the knee during walking*. in *48th Annual Trans Orth Res Soc*. 2002. Dallas, TX.

265. Manal, K., et al., *The accuracy of estimating proximal tibial translation during natural cadence walking: bone vs. skin mounted targets.* Clin Biomech (Bristol, Avon), 2003. **18**(2): p. 126-31.

266. Cappozzo, A., et al., *Position and orientation in space of bones during movement: experimental artefacts.* Clin Biomech (Bristol, Avon), 1996. **11**(2): p. 90-100.

267. Stagni, R., et al. *Effect of skin motion artefacts on knee joint kinematics*. in *American Society of Biomechanics IV World Congress of Biomechanics*. 2002. Calgary, Alberta, Canada.

268. Fantozzi, S., et al. *Skin motion artefact characterization from 3D fluoroscopy and stereophotogrammetry*. in *American Society of Biomechanics IV World Congress of Biomechanics*. 2002. Calgary, Alberta, Canada.

269. Tashman, S. and W. Anderst. *Skin Motion Artifacts at the Knee During Impact Movements*. in *Gait and Clinical Movement Analysis Society*. 2002. Chattanooga, TN.

270. Karlsson, D. and R. Tranberg, *On skin movement artefact-resonant frequencies of skin markers attached to the leg.* Human Movement Science, 1999. **18**: p. 627-635.

271. Fuller, J., et al., *A comparison of lower-extremity skeletal kinematics measured using skin and pin mounted markers.* Human Movement Science, 1997. **16**: p. 219-242.

272. Reinschmidt, C., et al., *Effect of skin movement on the analysis of skeletal knee joint motion during running.* J Biomech, 1997. **30**(7): p. 729-32.

273. Levens, A.S., V.T. Inman, and J.A. Blosser, *Transverse rotations of the segments of the lower extremity in locomotion.* JBJS, 1948. **30-A**(4): p. 859-872.

274. Ronsky, J.L., et al. *The kinematics of the stable and unstable ovine stifle joint during walking, incline walking, and running*. in *ASME Bioengineering Conference*. 2001: Snowbird, UT.

275. Ramsey, D.K., et al., *Assessment of functional knee bracing: an in vivo three-dimensional kinematic analysis of the anterior cruciate deficient knee.* Clin Biomech (Bristol, Avon), 2001. **16**(1): p. 61-70.

276. Ramsey, D.K., et al., *Methodological concerns using intra-cortical pins to measure tibiofemoral kinematics.* Knee Surg Sports Traumatol Arthrosc, 2003. **11**(5): p. 344-9.

277. Spoor, C.W. and F.E. Veldpaus, *Rigid body motion calculated from spatial co-ordinates of markers.* J Biomech, 1980. **13**(4): p. 391-3.

278. Peterson, S. *Yet another algorithm for computing rigid body displacements from landmark displacement data*. in *ASME Biomechanics Symposium*. 1987. Cincinnati, OH.

279. Soderkvist, I. and P.A. Wedin, *Determining the movements of the skeleton using well-configured markers.* J Biomech, 1993. **26**(12): p. 1473-7.

280. Holden, J.P., et al., *Surface movement errors in shank kinematics and knee kinetics during gait.* Gait Posture, 1997. **5**: p. 217-227.

281. Manal, K., et al., *Comparison of surface mounted markers and attachment methods in estimating tibial rotations during walking: an in vivo study.* Gait Posture, 2000. **11**(1): p. 38-45.

282. Cheze, L., B.J. Fregly, and J. Dimnet, *A solidification procedure to facilitate kinematic analyses based on video system data.* J Biomech, 1995. **28**(7): p. 879-84.

283. Cappello, A., et al., *Multiple landmark calibration for optimal bone pose estimation.* Human Movement Science, 1997. **16**: p. 259-274.

284. Lucchetti, L., et al., *Skin movement artefact assessment and compensation in the estimation of knee-joint kinematics.* J Biomech, 1998. **31**(11): p. 977-84.

285. Alexander, E.J. and T.P. Andriacchi, *Correcting for deformation in skin-based marker systems.* J Biomech, 2001. **34**(3): p. 355-61.

286. Stagni, R., et al. *Validation of the interval deformation technique for compensating soft tissue artifacts in human motion analysis*. in *International Symposium on Surgery Simulation & Soft Tissue Modeling*. 2003. Juan-Les-Pins, France.

287. Gamage, S.S. and J. Lasenby, *New least squares solutions for estimating the average centre of rotation and the axis of rotation.* J Biomech, 2002. **35**(1): p. 87-93.

288. Fischer, K.J., et al., *A method for measuring joint kinematics designed for accurate registration of kinematic data to models constructed from CT data.* J Biomech, 2001. **34**(3): p. 377-83.

289. Courtine, G. and M. Schieppati, *Human walking along a curved path. II. Gait features and EMG patterns.* Eur J Neurosci, 2003. **18**(1): p. 191-205.

290. Ingber, A.L., *Simulated annealing: practice versus theory.* J. Mathl. comput. Modelling, 1993. **18**(11): p. 29-57.

291. Yuan, X., L. Ryd, and L. Blankevoort, *Error propagation for relative motion determined from marker positions.* J Biomech, 1997. **30**(9): p. 989-92.

292. Shellock, F.G., *Functional assessment of the joints using kinematic magnetic resonance imaging.* Semin Musculoskelet Radiol, 2003. **7**(4): p. 249-76.